Towards A Novel Minimally Invasive 3D Ultrasound Imaging Based Computer Assisted Orthopaedic Surgery System for Bone Fracture Reduction

by

ILKER HACIHALILOGLU

B.Sc., Istanbul Technical University, Istanbul, Turkey, 2001
M.Sc., Istanbul Technical University, Istanbul, Turkey, 2004

A THESIS SUBMITTED IN PARTIAL FULFILLMENT OF THE REQUIREMENTS FOR THE DEGREE OF

DOCTOR OF PHILOSOPHY

in

THE FACULTY OF GRADUATE STUDIES

(Electrical and Computer Engineering)

THE UNIVERSITY OF BRITISH COLUMBIA

(Vancouver)
April 2010

Abstract

Current practice in orthopaedic surgery relies on intra-operative two dimensional (2D) fluoroscopy as the main imaging modality for localization and visualization of bone tissue, fractures, implants, and surgical tool positions. However, with such projection imaging, surgeons typically face considerable difficulties in accurately localizing bone fragments in three dimensional (3D) space and assessing the adequacy and accuracy of reduced fractures. Furthermore, fluoroscopy involves significant radiation exposure. Ultrasound (US) has recently emerged as a potential non-ionizing imaging alternative that promises safer operation while remaining relatively cheap and widely available. US image data, however, is typically characterized by high levels of speckle noise, reverberation, anisotropy and signal dropout which introduce significant difficulties in interpretation of captured data, automatic detection and segmentation of image features and accurate localization of imaged bone surfaces.

In this thesis we propose a novel technique for automatic bone surface and surgical tool localization in US that employs local phase image information to derive symmetry-based features corresponding to tissue/bone or tissue/surgical tool interfaces through the use of 2D Log-Gabor filters. We extend the proposed method to 3D in order to take advantage of correlations between adjacent images. We validate the performance of the proposed approach quantitatively using realistic phantom and in-vitro experiments as well as qualitatively on in-vivo and ex-vivo data. Furthermore, we evaluate the ability of the proposed method in detecting gaps between fractured bone fragments. The current study is therefore the first to show that bone surfaces, surgical tools and fractures can be accurately localized using local phase features computed directly from 3D ultrasound image volumes.

Log-Gabor filters have a strong dependence on the chosen filter parameters, the values of which significantly affect the outcome of the features being extracted. We present a novel method for contextual parameter selection that is autonomously adaptive to image content. Finally, we investigate the hypothesis that 3D US can be used to detect fractures reliably in the emergency room with three clinical studies. We believe that the results presented in this work will be invaluable for all future imaging studies with US in orthopaedics.

Table of Contents

List of Tables

List of Figures

List of Acronyms

2D	Two Dimensional
3D	Three Dimensional
CAS	Computer Assisted Surgery
CAOS	Computer Assisted Orthopaedic Surgery
CCD	Charger Coupled Device
CT	Computed Tomography
CREF	Closed Reduction and External Fixation
DRF	Dynamic Reference Frame
ED	Emergency Department
EPS	Empirical Phase Symetry
FRE	Fiducial Registration Error
FOOSH	Fall Onto Outstretched Hand
ICP	Iterative Closest Point
IRLED	Infrared Light Emitting Diode
ME	Mean Error
MIS	Minimally Invasive Surgery
MR	Magnetic Resonance
MREM	Millirem
MRI	Magnetic Resonance Imaging
NCC	Normalized Cross Correlation
OPS	Optimized Phase Symmetry
OR	Operating Room
ORIF	Open Reduction and Internal Fixation
PS	Phase Symmetry
RD	Radiology Department
RT	Radon Transform
ROI	Region of Interest
STD	Standard Deviation
THR	Total Hip Replacement
TKR	Total Knee Replacement
UKF	Unscented Kalman Filter
US	Ultrasound
VGH	Vancouver General Hospital

Acknowledgements

Looking back at this entire process I realize that there were a lot people that were involved and helped me to shape this work. Surely, though, the principle influence on any student is their supervisor and I was fortunate enough to have three. I would like to express my deep and sincere gratitude to Dr. Rafeef Abugarbieh, Dr. Antony Hodgson and Dr. Robert Rohling for their guidance and support which helped me to complete this work and look forward to new challenges. Their superior knowledge and expertise in the fields of medical image processing, orthopedics and ultrasound together with their patience made this project happen. Many thanks as well for keeping that special balance of guidance and freedom which I believe is so important in an open ended research. I would also like to thank the committee members Dr. Purang Abolmaesumi, Dr. Boris Stoeber and Dr. Tim Salcudean for their constructive feedback.

I would also like to thank my colleagues at The Signal and Image Processing Laboratory and The Biomedical Signal and Image Computing Laboratory.

The doctor I worked with during this thesis is extraordinary. Dr. Pierre Guy always found time in his busy schedule for my work. Without his help I would have never seen the big picture. I also would like to thank Dr. Peter O'Brien being part of this work. I will always remember the days at the hospital trying to get an approval for our clinical study and OR 20.

The two people who have been the biggest part of this process are my parents. They have been involved in this for almost thirty years and have provided the love, support, and encouragement throughout. I also would like to thank my twin brother for being so different than me.

I would also like to thank my friends for always being there. Finally, I would like to thank that special person. Without you, this thesis and life in general wouldn't have been half as much fun. Thanks for always being there.

Dedication

Dedicated to my parents…

Co-authorship Statement

This thesis presents research work conducted by Ilker Hacihaliloglu under the supervision of Dr. Rafeef Abugharbieh and Dr. Antony Hodgson, with collaboratoin with Dr. Robert Rohling. This is a Manuscript based thesis prepared following the guidelines of UBC and is constructed around the four manuscripts described below:

Manuscript 1: “Bone Surface Localization in Ultrasound Using Image Phase Based Features”, *Ultrasound in Medicine and Biology*, 2009. This manuscript is the work of Ilker Hacihaliloglu who received suggestions and feedback from, Dr. Rafeef Abugharbieh, Dr. Antony Hodgson, and Dr. Robert Rohling.

Manuscript 2: “Automatic Bone Localization and Fracture Detection from Volumetric Ultrasound Images Using 3D Local Phase Features.”, will be submitted for publication.This manuscript is the work of Ilker Hacihaliloglu who received suggestions and feedback from, Dr. Rafeef Abugharbieh, Dr. Antony Hodgson, and Dr. Robert Rohling.

Manuscript 3: “Data-Driven Parameterization for Automatic Bone Localization in Ultrasound using Log-Gabor Filter Based Phase Features”, will be submitted for publication.

Manuscript 4: “Local Phase Features of Ultrasound Images for Orthopaedic Surgery: First Clinical Results”, will be submitted for publication.

This manuscript is the work of Ilker Hacihaliloglu who received instructions suggestions and feedback from, Dr. Rafeef Abugharbieh, Dr. Antony Hodgson, and Dr. Robert Rohling.

The first and last chapters of the thesis were written by Ilker Hacihaliloglu, with editing assistance and consultation from Dr. Rafeef Abugharbieh, Dr. Antony Hodgson.

The conception and design of the studies presented in this Thesis as well as the analysis and interpretation of the data and results are the original work of Ilker Hacihaliloglu under the direct and close supervision of his co-supervisors Dr. Rafeef Abugharbieh and Dr. Antony Hodgson.

Dr. Rafeef Abugharbieh, Dr. Antony Hodgson and Dr. Robert Rohling aided revising the manuscripts for critically important intellectual content. They provided numerous suggestions throughout the course of concept development and evaluation.

Chapter 1
Introduction

1.1 Thesis Objective

The focus of this work was to develop robust, accurate and automatic segmentation techniques in the field of ultrasound (US) guided minimally invasive surgery. Ultimately this research was intended to advance the larger goal of developing a novel three dimensional (3D) US based computer assisted orthopaedic surgery (CAOS) system for minimally invasive bone reduction procedures. Such a system will ultimately address a variety of problems with the planning and execution of orthopaedic surgery procedures. Specifically we have investigated the potential and feasibility in using 3D US imaging modality for real-time identification of fractures in emergency departments (ED). The specific clinical application of focus was distal radius and pelvic fractures. The goals of this research include the following:

- Develop new and robust image processing methods that can allow automatic and real-time extraction of bone surfaces and surgical tools from two dimensional (2D) and 3D US scans with sufficient accuracy.
- Develop new and robust image processing methods that can automatically extract fractured bone fragments from 3D US data with sufficient accuracy.
- Perform extensive validation studies that will allow to address the engineering challenges found in real clinical situations.
- Validate the proposed methods with clinical studies.

This in turn will help us in the future design, develop, and evaluate a 3D US based CAOS system which could:

- Improve performance by providing better assessment and placement of the fracture fragments which could in turn improve reduction and decrease the operation time
- Promote minimally invasive surgery (MIS) by minimizing soft tissue exposure
- Decrease cost and improve efficiency by replacing fluoroscopy at key points in the diagnosis and treatment
- Decrease the amount of radiation exposure to patients and to staff
- Decreasing the post operative complications related to fracture fragment reduction and implant position, which are encountered because of imaging limitations.

This study has introduced the concept of using radiation-free real time 3D US imaging modality for fracture assessment in ED. It provided a method which is robust, fast and easy to use and which allows imaging of the fracture at the time of presentation and during surgery. The proposed method also allows accurate and robust extraction of bone surfaces and surgical tools from 3D US volumes. We believe that the results presented in this study are invaluable for all future ultrasound guided computer assisted orthopaedic surgery studies.

1.2 Thesis Motivation and Problem Statement

During 1986–1995, annual medical-care costs for fractures in United States among older adults (aged ≥65) ranged from $7 billion to $10 billion in 1986 to $13.8 billion in 1995. The statistics also show that the number of persons aged ≥65 years is projected to increase from 32.0 million to 51.5 million during 1990–2020 [1]. In a study made by National Center for Health Statistics (NCSH) it was shown that the number for annual ED visits for fractures was 3,443,000 from a total of 21,163,000 visits for all types of injuries. Among the injury types which require hospitalization they are the most common one with 70% [1]. The study also showed that 17,706 people died from fracture related injuries in 2003, which accounts for 10% of the total deaths in ED [1]. According to the Canada National Trauma Registry (CNTR) bulletin the three most common injury diagnoses for trauma hospitalization in 1998/1999 were fractures and dislocations of the lower and upper limb accounting for 51.2% of all injury types [2].

Distal radius fracture is the most common fracture type in the forearm region. It is usually caused by a fall onto an outstretched hand (FOOSH). It can also result from direct impact or axial forces. In the United States, fractures of the distal radius constitute about one sixth of all fractures seen in emergency room [3, 4], and this number increases to 20% in United Kingdom [5]. It is more frequently seen in patients between the ages of 5-14 and 60-69 years [6]. On the other hand pelvic injuries commonly result from high energy trauma. Motor vehicle accidents accounting for up to 73% of injuries are the most common cause of pelvic fractures [7]. The incidence of pelvic fractures in the United States is estimated to be more than 100,000 per year [8]. The Canadian National Trauma Registry have recorded that out of 109,738 major injuries occurring in 1999, 4531 had a pelvis fracture (4%) [7]. Furthermore, mortality rates following pelvic trauma have ranged from 9 to 27% [7]. Due to these high incident rates and the problems faced during the fixation of distal radius and pelvic fractures, which will be explained in section 1.3, the clinical focus of this thesis was on distal radius and pelvic fractures.

1.2.1 Current Fracture Treatment in Orthopaedic Surgery

A range of operative and non-operative treatment options are recommended based on injury and patient characteristics. In today's practice, methods for distal radius fracture fixation are based on either cast immobilization, percutaneous pinning, external fixation, internal fixation with plates, or combination treatments [9], while pelvic fractures are either managed non-operatively with protected mobilization or with internal and external fixation devices following reduction (realignment) of the fracture fragments [10,11,12]. Management for either injury is generally based on the fracture pattern, degree of displacement, other associated injuries, and the individual patient's needs and demands.

For distal radius fractures, other than casting, external fixation is considered the next least invasive procedure, which can be used to correct radial shortening and metaphyseal angulation, but may not always restore articular congruity in intra-articular fractures. For these situations a combination of open reduction and percutaneous pinning or internal fixation under fluoroscopic visualization is usually the favored option and in many cases offers more secure fixation [13, 14].

In complex intra-articular fractures, open reduction and internal fixation (ORIF) with metal implants (T-plates) on the surface of the distal radius allows better reduction of the fracture fragments and in many cases offers more secure fixation. However, this treatment method demands more extensive surgical exposure and more aggressive use of retractors that can be dangerous for the skin and other soft tissues which may devascularize the fracture fragments. This may contribute to necrosis caused by trauma and, consequently, increase the risk of delayed healing and infection. Hardware problems may also require removal of the implant. Furthermore, due to the difficulties encountered during the fixation of the fracture the distal bone fragment may fail to realign to its proper anatomical position during healing which can lead to pain and reduced range of motion in the wrist and accelerated wear which may warrant another surgery for deformity correction. The list of complications in malunited distal radius fractures is extensive and includes limitation of wrist mobility due to joint incongruencies, loss of radial length leading to impingement or subluxation of the distal radial joint, all causing a painful wrist, reduced grip strength, problems with the median nerve and, in later stages, carpal instability and secondary arthritic changes [15]. The treatment goals have therefore aimed at improving the radiographic alignment of fragments using the least invasive approach which will achieve this.

Similar treatment options, ranging from external fixation methods to open reduction and stabilization, are also available for pelvic ring fractures [10, 11, 12]. External fixation devices cannot restore enough stability in the unstable complex fractures to allow mobilization of the patient without risk of redisplacement of the pelvis, which may lead to suboptimal functional results. In such cases, additional reduction manoeuvres are carried out, followed by internal fixation. The goal of the surgical treatment is to maintain anatomical shape of the pelvis and to reduce the fragments within 5-10mm of their normal location to maximize function.

Complications after operatively treated pelvic fractures include loss of the reduction; wound infection, neurological and/or vascular injuries, pain syndromes and leg length discrepancies which may result in permanent disability [10]. Of these, some may be related to inability to reduce the pelvis to an acceptable position or may be related to improper placement of implants.

1.3 Current Challenges in Orthopaedic Surgery

1.3.1 Imaging and Visualization

Imaging is one of the main components of all fracture treatments. The most commonly used medical imaging modalities in orthopaedic surgery are preoperative X-ray or computed tomography (CT) and intra-operative fluoroscopy (Fig.1.1) for guidance during the surgery. Although these imaging modalities provide high quality visualization of bones, they nevertheless pose several challenges.

Because traditional fluoroscopic images provide two dimensional (2D) representations of a 3D structure, scans from different directions must be obtained in order to visualize the anatomical region being operated on. A lot of skill is required to visualize 3D anatomy based on information obtained from

2D scans and to properly perform the necessary surgical action accordingly. The surgeon must position the implant in one view, and then obtain additional images in other planes using trial and error placements of guide wires or screws. In order to determine the drill trajectory of K-wires, commonly used for fixation during distal radius fracture surgeries as a provisional fixation step prior to plating or as definitive fixation, different 2D fluoroscopy images are taken. The same procedure is also used for screw fixation for T-plates and for assessing the proximity of the plate to the articular joint surface.

The quality of the reduction of distal radius fractures also depends on the restoration of anatomical parameters. Visually investigating 2D fluoroscopic images intraoperatively may not be enough to assess anatomic reduction, especially for determining articular step off, which is one of the major determinants of the functional outcome in distal radius fractures. In a recent study, the in-vivo accuracy of fluoroscopy and plain radiographs (X-ray) in measuring the articular step off was investigated. The results showed that none of these imaging modalities allowed for consistent measurement of anatomic reduction [16].

Recently introduced 3D fluoroscopy units [17, 18, 19] provide 3D information about the anatomical area but are almost twice as expensive as conventional 2D fluoroscopy. Also in extremely obese individuals, image quality can be suboptimal for navigation. Furthermore the accuracy of 3D fluoroscopy depends on the rigid relationship between the reference arc and the navigated anatomy. Current radiopaque retractors must be removed before the image acquisition. Re-placing the retractor could affect the accuracy of the navigation system [20].

CT imaging on the other hand provides 3D information about the anatomical area with very good resolution but is limited to imaging before and after the surgical procedure. The preoperatively obtained 3D scans can not be updated in the operating room (OR) after reduction is achieved and it is not possible to use this imaging modality in real time.

(a)

(b)

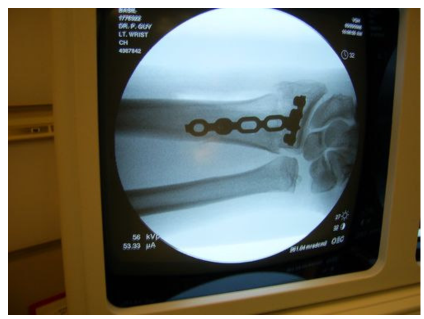

(c)

Fig.1.1 (a) Intra-operative 2D Mini-C arm (fluoroscopy), (b) 2D fluoroscopy scan showing the fractured distal radius and inserted K-wire, (c) 2D fluoroscopy scan showing the fractured distal radius and metal T-plate used during the surgery. The images are taken during a distal radius surgery at Vancouver General Hospital (VGH), Vancouver, BC, Canada.

1.3.2 Navigation and Guidance

Positioning of surgical tools or implants relative to bones, moving a drill guide sleeve or a cutting jig, drilling K-wires, and T-plate screw fixation are mainly based on the surgeon's knowledge about the target anatomy and experience obtained from performing various surgeries. Surgeons typically localize their targets by placing a radiologically opaque instrument near the region of interest. From this view, the surgeon visually estimates the location of the target structure and plans the trajectory. Throughout the surgery the accuracy of the trajectory estimate is controlled with additional fluoroscopic images. Operation time, quality and accuracy of the surgical procedure and reproducibility of the surgical actions therefore largely depend on information obtained from 2D fluoroscopy images and the experience of the surgeon.

1.3.3 Safety and Accuracy

The pre and intraoperative imaging modalities currently employed in orthopaedic surgeries require the use of X-rays therefore exposing the surgical team and patients to potentially harmful ionizing radiation. It is reported that more than 15 million skeletal studies are performed yearly in the United States using radiography [21]. A recent study investigating the exposure of the orthopaedic surgeon's hands to radiation during the surgery found an exposure of 20mrem/case which is reported to be 187 times greater than the amount predicted by the manufacturer [21] (mrem represents the unit in radiation dose). For comparison, a chest x-ray exposes the patient to about 20mrem. The surgeries included in this study were treatments for distal radius fractures and malunions, scaphoid nonunion, small joint fusion, perilunate dislocation, and metacarpaophalangeal joint arthoplasty. Both the National Council on Radiation Protection and the International Commission of Radiological Protection recommend a maximum exposure of the hands of 50000mrem, which allows up to 2500 cases per year. Though 20mrem/case is below this limit, however, receiving nearly the equivalent of a chest X-ray per case indicates special care must be taken especially if we think the amount of surgeries a surgeon has to perform. It is reasonable to keep the radiation exposure as low as possible, regardless of safety regulations.

Since images used for guidance and fracture reduction assessment are 2D, the number of fluoroscopy images taken during the surgery increases depending on the experience of the surgeon. In a recent study, Blattert et al. [22] formed two teams according to their professional qualification and clinical appointment in order to determine whether skill dependence affects the amount of radiation exposure to orthopaedic surgeons. The study showed that the mean time of fluoroscopy per operation was higher for the team which had less experienced surgeons.

Misdiagnosis of a fracture is a very common occurrence in ED and can have serious consequences because of delays in treatment and resulting long term disability [23]. In a study which was made in order to find out the diagnostic errors in emergency departments it has been shown that fractures were the leading types among the other diagnostic errors with 19% [24]. Guly et al. [25] reported that the primary reason for diagnostic error was due to abnormalities missed on radiographs with a rate of 77.8%.

Another important issue to mention is the overload of imaging studies requested from the ED to the radiology department (RD). In a recent study Blane et al. [26] reported that 72,886 imaging studies were requested from the ED to the RD in a year period. 65,7% of these studies were plain radiographs and 21.4% CT. These numbers show that the volume of imaging studies requested through the ED is significant. With the increasing importance of imaging for both diagnosis and management in patient care in ED there is a need for quick, accurate, and easy to use imaging modality for preoperative fracture assessment which will decrease both the overload and amount of plain radiographs to the RD.

Due to the many problems associated with fracture reduction treatments, there is an immediate need for improved safe, accurate and efficient CAOS systems that can potentially reduce surgical complications, improve the quality of the surgical outcome, decrease the time spent in the operating room (OR), and produce less invasive new treatment options.

1.4 Computer Assisted Orthopaedic Surgery (CAOS) Systems

The importance and demand for precise, efficient and minimally invasive surgery is driving the search for new ways to integrate computer systems into surgical procedures. Higher accuracy in surgical interventions, less invasive operation, better planning and simulation, and reduction of radiation exposure to both patient and surgeon are some of the potential advantages of such systems. Computer assisted surgery (CAS) systems were first introduced to locate brain tumors based on stereotactic principles [27]. Following that, the CAS field started to grow in different subspecialties with CAOS being one of them. Due to the rigid structure of bone, orthopaedic surgeries are particularly suitable for CAS systems [28, 29].

The first application of CAS in orthopaedics was developed for the spinal surgical procedure of placing pedicle screws [30]. That paper described an in-vitro setup for drilling pedicle holes in lumbar vertebrae. Since then, many authors have reported clinical series on computer assisted pedicle screw insertion [31, 32, 33]. The good results obtained in computer assisted pedicle screw placement opened new opportunities for CAS in other fields of orthopaedic surgery such as total hip replacement (THR) [34, 35], total knee replacement (TKR) [36, 37], intramedullary nail locking [38], tibial [39], femoral and pelvic [40, 41, 42], and distal radius [15] osteotomies.

Navigation is one of the main components of a CAS system. It is required in order to visualize surgical actions performed with different instruments and provide positional information about these surgical tools or implants relative to the target organ on a computer screen in real time. Navigation can be divided into three major components:

The ***target*** represents the anatomical location in the body where the surgical action is performed. In orthopaedic surgery target object are bones or bone fragments.

The ***virtual target*** is a virtual representation of the target object obtained from preoperative CT or MRI scans. It allows the surgeon to plan the intervention before the surgery without visual contact with the target object.

The ***real-time tracker*** is used to provide real-time guidance during the surgery. In order to achieve this position of surgical tools, bone fragments and the patient must be simultaneously tracked in the OR. Typically a specially constructed tracking device is attached rigidly to each surgical object the bone fragments and the patient and tracked by the real-time tracker. The two most commonly used real-time tracking devices in CAOS are optical tracking systems and magnetic tracking systems. In optical systems position information is acquired using charged couple device (CCD) cameras in order to detect infrared lights. The infrared lights are created from infrared light emitting diodes (IRLEDs) or passive markers such as retro-reflective spheres or disks. Shields with at least two but usually four or six IRLEDs/passive markers are attached to the instruments and the operated bone (Fig. 1.2). To allow freedom of movement of the operation field during surgery, the position of the target bone also has to be tracked. Therefore, a frame with IRLEDs or passive markers is attached to the skeleton, the so-called dynamic reference frame (DRF). Measurements by optical sensors are highly accurate and fast; and many IRLEDs can be tracked simultaneously, although an uninterrupted line of sight must be maintained between the CCD camera and DRF and tracked objects. On the other hand in a magnetic tracking system instead of the infrared light a magnetic field is detected created by a transmitter. There is no line of sight problem with magnetic tracking systems. However, there are concerns about their accuracy, which may be disturbed by the motor of the OR table or metallic tools.

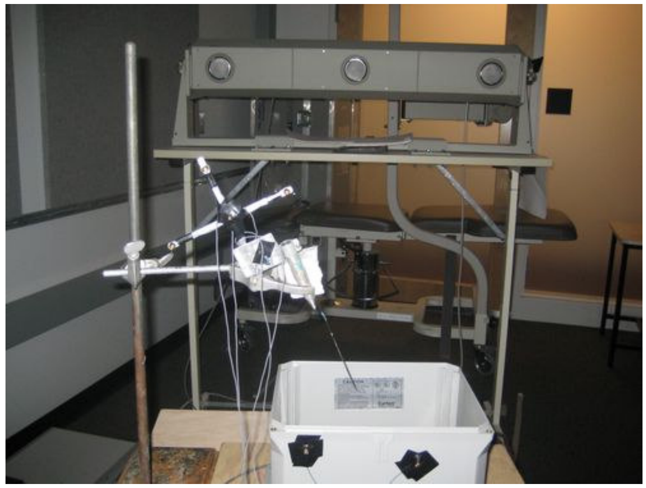

(a)

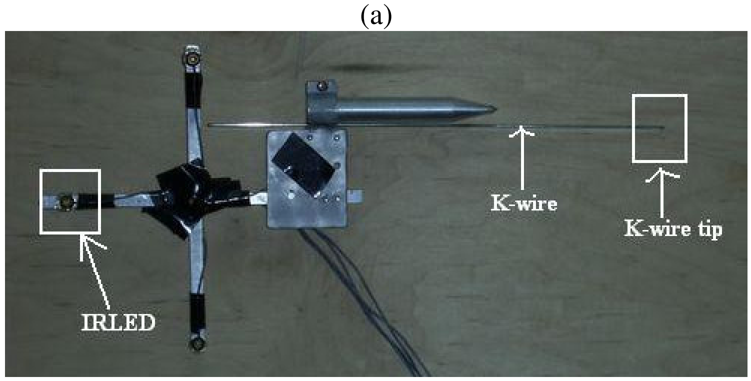

(b)

Fig.1.2 (a) An experimental system constructed with OPTOTRAK tracking system with three CCD cameras. (b) K-wire with infrared light emitting diodes attached.

A relationship between the target (current patient anatomy in the operating field) and the virtual target (patient anatomy obtained from preoperative scans) is obtained through a procedure known as registration. During the registration a set of intra-operatively obtained scans together with their corresponding position information are obtained. These intra-operative images are than mapped to the preoperative scans by using a 3D transformation matrix which is calculated during the registration procedure. There are three main types of registration techniques used in CAOS system:

Fiducial based registration: In this method, corresponding anatomical landmarks, also known as fiducial markers, are identified in both reference and target images and registered. In CAOS systems, fiducial markers are implanted on the bone surface and are identified from preoperative CT volumes. These identified landmarks are then registered to intraoperative fluoroscopy scans. Fiducial marker registration methods are usually used as a gold standard registration method in order to evaluate accuracy of other registration methods [43, 44]. The major disadvantage of this approach is the high invasiveness and the increase in operation time. During the placement of markers, there also are risks of infection, damage to soft tissue, and extra pain to the patient.

Intensity based registration: This method uses intensities in the two images without the need for segmenting or extracting geometric features. If the registration involves two images from same modality this is called intra-modality registration, if different modalities are used than this is called inter-modality registration. In orthopaedic applications this kind of registration is used for preoperative CT to intraoperative fluoroscopy registration [45, 46, 47, 48].

Feature based registration: This is a shape based or surface based registration algorithm and has been used in many applications [49, 50, 51, 52, 53, 54, 55, 56]. In this method, anatomical structures such as bone surfaces are extracted from preoperative and intraoperative scans. To identify and extract bone surfaces from these images segmentation algorithms need to also be developed. After segmenting the surfaces automatically or manually, rigid body registration is applied in order to match the surfaces using methods like Iterative Closest Point (ICP) [57] or recently introduces Unscented Kalman Filter (UKF) [58]. The accuracy of the surface based registration depends on the accuracy of generating 3D surface models from preoperative CT volumes and the quality and quantity of intraoperative data sampling.

Based on the imaging modality used and principles to provide navigation, CAOS systems can be divided into two main parts: one that makes use of intraoperative fluoroscopy, and another that uses volumetric images such as magnetic resonance imaging (MRI) or CT.

1.4.1 Fluoroscopy Based CAOS Systems

Fluoroscopic navigation is less expensive than volumetric image based navigation. In these systems, a fluoroscopy device, also called a C-arm or mini C-arm based on it's size, is used intraoperatively for guidance in the OR [45, 46, 47, 59] (Fig. 1.3) . To determine the position of the images relative to the patient, position tracking devices are attached to the C-arm device and the target bones. This facilitates superimposing tracked surgical tools in the images without the need for registration. This approach has gained some popularity as it is based on imaging technology familiar to all orthopaedic surgeons, and has the advantage that images are acquired during surgery, which allows the pose of instruments and prosthetic components to be assessed directly as the surgery progresses. Furthermore, since the first several images are used repeatedly to guide operative procedures it reduces the imaging time and radiation dosage. However, in practice, there is a significant degree of uncertainty in determining the pose of 3D objects from 2D projection images, and under some circumstances this can lead to inaccurate navigation. Finally, there is still a substantial amount of exposure to radiation.

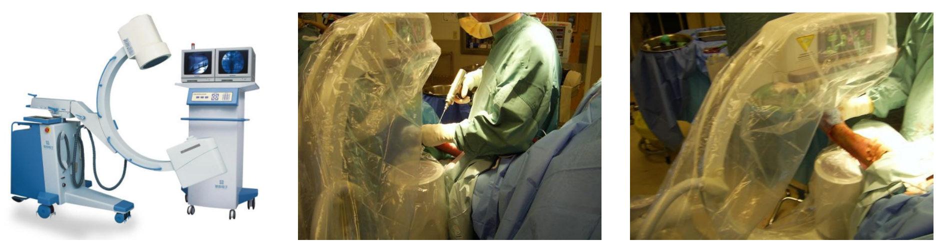

(a) (b) (c)

Fig.1.3 (a) Intra-operative 2D fluoroscopy, (b) and (c) 2D fluoroscopy is used during a distal-radius fracture surgery. (Images courtesy of Vancouver General Hospital, Vancouver, Canada)

1.4.2 Volumetric Image Based CAOS Systems

Recent state of the art CAOS systems are based on volumetric image guided techniques which use CT or MRI imaging modalities. Because of its high resolution, high contrast between the bone and its surrounding soft tissues, long scanning range, and short scanning time, CT is the preferred modality in CAOS. The latest research based in this area involves high tibial osteotomy [39], distal radius osteotomy [15], spine pedicle screw insertion [32, 33], total hip arthoplast [34, 35], and total knee arthoplast [35, 36, 37, 38].

Usually in such systems, a preoperative plan is developed based on CT scans. This is achieved based on one of two methods. The first method is multi image slice based where the patient’s anatomy is displayed in three orthogonal slices and the position and orientation of implants and surgical tools are superimposed onto these views. The other method is volume rendering or surface modeling based where the 3D surface of the anatomy is reconstructed using state of the art segmentation algorithms. This pre-operative plan is then registered with intra-operative scans obtained from the patient during the surgery.

Several research groups who proposed volumetric CAOS systems that used 2D fluoroscopy as the intra-operative imaging modality and showed promising improvements in overall surgical accuracy, decreased invasiveness of the surgeries. Furthermore, a decrease in the total amount of radiation exposure was also reported [60, 61, 62, 63]. However, these techniques still involve the use of ionizing radiation during surgery and require a CT scan which may not always be acquired in conjunction with a conventional procedure.

In order to address some of these issues, a recent approach proposed the use of statistical shape models built from CT scans of a patient population and registered using intraoperatively-obtained patient-specific geometric data [64]. The geometric data is acquired by digitizing the surgically exposed bone surface using a tracked pointer. Though promising, this technique requires prior models for each fragment of interest; given the high variability of fracture patterns, it is difficult to produce a library which describes the range of possible fragments.

Recently, 3D fluoroscopy (e.g. Siemens Siremobil ISO-C 3D) has been introduced for intra-operative use [17, 18, 19]. However, 3D fluoroscopy machines are currently approximately twice as expensive as conventional 2D fluoroscopy machines and are used by relatively few hospitals. Radiopaque surgical instruments such as retractors can interfere with the registration process linking the 3D image and the bone fragments, which can complicate the process and affect registration accuracy [20]. Finally, this technique still involves radiation exposure to the patient and surgical team.

1.4.3 Ultrasound Based CAOS Systems

Ultrasound has traditionally been used to image the body's soft tissue, organs, and blood flow in real time. Since there is no clinically reported risk of using US, it is still regarded the only safe method to image a fetus. Consequently, in order to eliminate the substantial exposure of ionizing radiation to both the surgical teams and patients, which is inherent to fluoroscopic imaging, special attention has been recently given to incorporating US imaging instead of fluoroscopy [49, 53, 65-70]. Though preoperative MRI and CT scans still remain a valuable source of information for surgeons in planning the intervention, US features such as real time operation, lack of radiation, and low cost make it a very suitable modality for intraoperative imaging. Many of the reported results showed promising improvements in overall surgical accuracy, decreased invasiveness of the surgeries and a decrease in the overall radiation exposure time [66, 68].

In order to enable more efficient image guidance the registration of the pre-operative volume to the intra-operative US data must be achieved, automatically, and rapidly with sufficient accuracy. Consequently a lot of attention was given to develop automatic US registration methods.

1.5 Ultrasound Image Registration

Previous research on registering intra-operative US to preoperative CT images in orthopaedic surgery involved registration of vertebrae [65, 67, 76], pelvis [49, 53, 66, 67, 77, 78] long bones [79, 80], scaphoid [68], and shoulder [81].

Since the first introduction of computer assisted surgery (CAS) [27] a number of registration methods have been developed by different research groups. Normalized cross correlation (NCC) [53], iterative closest point (ICP) [49, 78, 81], unscented kalman filtering (UKF) [58] based algorithms are largely dominant in CAOS applications and have shown promising results.

However, most state of the art registration methods require either manual interaction from the user or are not robust enough to the typical US artifacts, such as speckles and shadows. Furthermore, one of the major stumbling blocks facing all of the proposed registration methods is the requirement of an optimization procedure during the registration which is time consuming and not robust enough if the misalignment between the two registered data sets is large.

1.6 Bone Imaging With Ultrasound

US images are obtained by using a pulse-echo approach. This process is illustrated in Fig. 1.4 A small, spatially localized pulse of ultrasound is produced by a device called a *transducer* (positioned at the top of the US image shown as a sketch in Fig.1.4) and is transmitted into the patient. Ultrasound echoes directed back toward the transducer are produced as the pulse travels along a straight line through the tissues. The straight line is (shown as dotted red line in Fig. 1.4) is usually referred to as an US *scanline* or US *beam line*. The direction of ultrasound pulse propagation along the beam line is referred to as the *axial direction*, the direction in the image plane perpendicular to axial is called the *lateral direction*, and the direction perpendicular to the image plane is called *elevational direction.* Usually, only a very small fraction of the ultrasound pulse is reflected as an echo from any point in the patient, with the remainder of the pulse continuing along the beam line to greater tissue depths. As the pulse travels deeper into the body, in general there will be a long train of echoes reflected back towards the transducer and received by the imaging arrays (piezoelectric crystals), where they will be detected. The different reflectivities of various structures encountered by the pulse cause a corresponding variation of the detected echo amplitude. The detected echo signals are processed and translated into luminance, resulting in a “brightness- mode” or B-mode image display. In B-mode images, more reflective structures appear brighter than less reflective structures. A complete image is obtained by repeating this pulse-echo cycle for many coplanar scanlines. Pulses for successive scanlines are transmitted after all of the echoes from the previous scanline have been detected by the transducer. After all of the echoes from all of the scanlines have been detected and processed, these signals are mapped to the proper locations in the image pixel matrix, and the complete B-mode image is displayed. The location is determined by measuring the time the reflected echo is detected by the transducer.

A high intensity pixel in an US image indicates a strong likelihood of the presence of a boundary, such as soft tissue interface or bone. In order to use US imaging successfully in CAOS systems the bone boundaries must be localized with sufficient accuracy. The bone surface is highly specular, creating a very high intensity feature in the image followed by a shadow which is a black region followed right after the high intensity bone boundary. The shadow region is one of the typical US imaging artifacts and is caused due the strong reflection (high attenuation) of US pulses from strong reflectors (Fig. 1.4 (a)).

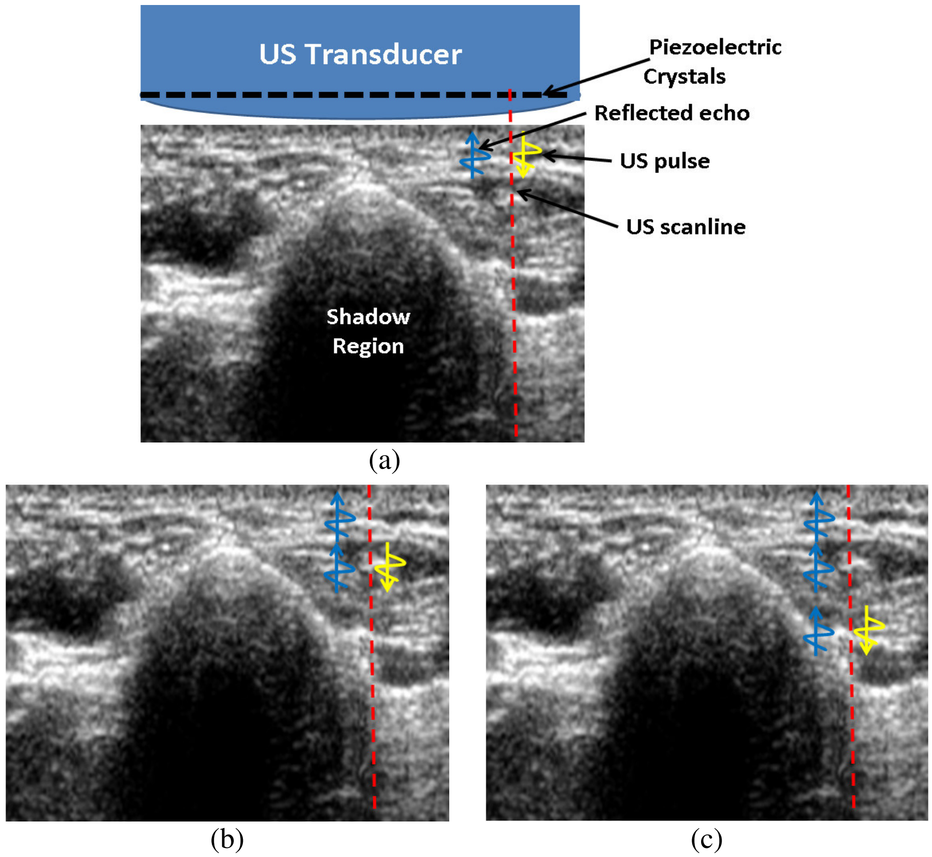

Fig.1.4 Sequence of images showing the propagation of an ultrasound pulse (yellow shape) along one particular scanline (dotted red line). Echoes (blue shapes) are generated by reflections of the pulse from structures in the tissue medium all along this path, and the echoes travel back to the transducer. The images are obtained by scaning an in-vivo human distal radius.

The high intensity feature depicting bone boundary response looks like a line with a shape closely resembling the surface. However the thickness of this line can reach a value of 4mm in certain cases. The actual location of the bone surface may merge within this response where the amount of migration is dependent on the local 3D geometry of the imaged bone surface. Each piezoelectric crystal will receive reflections from surfaces outside its direct line of sight and will record a thicker response along its own scanline. The greater the inclination of the imaged surface the greater is the response thickness. Furthermore, the finite beam width in the elevational direction produces a thick response when it is projected to a 2D plane (Fig. 1.5).

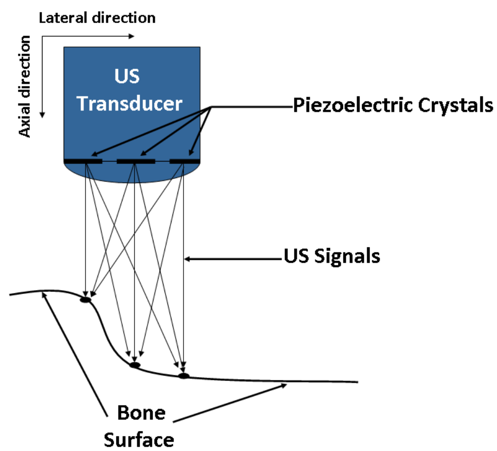

(a)

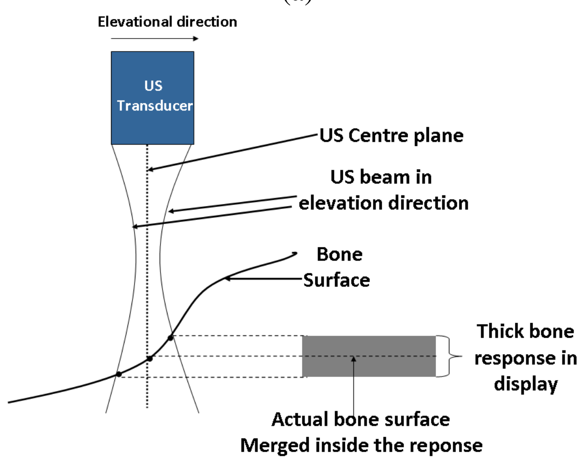

(b)

Fig.1.5 Bone surface response thickness in US images. (a) Affect of 3D geometry of the bone on the bone surface response where each imaging array receives reflections outside its direct line of sight and causes a thicker bone reponse, (b) elevational beam width artifact causes a thicker bone surface response where the actual surface is merged inside this response.

1.7 Bone Segmentation from Ultrasound

One of the most important tasks in analyzing US images is segmentation of the relevant anatomical structures. US image data, however, is typically characterized by high levels of speckle noise, reverberation, anisotropy and signal dropout which introduce significant difficulties in interpretation of captured data, automatic detection of image features and accurate localization of imaged bone surfaces [74]. In particular, the appearance of bone surfaces in US remains strongly influenced by beam direction and regions corresponding to bone boundaries appear blurry (Fig.1.6). Furthermore, since the final clinical application is orthopaedic surgery, the scanned bone surfaces may have discontinuities over fractured regions which affect many of the common segmentation algorithms that assume continuity. Due to these difficulties faced in extraction of the bone surfaces, in most of the recently proposed ultrasound guided CAOS systems, the main interest was in developing fast and accurate surface based registration methods in order to find a transformation between intraoperative US scans and preoperative CT volumes. In most of these studies the bone surfaces were segmented manually. Reports were given about the accuracy of the proposed registration method and little attention was given to the bone surface localization accuracy from US images.

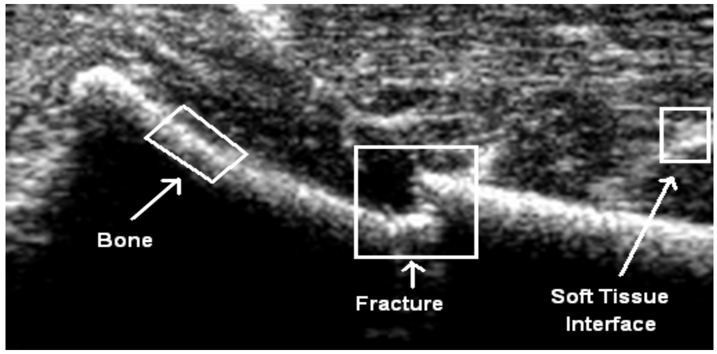

(a)

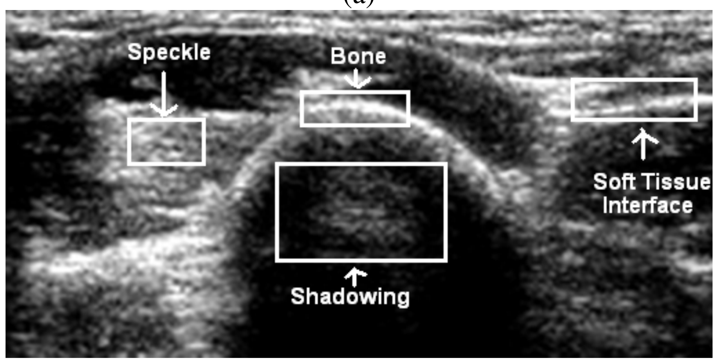

(b)

Fig.1.6 Examples of 2D US images acquired. (a) Phantom Sawbone with bovine soft tissue overlaid on top. (b) In-vivo distal radius. Regions within white rectangles highlight typical bone responses and common artefacts in bone US. Note the highly realistic nature of our phantom data in (a) and its close likeness to real in-vivo data in (b).

To successfully use US scans in image guided procedures the bone surface localization error should be within the allowable limits which also depends on the anatomical area being operated. This accuracy will also affect the registration error results; therefore special care must be given not only to registration but also to bone surface extraction from ultrasound.

US imaging has the potential of providing a powerful new tool for practical and real-time guidance during orthopaedic surgery as long as anatomical structures of interest can be visualized and localized with sufficient accuracy and efficiency.

Manual identification is still the most common way of identifying bone surface points from the US data [52, 66, 68]. Tonetti et al. [66] used manually digitized bone contour points from B-mode ultrasound images of a pelvis for the registration to a CT dataset. The clinical validation of the proposed method, which was percutaneous iliosacral screwing surgery, showed sufficient accuracy for the placement of screws. The study also confirmed that the amount of radiation exposure decreased compared to the standard fluoroscopy-based approach. In a different study on human cadavers, Barratt et al. [52], manually segmented the pelvis and femur bone surfaces from US data and registered them to the corresponding CT dataset. They reported an average RMS target registration error of 1.6mm. Beek et al. [68] used a maximum of 5 manually selected seed pixels from the US image of a scaphoid phantom bone to obtain a point cloud which is then used during the registration algorithm. The reported CT to US registration error was 0.54mm (max error: 0.68 mm; STD: 0.07 mm). Despite the accurate results obtained in these studies, a major drawback was the time needed for manual segmentation. The accuracy of the systems also depends on the operator performing the manual segmentation which may introduce significant inter- and intra-user variability [52, 68].

Several groups have explored ways to automate US image segmentation for various applications [82]. For bone segmentation traditional methods based on image intensity and local gradient information have been used [72, 67, 51]. Kowal et al. [67] used depth weighted thresholding followed by morphological operations and connected component labeling in his proposed framework. The algorithm was tested in porcine and bovine specimens. Mean accuracy of 0.42mm and a 0.8s average processing time for each ultrasound image frame was reported. Daanen et al. [72] proposed an automated segmentation method for delineation of the bone soft tissue interface from US images. The method was tested on three different cadavers and real patients. Results were compared with manual expert segmentation. For patients, the maximum mean error was 8.8 pixels, with a pixel size of 0.112mm $\times$0.109mm, while the minimum mean error was 4.545 pixels. For cadavers, the maximum mean error was 4.056 pixels and the minimum mean error was 2.679 pixels. The time to delineate one image was less than 4s and a dataset of 69 images took about 4 minutes. However, it remains difficult to manage the sensitivity of intensity and gradient-based techniques to US artifacts, machine settings and algorithm parameters. In particular, small scale variations resulting from speckle must be addressed explicitly to reduce the incidence of false bone edge detection. The dependence of the appearance of bone on the US beam direction and shadowing beneath the bone increases the number of false and missed edges.

In order to render the problem more tractable, some researchers have tried to incorporate *a priori* bone appearance information into their framework [72, 74, 83]. This was achieved by mathematically modeling bone surface regions. Combining such models with intensity and gradient information gave promising results. However, fractured bone surfaces in orthopaedic surgery applications, as well as reduced bones secured with internal fixation devices, do not have a continuous smooth surface and often significantly violate prior assumptions regarding bone shape. This is also an important drawback for methods which use active shape models in their framework [84]. Therefore, building reasonable models of all possible fracture scenarios into the system is not currently practical. Furthermore, the evolving contour will have difficulties near the fractured regions where it will start to 'leak' into the soft tissue regions.

Some groups have proposed methods combining segmentation techniques with multimodal registration of US to CT [49, 79, 85]. Amin et al. [49] combined three sources of information: the bone surface reflection indicated by image intensity, edge information obtained from the bone shadow region by using a directional edge detector, and a spatial prior obtained by processing a CT volume. Instead of segmenting the bone surface explicitly from the US image, these three sources of information were used to obtain a set of regions which are likely to contain bone surfaces. During the registration process, the regions were refined to select data that is most consistent with the 3D shape of the bone surface. The overall accuracy of the system is directly related to the accuracy of the initial registration estimate which will also depend on the experience of the surgeon and the imaged anatomical region. No accuracy results for the bone surface extraction were given; rather, registration error results were reported which were 1.94mm for average translation and 0.90 degrees for average rotation. Brendel et al. [79] first segmented 3D bone surfaces from the CT data set. Then, the part of the bone surface, which should be visible in the ultrasound data, is segmented considering the restrictions of bone imaging with ultrasound. The segmented bone surfaces were then registered to the US image using an average grey value sum. This sum should reach a maximum for a correct registration. Ionescu et al. [85] used a similar approach; the main difference was that the US images were segmented as well using classical image segmentation techniques based mainly on linear filtering or mathematical morphology. This segmentation is then updated using US-CT registration. The purpose of these studies was to overcome the limitations of US by fusing US with information from CT datasets where bone is more easily identified. However, in orthopaedic surgery, CT is not routinely used for many types of fractures, but is reserved for cases where the fracture is complex and the identification of the fractured parts has proven difficult with standard fluoroscopy. CT scanning of all fracture cases for the purpose of US segmentation would increase the associated costs and radiation exposure, which defeats one of the main advantages of employing US.

Due to these difficulties, US has only been used intra-operatively in CAOS as a surface digitization tool in order to obtain patient-specific data rather than as an imaging modality. The possibility of using 3D US as an alternative to fluoroscopy imaging for guiding basic surgical tasks and assessing fracture reduction in orthopaedic surgery has so far not been well studied. Furthermore, none of the previous studies presented a bone detection and localization framework for 3D US that is sufficiently accurate, robust and efficient for routine intraoperative use. This possibility is explored in this thesis.

1.8 Thesis Contributions

The thesis makes contributions both in the areas of image feature extraction from ultrasound data and in the areas of computer assisted orthopaedic surgery. The main contributions of this thesis are summarized as follows:

- We introduce an automatic, fast and accurate method for extracting bone surfaces from 2D US data. The method is based on the design and use of 2D Log-Gabor filter in order to construct a local phase symmetry measure that produces strong responses at bone surfaces and suppresses responses elsewhere.
- We extend our original local phase based image processing technique from 2D to 3D US using 3D Log-Gabor filters. Extending the 2D method to 3D enables the extraction of much smoother and continuous bone surfaces with increased localization accuracy. Furthermore, integrating the surface information along the axis perpendicular to the scan plane direction makes the proposed 3D algorithm less sensitive to soft tissue artifacts and more sensitive to weak bone surface responses.
- We analyze the ability of our proposed 2D/3D local phase based method to localize surgical tools from 2D/3D US scans. Using the proposed method we show that even relatively small surgical tools (less than 2 mm in diameter) can be localized with sub-millimeter resolution in a soft tissue model.
- We present extensive validation studies using carefully designed phantom, in-vitro and in-vivo experiments, and demonstrate the accuracy and robustness of our proposed approach for localizing fractured bone segments from 2D and 3D ultrasound data.
- We investigate the effects of Log-Gabor filter parameters on local phase-based feature extraction, specifically for bone surface

localization. Although local phase measures can be quite successful in extracting important image features, they remain somewhat sensitive to the underlying filter parameters used. Therefore, we present a novel method for contextual parameter selection that is adaptive to image content. Our technique automatically selects the scale, bandwidth and orientation parameters of Log-Gabor filters for optimizing the local phase symmetry in ultrasound images. The proposed approach incorporates principle curvature computed from the Hessian matrix and directional filter banks in a phase scale-space framework.

- We demonstrate the clinical feasibility and effectiveness of the proposed method with two clinical studies.

1.9 Thesis Overview

The remainder of this dissertation presents formulation and experimental validation studies for the proposed system. In addition to this introductory chapter, the thesis includes five chapters. The final chapter discusses the conclusions and directions for future work.

Chapter 2 presents the theoretical framework and formulation of the proposed 2D local phase based feature extraction method for segmenting bone surfaces from US data. It explains the experiments designed in laboratory conditions that are used in order to evaluate the performance of the proposed phase-based US data processing method and represents quantitative results. Finally, the ability of the proposed approach for segmenting surgical tools from 2D US data is also provided in this chapter together with the validation studies.

In chapter 3 we extend the proposed local phase based bone segmentation algorithm to 3D by constructing a 3D local phase symmetry metric. We validated the proposed 3D method by carefully designed experiments and show the improvement achieved in terms of bone surface localization accuracy. We report qualitative results obtained from in-vivo, in-vitro scans and show that more smooth and continues 3D bone surfaces could be extracted using the proposed method. Finally, we present surgical tool localization results using the proposed method.

Chapter 4 describes the proposed novel data driven parameterization method for phase based bone localization from US data using Log-Gabor filters. By automatically selecting the filter parameters we show that an improvement in terms of surface localization could be achieved. We also show that by correct filter parameter selection the proposed method becomes less sensitive to the typical US artifacts. We also compare the filter parameters obtained using the proposed method with the filter parameters obtained after an exhaustive search method.

Chapter 5 describes the three clinical pilot studies that have been conducted in order to demonstrate the feasibility of using 3D US imaging modality for assessing distal radius fractures in the ED.

Chapter 6 summarizes the contributions of this dissertation and presents promising directions for future applications in the concept of orthopaedic surgery. The particular surgical procedures that are likely to benefit from ultrasound based CAOS system are highlighted. Furthermore, the relative ease of achieving widespread utilization of US based fracture assessment is ER and orthopaedic surgery is outlined as well as the possible improvements for future generations of US imaging.

1.10 References

[1] National Center for Health Statistics, http://www.cdc.gov/nchs/, June, 2006.

[2] National Trauma Registry Bulletin , http://secure.cihi.ca/cihiweb/en/downloads/bl_ntraug2001_e.pdf 2001.

[3] D.P. Hanel, M.D.Jones, T.E. Trumble, "Wrist fractures", *Orthop Clin North Am*, vol. 33, no. 1, pp.35-57, 2002.

[4] R.Y. McMurtry, J.B. Jupiter, B.D. Browner, "Skeletal Trauma: Fractures, Dislocations, Ligamentous Injuries", 1997, pp. 1063-91.

[5] S. Batra, A. McMurtie, M. Batra, A. Gul, R. Kanvinde, "Distal radius fracture management in the emergency departments in UK: are we doing enough?", *International journal of Clinical Practice*, vol. 61, no. 7, pp.1131-6, 2007.

[6] M.W.T. Armander, K.J.H Newman, "Fractures of the distal radius", Surgery (Oxford), pp. 429-432, 2006.

[7] B. Petrisor, M. Bhandari, "(i) Injuries to the pelvic ring: Incidence, classification, associated injuries and mortality rates", *Current Orthopaedics*, Vol. 19, No. 5, pp. 327-333.

[8] L.P. Rice, M.Rudolph, "Pelvic Fractures", *Emergency Medicine Clinics of North America*, vol. 25, pp. 795-802, 2007.

[9] M.E. Muller, M. Allgower, R. Schneider, H. Willenegger, Manual of Internal Fixation, Springer-Verlag, 1991.

[10] E. Hirvensalo, J. Lindahl, V. Kiljunen, "Modified and new approaches for pelvic and acetabular surgery", Injury, vol. 38, no.4, pp. 431-441, 2007.

[11] T. Nunn, I. Pallister, "Fractures of the pelvic ring", *Surgery (Oxford)*, vol. 25, no.10, pp. 420-423, 2007.

[12] D.J.G. Stephen "Management of high-energy pelvic fractures", *Current Orthopaedics*, vol. 17, no.5, pp: 335-345, 2003.

[13] W. Geissler, D. Fernandez, "Percutaneous and limited open reduction of intra-articular distal radial fractures", *Journal Hand Surgery*, vol.5, pp. 85-92, 2000.

[14] R. Grewal, B. Perey, M. Wilmik, K. Stothers," A randomized prospective study on the treatment of intra-articular distal radius fractures: Open reduction and internal fixation with dorsal plating versus mini open reduction, percutaneous fixation, and external fixation", *Journal of Hand Surgery*, vol. 30A, pp 764-772, 2005.

[15] H. Croitoru, R.E. Ellis, C.F. Small, D.R. Pichora, "Fixation based surgery: A new technique for distal radius osteotomy", *Proc. of Medical Image Computing and Computer Assisted Intervention*, pp. 1126-1135, 2000.

[16] C.C. Edwards II, J.H. Christopher, G.R. McGillivary, A.P. Gutow, "Intra-articular distal radius fractures: arthroscopic assessment of radiographically assisted reduction", *The Journal of Hand Surgery*, vol. 26, no.6, pp.1036-1041, 2001.

[17] U. Stockle, B. König, A. Schäffler, T. Zschernack, N.P. Haas, "Clinical experience with the Siremobil Iso-C(3D) imaging system in pelvic surgery", *Unfallchirurg,* vol. 109, no.1, pp.30-40, 2006.

[18] U. Linsenmaier, C. Rock, E. Euler, S. Wirth, R. Brandl, D. Kotsianos, Mutschler W,Pfeifer KJ. "Three-dimensional CT with a modified C-arm image intensifier: feasibility", *Radiology*, vol. 224, no.1, pp. 286–292, 2002.

[19] L.P. Nolte, H. Walti, H. Fujita, G. Zheng, W. Seissler, J. Hey, "A novel mobile C-arm system for use in image-guided surgery – a feasibility study", *Proc. Computer Assisted Orthopaedic Surgery CAOS,* 2002.

[20] J.S. Hott, V.R. Deshmukh, J.D. Klopfenstein, V.K.H. Sonntag, C.A. Dickman, R.F. Spetzler, S.M. Papadopoulos, "Intraoperative Iso-C C-arm navigation in craniospinal surgery: the first 60 cases", *Neurosurgery*, vol. 54, no.5, pp.1131-7, 2004.

[21] D. Herscoici, R.W. Sanders, "The effects, risks, and guidelines for radiation use in orthopaedic surgery", *Clinical Orthopaedics and Related Research*, vol. 375, pp 126-132, 2000.

[22] G. Singer, "Radiation exposure to the hands from mini C-arm fluoroscopy", *The Journal of Hand Surgery*, vol 30, no.4, pp. 795-198, 2005.

[23] R.T. Blattert, U.A. Fill, E. Kunz, W. Panzer, A. Weckbach, F.R. Dieter, "Skill dependence of radiation exposure for orthopaedic surgeon during interlocking nailing of long bone shaft fractures: a clinical study", *Arch. Of Orthopaedic Trauma Surgery*, vol.124, no. 10, pp. 659-664, 2004.

[24] A. Kachalia, T.K. Gandhi, A.L. Puopolo, C. Yoon, E.J. Thomas, R. Griffey, T.A. Brennan, A.M. Studdert, " Missed and delayed diagnoses in the emergency department: a study of closed malpractice claims from 4 liability insurers", *Annals of Emergency Medicine*, vol. 92, no.2, pp.196-205, 2007.

[25] H.R. Guly, "Diagnostic errors in accident and emergency department", *Emergency Medicine Journal*, vol.18, no.4, pp. 263-269, 2001.

[26] C.E. Blane, J.S. Desmond, M.A. Helvie, B.J. Zink, J.E. Bailey, L.D. Yang, N.R. Dunnick, "Academic radiology and the emergency department: does it need changing?", Academic Radiology, vol.14, no.5 pp. 625-630, 2007.

[27] R.A. Bown, "A computerized tomography- computer graphics approach to stereotaxic localization", *Journal of Neurosurgery*, vol. 50, no.6., pp.715-720, 1979.

[28] N. Sugano, "Computer assisted orthopaedic surgery", *Journal of Orthopaedic Science,* vol.8, no.3, pp.442-448, 2003.

[29] N.W.L. Shep, I.A.M.J. Broeders, "Computer assisted orthopaedic and trauma surgery: state of the art and future perspective", *Injury*, vol. 34, no.4, pp.299-306, 2003.

[30] L.P. Nolte, L.J. Zamorano, Z. Jiang, Q. Wang, F. Langlotz, U. Berlemann, ”Image-guided insertion of transpedicular screws. A laboratory set-up”, *Spine*, vol. 20, no.4, pp.497-500, 1995.

[31] T. Laine, D. Schlenzka, K. Makitalo, K. Tallroth, L.P. Nolte, H. Visarius, “Improved accuracy of pedicle screw insertion with computer-assisted surgery. A prospective clinical trial of 30 patients”, *Spine*, vol. 22, no.4, pp.1254-1258, 1997.

[32] P. Merloz, J. Tonetti, A. Eid, C. Faure, S. Lavallee, J. Troccaz, P. Sautot,A. Hamadeh, P. Cinquin,”Computer assisted spine surgery”, *Clinical Orthop.,* pp.86-96, 1997.

[33] P. Merloz, J. Tonetti, L. Pittet, M. Coulomb, S. Lavallee, P. Sautot, “Pedicle screw placement using image guided techniques”, *Clinical Orthop*., vol. 9, pp.39-48, 1998.

[34] B. Jaramaz B., A.M. DiGioia, M. Blackwell, C. Nikou, “Computer assisted measurement of cup placement in total hip replacement”, *Clinacal Orthop*., vol. 354, pp.70-81, 1998.

[35] A. M. DiGioia, B. Jaramaz, M. Blackwell, D.A. Simon, F. Morgan, J.E. Moody, C. Nikou, B.D. Colgan, C.A. Aston, R.S. Labarca, E. Kischell, T. Kanade , “Image guided navigation system to measure intraoperatively acetabular implant alignment”, *Clinical Orthop.,*vol.355, pp. 8-22, 1998.

[36] D. Saragaglia, F. Picard, C. Chaussard, E. Montbarbon, F. Leitner, P. Cinquin, “Computer assisted total knee arthroplasty: comparison with a conventional procedure. Results of a 50 cases prospective randomized study”, *Rev Chir Orthop Reparatrice Appar Mot,* vol. 87, no.1, pp.18-28, 2001.

[37] H. Kiefer, D. Langemeyer, U. Scherwitz, F. Krause, “Computer aided knee arthroplasty versus conventional technique- first results”, *Computer Assisted Orthopaedic Surgery (CAOS)*, 1th annual meeting, Davos,Switzerland. 2001.

[38] M.A. Slomczykowski, R. Hofstetter, M. Sati, C. Krettek, L.P. Nolte, “Novel computer-assisted fluoroscopy system for intraoperative guidance: feasibility study for distal locking of femoral nails”, *J. Orthop. Trauma*, vol. 15, no.2, pp. 122-131, 2001.

[39] R.E. Ellis, C.Y. Tso, J.F. Rudan, M.M. Harrison, “A surgical planning and guidance system for high tibial osteotomy”, *Computer Aided Surgery*, vol.4, no.5, pp.264-274, 1999.

[40] U. Langlotz, J. Lawrence, Q. Hu, M.E. Muller, “Computer assisted total hip replacement: preoperative planning and intraoperative execution”, *Computer Aided Surgery*, pp. 4:160, 1999.

[41] F. Langlotz, R. Bachler, U. Berlemann, L.P. Nolte, R. Ganz, “Computer assistance for pelvic osteotomies”, *Clinical Orthop.*, vol. 354, pp.92-102, 1998.

[42] F. Langlotz, M. Stucki, R. Bachler, C. Scheer, R. Ganz, U. Berlemann, L.P. Nolte L,”The first twelve cases of computer assisted periacetabular osteotomy”, *Computer Aided Surgery*, vol.2, no. 6, pp.317-326, 1997.

[43] R.E. Ellis, M. Marcacci M., D. Caramella, M. Fadda, “Use of a biocompatible fiducial marker in evaluating the accuracy of CT image registration”, *Investigate Radiology*, vol. 31, no.10, pp.658-667, 1996.

[44] T.S.Y. Tang, R.E. Ellis, G. Fichtinger, “Fiducial registration from a single x-ray ray image: A new technique for fluoroscopy guidance and radiotherapy”, *Proc Int. Conf. Med. Image Compt. Computer- Assisted Intervention*, pp. 502-511, 2000.

[45] J. Knaan, L. Joskowicz, “Effective intensity based 2D/3D rigid registration between fluoroscopy x-ray and CT”, *Proc Int. Conf. Med. Image Compt. Computer- Assisted Intervention*, pp. 351-358, 2003.

[46] G.P. Penney, H.D.L. Batchelor, D.J. Hawkes, J. Weese, “Validation of two to three dimensional registration algorithm for aligning preoperative CT images to intraoperative fluoroscopy images”, *Medical Physics*, vol.28, no.6, 1024-1032, 2001.

[47] Gong R.H., Stewart A.J., Abolmaesumi P., “A new mthod for CT to fluoroscope registration based on unscented kalman filtering”, *Proc Int. Conf. Med. Image Compt. Computer- Assisted Intervention*, pp. 891-898, 2006.

[48] Weese J. Penney G.P., Desmedt P., “Voxel based 2D 3D registration of fluoroscopy images and CT scans for image guided surgery”, IEEE Transaction on Information Technology in Biomedicine, pp 284-293, 1997.

[49] D.V. Amin, T. Kanade, A.M. DiGioia, B. Jaramaz, “Ultrasound registration of bone surface for surgical navigation”, *Computer Aided Surgery*, vol.8, no.1,pp.1-16, 2001.

[50] J.L. Herring, B.M. Dawant, C.R. Maurer, “Surface based registration of CT images to physical space for image guided surgery of the spine: a sensitivity study”, *IEEE Transactions on Medical Imaging*, vol. 15, no. 23, pp.743-752, 2002.

[51] A. Kryvanos, Computer assisted surgery for fracture reduction and deformity correction of the pelvis and long bones, PhD thesis, University of Manheim, Germany, 2002.

[52] D.C. Barratt, P.G. Penney, S.K. Chan, M. Slomczykowski, T.J. Carter, P.J. Edwards, D.J. Hawkes, “Self calibrating 3D-ultrasound-based bone registration for minimally invasive orthopaedic surgery”, *IEEE Transactions on Medical Imaging*, vol. 25, no. 3, 2006.

[53] G.P. Penney, D.C. Barratt, C.S.K. Chan, M. Slomczykowski, T.J. Carter, P.J. Edwards, D.J. Hawkes, “Cadaver validation of intensity-based ultrasound to CT registration ” , *Medical Image Analysis*, vol.10, no. 3, June 2006.

[54] D.M. Muratore, Towards an image guided spinal surgical system using three dimensional ultrasound: from concept to clinic, PhD thesis, Vanderbilt University, USA, 2002.

[55] L. Carrat, J. Tonetti, S. Lavallee, “Percutaneous computer assisted iliosacral screwing”, *Proc Int. Conf. Med. Image Compt. Computer-Assisted Intervention*, pp.84-91, 1998.

[56] L. Carrat, J. Tonetti, P. Merloz, “Percutaneous computer assisted iliosacral screwing: Clinical validation”, *Proc. Medical Image Computing and Computer Assisted Intervention Conference*, pp.1229-1237, 2000.

[57] P. Besel and N. Mckay: “A method for registration of 3D-shapes”. *IEEE Transactions on Pattern analysis and Machine intelligence*, vol. 14, no.2, pp.239-256, 1992.

[58] M.H. Moghari, P. Abolmaesumi, "Point-based rigid-body registration using an unscented Kalman filter", *IEEE Transactions on Medical Imaging,* Vol. 10, No. 12, pp. 1708-1728, 2007.

[59] P.A. Grutzner, G. Zheng, U. Langlotz, J. von Recum, L.P. Nolte, A. Wentzensen, K.H. Widmer, K. Wendl, “C-arm based navigation in total hip arthroplasty-background and clinical experience”, *Injury*, vol. 35, no.1, pp. 90-95, 2004.

[60] A. Hamadeh, S. Lavallee , P. Cinquin, “Automated 3-dimensional computer tomographic and fluoroscopic image registration”, Journal of Computer Aided Surgery, vol 3(1), pp.11-19, 1998.

[61] L. Joskowicz, C. Milgrom, A. Simkin, L. Tockus, Z. Yaniv, “FRACAS: A system for computer aided image guided long bone fracture surgery”, Journal of Computer Aided Surgery, vol 3, pp. 271-288, 1998.

[62] J. Wesse, G.P. Penney, P. Desmedt, T.M. Buzug, D.L. Hill, D.J. Hawkes, “Voxel based 2D/3D registration of fluoroscopy images and CT scans for image guided surgery”, IEEE Trans on Information Technology Biomedicine, vol. 1, no. 4, pp. 284-293, 1997.

[63] G. Zheng, M.A. Ballester, M. Styner, L.P. Nolte, “Reconstruction of patient-specific 3D bone surface from 2D calibrated fluoroscopic images and point distribution model”, *Proc Int. Conf. Med. Image Compt. Computer- Assisted Intervention*, 2006, vol. LNCS 4190, pp. 25–32.

[64] K.T. Rajamani, M.A. Styner, H. Talib, G. Zheng, L.P. Nolte, G.M.A. Ballaster, "Statistical deformable bone models for robust 3D surface extrapolation from sparse data", Medical Image Analysis, vol 11, no.2, pp. 99-109, 2007.

[65] D.M. Muratore, J.H. Russ, B.M. Dawant, "Three dimensional image registration of phantom vertebrae for image guided surgery: A preliminary study", *Computer Aided Surgery*, pp.342-352, 2002.

[66] J. Tonetti, L. Carrat, S. Blendea, P. Merloz, J. Troccaz, S. Lavallee, J.P. Chirossel, " Clinical results of percutaneous pelvic surgery: Computer assisted surgery using ultrasound compared to standard fluoroscopy", *Computer Aided Surgery*, vol. 6, January 2001.

[67] J. Kowal, C. Amstutz, F. Langlotz, H. Talib, M.G. Ballester, "Automated bone contour detection in ultrasound B-mode images for minimally invasive registration in computer assisted surgery an *in vitro* evaluation", *The International Journal of Medical Robotics and Computer Assisted Surgery*, vol 3, pp. 341-348, 2007.

[68] M. Beek, M. Abolmaesumi, S. Luenam, R.E. Ellis, R.W. Sellens, D.R. Pichora, "Validation of a new surgical procedure for percutaneous scaphoid fixation using intra-operative ultrasound", Medical Image Analysis, vol 12, pp. 152-162, 2008.

[69] D.C. Barratt, C.S.K. Chan, P.J. Edwards, P.G. Penney, M. Slomczykowski, T.J. Carter, D.J. Hawkes, "Instantiation and registration of statistical shape models of the femur and pelvis using 3D ultrasound imaging", Medical Image Analysis, vol 12, pp.358-374, 2008.

[70] T. Chen, P. Abolmaesumi, D.R. Pichora, R.E. Ellis, "A system for ultrasound-guided computer-assisted orthopaedic surgery", *Computer Aided Surgery*, vol. 10, no. 5/6, pp. 281-292, 2005.

[71] H. Talib, K. Rajamani, J. Kowal, M. Styner, M.A.G. Ballester, "Assessing the feasibility of ultrasound initialized deformable bone models", Proc. of SPIE Medical Imaging, 2006.

[72] V. Daanen, J. Tonetti, J. Troccaz, “A fully automated method for the delineation of osseous interface in ultrasound images”, *Proc Int. Conf. Med. Image Compt. Computer- Assisted Intervention*, pp. 549-557, 2004.

[73] P. He , J. Zheng, “Segmentation of tibia bone in ultrasound images using active shape models”, Proc. of 23rd Annual conference- IEEE/EMBS, pp. 27112 -2715, 2001.

[74] A.K. Jain, R.H. Taylor, “Understanding bone responses in B-mode ultrasound images and automatic bone surface extraction using a bayesian probabilistic framework”, Proc. of SPIE Medical Imaging, pp. 131-142, 2004.

[75] J.G. Thomas, R.A. Peters, P. Jeanty, “Automatic segmentation of ultrasound images using morphological operators”, *IEEE Transactions on Medical Imaging,* vol. 10, vo.2, pp. 180-186, 1991.

[76] B. Brendel, S. Winter, A. Rick, M. Stockheim, H. Ermert, “Registration of 3D CT and ultrasound datasets of the spine using bone structures”, *Computer Aided Surgery*, vol7, July, 2002.

[77] D.C. Barratt, C.S.K. Chan, P.J. Edwards, G.P. Penney, G.P, Slomczykowski, M., Carter, T.J., Hawkes, D.J. Instantiation and Registration of Statistical Shape Models of the Femur and Pelvis using 3D Ultrasound Imaging. Med Image Anal 2008; 12: 358-374.

[78] P. Foroughi, D. Song, G. Chintalapani, R.H. Taylor, G. Fichtinger, "Localization of Pelvic Anatomical Coordinate System Using US/Atlas Registration for Total Hip Replacement", *Proc Int. Conf. Med. Image Compt. Computer- Assisted Intervention*, 2008, pp. 871-879.

[79] B. Brendel, S. Winter, A. Rick, M. Stockheim, H. Ermert, ”Bone registration with 3D CT and ultrasound data sets”, *Computer Assisted Radiology and Surgery*, 2003, pp. 426–432.

[80] B. Jaramaz, C. Nikou, B. Cavalier, S. Blendea, R. Labarca, A. DiGioia III, “Experimental validation of ultrasound registration of long bones. *3rd*

Annual Meeting of the International Society for Computer Assisted Orthopaedic Surgery. 2003., pp. 160–161.

[81] K. Tyryshkin, P. Mousavi, M. Beek, R. Ellis, D. Pichora, P. Abolmaesumi, "A navigation system for shoulder arthroscopic surgery", *Journal of Engineering in Medicine; Special Issue on Navigation Systems in Computer-assisted Orthopaedic Surgery*, pp. 801-812, 2007.

[82] A.J. Noble, D. Boukerroui, "Ultrasound image segmentation: a survey", *IEEE Transactions on Medical Imaging*, vol. 25, no. 8, pp. 987-1010, August 2006.

[83] P. Foroughi, E. Bocto, M.J. Swatrz, R.H. Taylor, G. Fichtinger, "Ultrasound bone segmentation using dynamic programming", *Proc. of IEEE Ultrasonics Sy*posium, pp. 2523-2526, 2007.

[84] P. He, J. Zheng, "Segmentation of tibia bone in ultrasound images using active shape models", *Proc. of 23rd Annual conference- IEEE/EMBS*, vol.3, pp. 2712-2715, 2001.

[85] G. Ionescu, S. Lavallee, J. Demongeot, "Automated Registration of Ultrasound with CT Images: Application to Computer Assisted Prostate Radiotherapy and Orthopedics",. *Proc Int. Conf. Med. Image Compt. Computer- Assisted Intervention*, vol.1679, pp. 768-777, 1999.

Chapter 2

Bone Surface and Surgical Tool Localization in Ultrasound Using Image Phase Based Features*

2.1 Introduction

Image phase information is a key component in the interpretation of a scene that has been long known to contribute more to the visual appearance of an image than magnitude information [1]. The importance of phase information is shown in Fig. 2.1. If we take the Fourier transform of two US images of bone and use the phase information from one image and the magnitude information of the other image to construct a new, synthetic Fourier transform and back-transform it to produce a new image we can clearly see that the dominant

---

* A version of this chapter has been published. I. Hacihaliloglu, R. Abugharbieh, A. Hodgson, R. Rohling. "Bone Surface Localization in Ultrasound Using Image Phase Based Features", *Ultrasound in Medicine and Biology*, vol.35, no.9, pp. 1475-1487, 2009.

feature in the new constructed image corresponds to the one where the phase information was combined (Fig. 2.1).

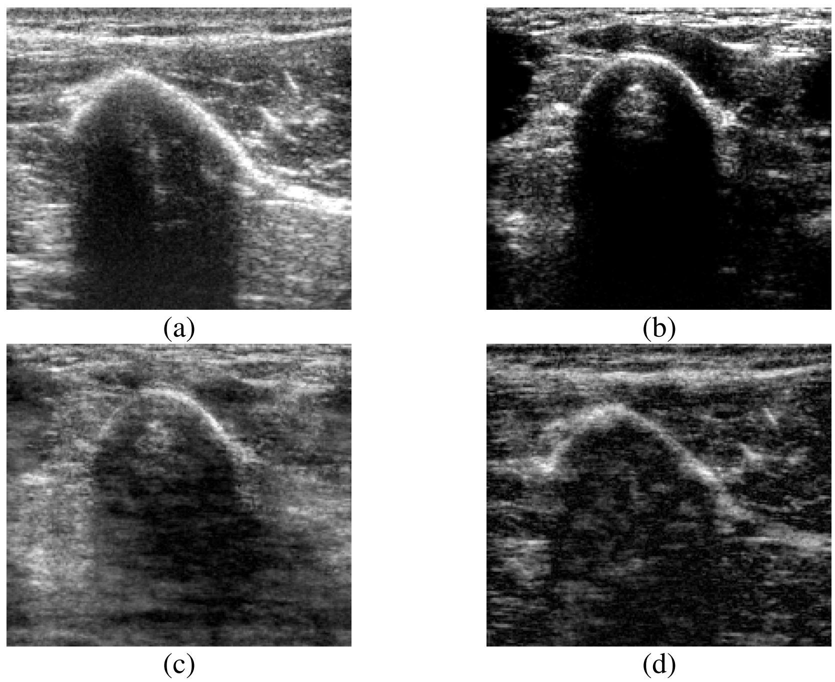

Fig.2.1 Importance of phase information. (a) In-vivo 2D B-mode US image of human distal radius, (b) different in-vivo 2D B-mode US image of human distal radius obtained by changing the US transducer position. (c) New image where the phase information was obtained from (b) and magnitude from (a), (d) new image where the phase information was obtained from (a) and magnitude from (b). Investigating (c) and (d) we can clearly see that the dominant feature corresponds to the image where the phase information was taken from.

In a seminal paper, Morone and Owens [2] proposed the use of a local energy model for phase-based feature detection where they argued that features are perceived at points in the signal where the Fourier components are maximally in phase, i.e., where phase congruency (PC) is maximal. Since then, phase information has been widely investigated as a basis for feature extraction in various medical image data such as feature extraction in magnetic resonance (MR) images [3], airway wall estimation from CT images [4], as an additional feature for guidance for livewire segmentation [5], and various combinations of registration: CT-fluoroscopy, MR T1-MR T2, and MR-CT [6, 7, 8]. In these applications, conventional approaches based on intensity thresholding or gradient-based edge detection were shown to pose problems due to non-uniform intensity variations across the images and smooth tissue transitions due to partial volume effects. Since image phase features are intensity invariant, phase-based techniques were found to be more robust than conventional intensity and gradient-based techniques.

Recently it has been used successfully for processing US images of various soft tissues. It has provided promising results in applications such as MR-US registration of brain [8], ultrasound compounding for echocardiography image enhancement [9], endocardial border detection and image enhancement in 3D echocardiography [10, 11, 12, 13]. However, to the best of our knowledge, phase-based image features have never before been applied to bone US nor was directed at assessing bone fractures.

2.1.1 Main Contributions

Main contributions of this chapter are:

1. We propose and evaluate the novel use of phase symmetry features derived from US images using 2D Log-Gabor filters for automatic segmentation of bone surfaces. We show that the proposed local phase method mostly captured continuous sections of the bone with little influence exhibited by soft-tissue interfaces.
2. We propose that local phase features provide accurate localization of fractured bone fragments from US data. For the first time we show that fractures could be identified from US imaging data using local phase information.
3. We present extensive validation studies using carefully designed phantom, in-vitro and in-vivo experiments, and demonstrate the

accuracy and robustness of the proposed approach in localizing bone surfaces from US data.

4. We propose that surgical tools such as K-wires, which are commonly used for fixation during fracture surgeries as a provisional fixation step prior to plating or as definitive fixation, could be extracted from US images successfully using the proposed local phase based symmetry features.

The remainder of this chapter is organized as follows. In section 2.2 we describe local phase features and how they are extracted for 1D signals. Section 2.3 presents the proposed phase based bone surface extraction method. Furthermore, we explain the laboratory experiments that were constructed in order to validate the method together with the obtained results. We also illustrate qualitative results in this section. Section 2.4 shows the application of the proposed method in localizing surgical tools from US images. We finally draw our conclusion in section 2.5.

2.2 Local Phase Based Image Features

Local properties (Amplitude and Phase) of a 1D real signal $f(x)$ are defined using the so called analytical signal $f_A(x)$:

$$f_A(x) = f(x) + if_H(x) = f(x) * \delta(x) + f(x) * \frac{i}{\pi x} \tag{2.1}$$

where $f(x)$ is the original signal and $f_H(x)$ is its Hilbert transform of $f(x)$defined by:

$$f_H(x) = \frac{1}{\pi} \int_{-\infty}^{\infty} \frac{f(\tau)}{x-\tau} d\tau \tag{2.2}$$

In the frequency domain the Hilbert transform is defined as:

$$F_A(\omega) = F(\omega) + F(\omega) sign(\omega) \quad \text{where} \quad sign(\omega) = \begin{cases} 1 & if \quad \omega > 0 \\ 0 & if \quad \omega = 0 \\ -1 & if \quad \omega < 0 \end{cases} \tag{2.3}$$

Investigating these three equations we can see that the analytical signal suppresses the negative frequencies of the signal and multiplies all the positive frequencies by two. The analytic signal plays an important role in one-dimensional signal processing. One of the main reasons for this fact is, that the instantaneous amplitude (*A(x)*) and the instantaneous phase (*Φ(x)*) of a real signal *f(x)* at a certain position *x* can be defined as the magnitude and the angular argument of the complex-valued analytic signal f_A at the position *x* as:

$$A(x) = \sqrt{f^2(x) + f_H^2(x)} \qquad \phi(x) = \arctan(f(x) / f_H(x)) \tag{2.4}$$

From equations (2.1-2.3) we can see that the analytic signal is a global concept. The value of the signal at a position *x* depends on the whole original signal and not only on values at positions near *x*.

In most of the image processing applications local concepts are highly desirable. They are of lower computational complexity than global concepts. Furthermore, it is reasonable that the local signal structure, like local phase and local amplitude should only depend on local neighborhoods. Therefore, designing an operator that approximates these quantities in a small, spatial interval and over a narrow range of frequencies which will enhance spatial localization is of spatial interest. Filtering the input signal is one of the most used methods in order to achieve this localization. In order to be invariant to grey level shift the filter should have zero response for a constant signal. This is achieved by designing a filter which is a band-pass filter (zero DC) and symmetric with constant phase so as not to change the phase information of the original signal. The symmetry condition suggests that the filter must be an even filter. The new localized analytical signal will be obtained as:

$$\begin{aligned} \hat{f}_A(x) &= f(x) * f_e(x) + iH(f_e(x) * f(x)) \\ \hat{f}_A(x) &= \quad (f_e(x) + iH(f_e(x)) * f(x) \\ \hat{f}_A(x) &= \quad (f_e(x) + if_o(x)) * f(x)) \end{aligned} \tag{2.5}$$

Here H denotes the Hilbert transform operation and $f_o(x)$ is the Hilbert transform of $f_e(x)$, hence these two filters ($f_o(x)$, $f_e(x)$) are in quadrature. From this the local phase and amplitude of the signal c ould be defined as:

$$\begin{aligned} \hat{A}(x) &= \sqrt{[f_e(x) * f(x)]^2 + [f_o(x) * f(x)]^2} \\ \hat{\phi}(x) &= \arctan(f_o(x) * f(x) / f_e(x) * f(x)) \end{aligned} \tag{2.6}$$

The analytical signal and the corresponding quadrature filters provide a very effective framework for extracting local phase information of signals. The extension of this analysis to two dimensions is performed via the use of steerable filters or by performing the analysis at a set of orientations and, then combining the output to provide the localized phase information at any orientation in the image [11, 12, 13,14].

2.2.1 Quadrature Filters

In US image processing the two most widely used quadrature filters for obtaining localized phase information are the Monogenic filter (Riesz filter) and Log-Gabor filter [11, 12, 13]. In this thesis we choose to work with Log-Gabor filters since they offer orientation selectivity. When imaged with US bone features appear as long elongated line like structures with specific orientation. When the orientation of the Log-Gabor filter is tuned to the orientation of bone surfaces it allows extraction of localized bone features from the US images while suppressing the unnecessary soft tissue interfaces or typical US artifacts. On the other hand since the monogenic filter can not be tuned to specific orientations the filter is sensitive to soft tissue interfaces as well as bone boundaries (Fig. 2.2).

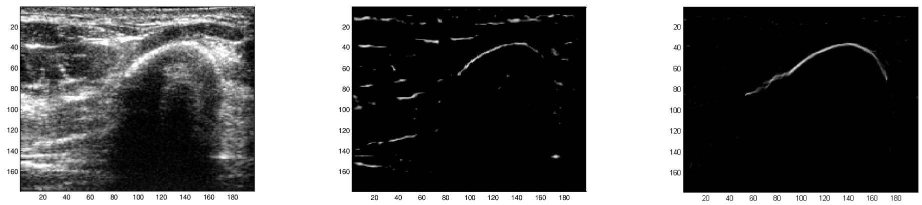

(a) (b) (c)

Fig.2.2 (a) B-mode US image, (b)local phase information extracted by processing the image shown in (a) using monogenic filter, (c) local phase information extracted by processing the image shown in (a) using 2D Log-Gabor filter.

Furthermore, Log-Gabor filters can be constructed with arbitrarily large bandwidths and still maintain a zero DC component which is of major importance for achieving intensity invariant local phase information. In US image processing large bandwidth filters are needed in order to differentiate soft tissue interface or speckle from bone surface response.

Log-Gabor filter [14, 15] is defined in the frequency domain as in (2.7) (note that equations for a one dimensional (1D) signal are shown for simplicity):

$$G(\omega) = \exp\left(-\frac{(\log(\omega/\omega_0))^2}{2(\log(\kappa/\omega_0))^2}\right) \tag{2.7}$$

Here κ is a scaling factor used to determine the bandwidth of the filter in the radial direction, and ω_0 is the filter's center spatial frequency. The ratio of these two variables is related to the filter's bandwidth *(β)* [17] as:

$$\beta = -\frac{2\sqrt{2}}{\sqrt{\ln 2}}\ln(\kappa/\omega_0) \tag{2.8}$$

Simultaneous localization of spatial and frequency signal information can hence be obtained by constructing a filter bank using a set of quadrature filters created from rescalings of the reference Log-Gabor filter. The filter bank is constructed at different scales that are multiples of a minimum user-defined wavelength, λ_{min}. The scaling of the Log-Gabor function is achieved by using different wavelengths that are based on multiples of the minimum wavelength, λ_{min}, which is a user-defined parameter. The relationship between the filter scale m, and the filter center frequency ω_0 is set as $\omega_0 = 2/(\lambda_{min} \times (\delta)^{m-1})$ where δ is a scaling factor defined for computing the center frequencies of successive filters. Let the signal to be analyzed be $I(x)$, and let $M^e_m(x) = real\ (F^{-1}(G(\omega))$ and $M^o_m(x) = imag\ (F^{-1}(G(\omega))$ denote the even and odd Log-Gabor filters at a scale m where F^{-1} denotes the inverse Fourier transform operation. The local amplitude $A_m(x)$, local phase $\varphi_m(x)$ at a given filter scale (m) can then be calculated as in (2.9):

$$
\begin{aligned}
&e_m(x) = I(x) * M^e_m(x); o_m(x) = M^o_m(x) \\
&A_m(x) = \sqrt{e_m(x)^2 + o_m(x)^2}; \phi_m(x) = \arctan(o_m(x)/e_m(x))
\end{aligned}
\tag{2.9}
$$

Accordingly, at each point x in the signal $I(x)$, a different response for each scale of the Log-Gabor filter can be obtained. These responses form the basis of a localized representation of the signal as we describe next.

2.3 Proposed US Image Features for Bone Localization and Fracture Identification

In US images, bone surfaces mostly appear blurred with non-uniform intensity and substantial shadowing beneath the surface. A 1D scanline profile through the bone surface (Fig.2.3) shows how the US response depicts a ridge edge rather than a step or ramp edge at the bone boundaries. However, due to the soft tissue interface and associated US artifacts, there are also different edge responses, present in the same intensity profile, which resemble the bone edge response (e.g. Fig. 2.3, region with yellow dotted line). Furthermore, on the other side of the ridge edge (e.g. Fig. 2.3, yellow continuous line), the intensity values of different edge responses decrease drastically due to shadowing. Based on the above observations, we argue that a ridge is an appropriate feature to detect in our application. The purpose of ridge detection is to capture the major axis of symmetry. Signals that have even symmetry about the origin will have real (and even) Fourier transforms, while signals that have odd symmetry will have imaginary (and odd) Fourier transforms. Signals that are neither perfectly odd nor perfectly even will have complex Fourier transforms (i.e. have both real and imaginary parts) where the resultant phase values describe their degree of symmetry.

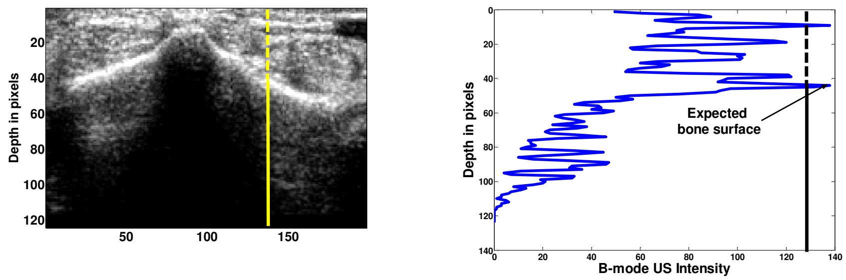

(a) (b)

Fig.2.3 (a) 2D in-vivo US image where the investigated 1D scanline profile is shown as a vertical line (yellow dotted and continuous). The US probe is pointing top to bottom in the image. (b) Corresponding scanline profile of the bone surface. The arrow indicates the ridge profile of the expected bone surface location.

Based on local phase information, as calculated in (2.9), a point of symmetry on the scale of the spatial extent of the filters will result in the response of the even filter ($e_m(x)$) dominating the response of the odd filter ($o_m(x)$) [16]. Taking the difference of these responses over a number of scales, a measure of phase symmetry (PS) can thus be defined as:

$$PS(x) = \frac{\sum_m \lfloor [|e_m(x)| - |o_m(x)|] - T \rfloor}{\sum_m \sqrt{e_m(x)^2 + o_m(x)^2} + \varepsilon} \tag{2.10}$$

where $\lfloor A \rfloor = \max(A,0)$, ε is a small number included to avoid division by zero, and T is a noise threshold calculated as a specified number (k) of standard deviations (σ) above the mean (μ) of the local energy distribution due to noise (Kovesi 1999). T is defined as: $T = \mu + k\,\sigma$ [17]. The response of the smallest scale filter is used to estimate μ and σ since it has the largest bandwidth and will give the strongest noise response. For different US machine settings and for different sequences, k can be tuned to provide a balance between the detected bone surface and speckle scale. At the tissue/bone interface, the *PS* value will be shown later in this chapter to be much higher compared to the *PS* values obtained from soft tissue interfaces and US artifacts.

If a 1D scanline profile is convolved with a pair of quadrature Log-Gabor filters, the result can be displayed graphically via a scalogram. Each row of the scalogram is created by convolving the signal with a pair of quadrature filters at a different scale. Figure 2.4 shows an example of scalogram calculated at different scales across a bone boundary using the same scanline profile given in Fig.2.3. Investigating this figure, we can see that using a small analysis scale (smaller filter wavelength) will treat each feature relatively independently from other features in the image. Each feature will be compared to a small number of other features that are nearby, and hence will be perceived as being more important locally. At the largest scale, each feature will be considered in relation to all other features, which will produce a measure of global significance for each feature. Therefore, a feature that may have high significance when analyzed at small scale may end up losing that significance when analyzed at a larger scale. By investigating the scalogram, the significance of the bone surface feature can be seen. The line corresponding to the bone feature starts from the smaller scale and extends downwards. Bone surface features give a localized response over a wide range of scales compared to features obtained from US artefacts.

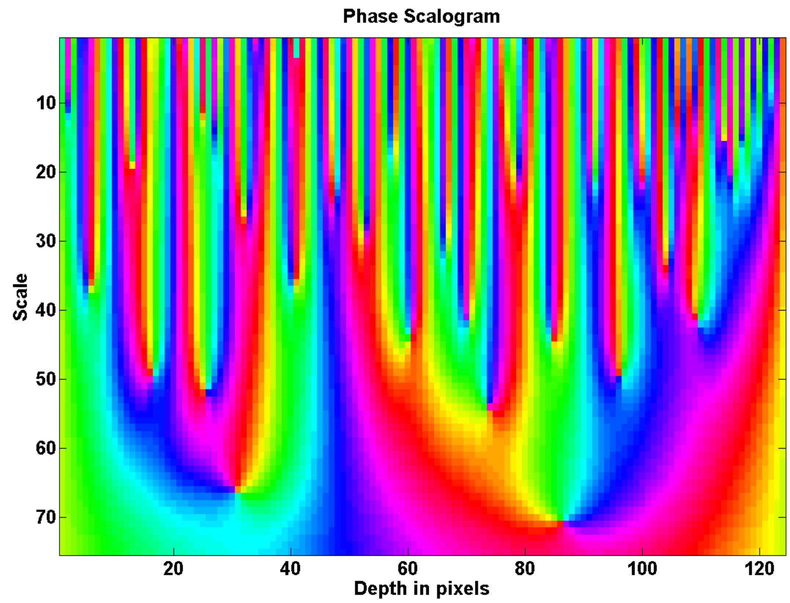

Fig.2.4 Local phase scalogram corresponding to the 1D scanline profile from fig. 2.1 (a). Phase is encoded with hue. The intensity values show the phase angle $\phi_m(x)$.

To extend the analysis into 2D for our US images, our feature detection is performed at a number of separate orientations (r) with the results subsequently combined. Accordingly, orientable 2D filters are defined by spreading a Log-Gabor function into two dimensions where a filter tuned to a particular orientation ϕ_0 is constructed by masking a radial Log-Gabor function with an angular Gaussian tuned to ϕ_0. The radial component controls the frequency band to which the filter responds and the angular component controls the orientation to which the filter responds. The resulting two components are then combined into a 2D Log-Gabor function as in (2.11):

$$G(\omega,\phi) = \exp[-(\frac{(\log(\omega/\omega_0))^2}{2(\log(\kappa/\omega_0))^2} + \frac{(\phi-\phi_0)^2}{2{\sigma_\phi}^2}] \qquad (2.11)$$

κ is a scaling factor used to determine the bandwidth of the filter in the radial direction, and ω_0 is the filter's center spatial frequency. Here $\sigma_\phi = \Delta\phi/s$ defines the angular bandwidth $\Delta\Omega$ given as:

$$\Delta\Omega = 2 \times \sigma_\phi \sqrt{2 \times \log 2} \qquad (2.12)$$

where $\Delta\phi$ is the angular separation between neighbouring orientations and is defined as $\Delta\phi = 180°/N_r$, where N_r denotes the total number of orientations used. The parameter s controls the angular overlap of the filters transfer function. We empirically found that setting $N_r=6$ ensured even spectral coverage of the spectrum with a sufficient number of bone surface response directions tested. Increasing the number of orientations, in our experience, had little effect on the quality of the outcome but increased the computational complexity of the algorithm. Our angular bandwidth was set to 25^0, which corresponds to $s=1.2$. During the construction of the angular component of the filter, σ_ϕ should be kept small in order to ensure good orientation resolution. On the other hand the angular component should contain an adequate range of frequencies to ensure its robustness to noise (setting $s=1.2$ ensured that this compromise was met). By using the above 2D filter over a number of scales *(m)* and at different orientations *(r)*, a 2D *PS* measure can then be defined as in (2.13):

$$PS(x, y) = \frac{\sum_r \sum_m \lfloor \left[|e_{rm}(x, y)| - |o_{rm}(x, y)| \right] - T_r \rfloor}{\sum_r \sum_m \sqrt{e_{rm}^{\,2}(x, y) + o_{rm}^{\,2}(x, y)} + \varepsilon} \qquad (2.13)$$

The orientation-dependent noise threshold T_r is calculated as previously explained (for the 1D case), however, with the response of the smallest scale filter belonging to a specific orientation being used which allows for the calculation of an independent noise compensation term for each orientation. Fig.2.5 demonstrates our proposed processing approach and shows an example line profile across the bone surface obtained from the extracted *PS* image overlaid on top of the corresponding profile in the original US image. It can be clearly seen that the *PS* image has a maximum at the bone boundary.

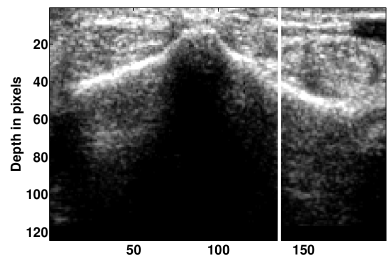

(a)

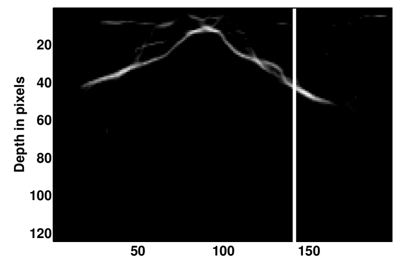

(b)

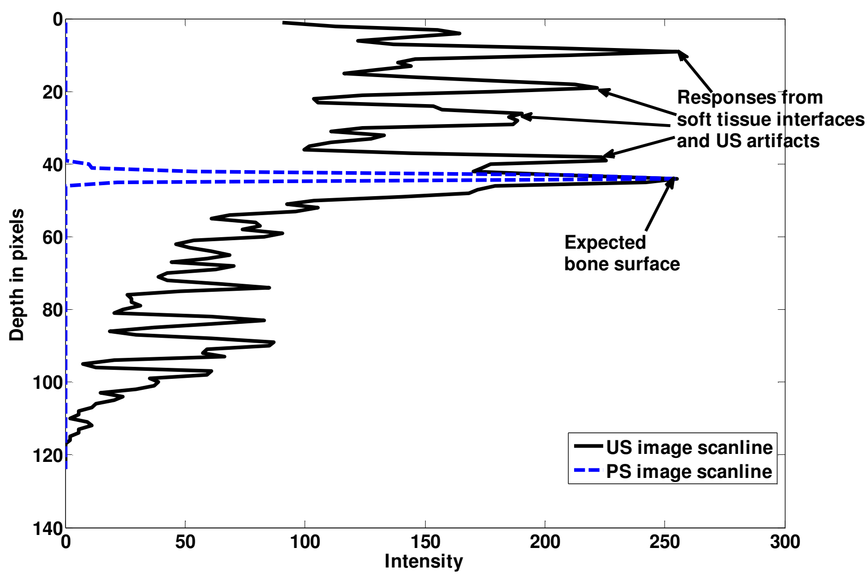

(c)

Fig.2.5 Illustration of the bone response in original and processed US images with an example (vertical) line profile shown. (a) Original 2D in-vivo image of a human distal radius (US probe is pointing top to bottom in the image). (b) Corresponding phase *PS* image obtained using our proposed phase based feature. (c) Example line profile across the bone surface in (a) shown in solid black, and across that in (b) shown in dashed blue. Note how the *PS* profile shows a high peak at the expected bone surface location (indicated by the arrow on the ridge-like bone profile in US). Note how *PS* facilitates robust detection of the bone edge even in the presence of many different edge responses that are due to the soft tissue interface and associated US artefacts.

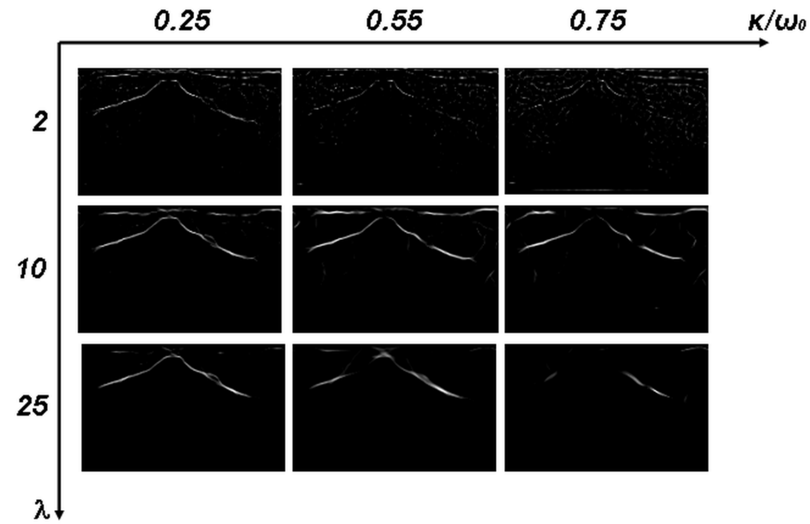

Fig.2.6 *PS* image results for different minimum wavelength (λ_{min}) and bandwidth (κ/ω_0). Increasing the bandwidth (decreasing κ/ω_0 ratio) and λ_{min} makes the location of the bone surface more distinct compared to the other responses from speckle and soft tissue interfaces.

A better understanding of the influence of minimum wavelength (λ_{min}) and bandwidth (β) on the *PS* image (hereafter, the term '*PS* image' will be used to refer to the phase symmetry feature image of an US image) results can be seen in Fig.2.6. Selecting an appropriate wavelength for the smallest scale filter and a constant bandwidth for all the filters will extract bone surfaces while reducing the influence the US artefacts. Fig. 2.6 shows different combinations of λ_{min} with κ/ω_0. Selecting an appropriate bandwidth and minimum wavelength is important during the design of the filters. We noticed that greatly increasing these values did not provide better localization results. If the bandwidth is increased, the local phase information will be averaged over larger regions of the spectrum. This will decrease the resolution at which the phase information is obtained, which will in turn affect the bone surface localization results.

2.3.1 Imaging and Experiments

The acquisition system consisted of an US scanner (Voluson 730, GE Healthcare, Waukesha, WI) with a 3D RSP5-12 probe. A tracking system (OPTOTRAK 3020, Northern Digital Inc., Waterloo, ON, Canada) was used to generate the gold standard measurement of relative bone fragment displacements. The acquired US volumes (each comprising cubic voxels of 0.19mm) were transferred from the US machine to a computational workstation using 3DView2000, a propriety software package from GE Medical Systems.

Experiment-1 Accuracy Assessment of Bone Surface Localization

In this experiment, we compared the surface localization accuracy obtained from both the original B-mode US image and the proposed PS feature image to the 'gold standard' measurement of the surface made with a stylus whose 3 mm diameter spherical tip was visible in the US image (Fig. 2.7). The echo from this tip was determined to be accurate down to a sub-pixel resolution, as will be shown later, so the bone can be considered to lie 3 mm distal to the near side of the spherical tip.

Two surface models were used; a flat metal block and a Sawbone model (#1018-3, Sawbones Inc., Vashon WA). Each model was immersed inside a water filled tank with the long axis of the model aligned with the scan plane to the best of the operator's ability. Images were obtained at three different depths by raising or lowering the probe position inside the water tank and realigning the model at each depth to ensure it was centred in the elevation direction. Two orientations of the model were also tested; horizontal and inclined at 20°, which we consider to be an upper limit for longitudinal angulation in the clinical situations for which we intend to use this imaging technique (Fig. 2.8).

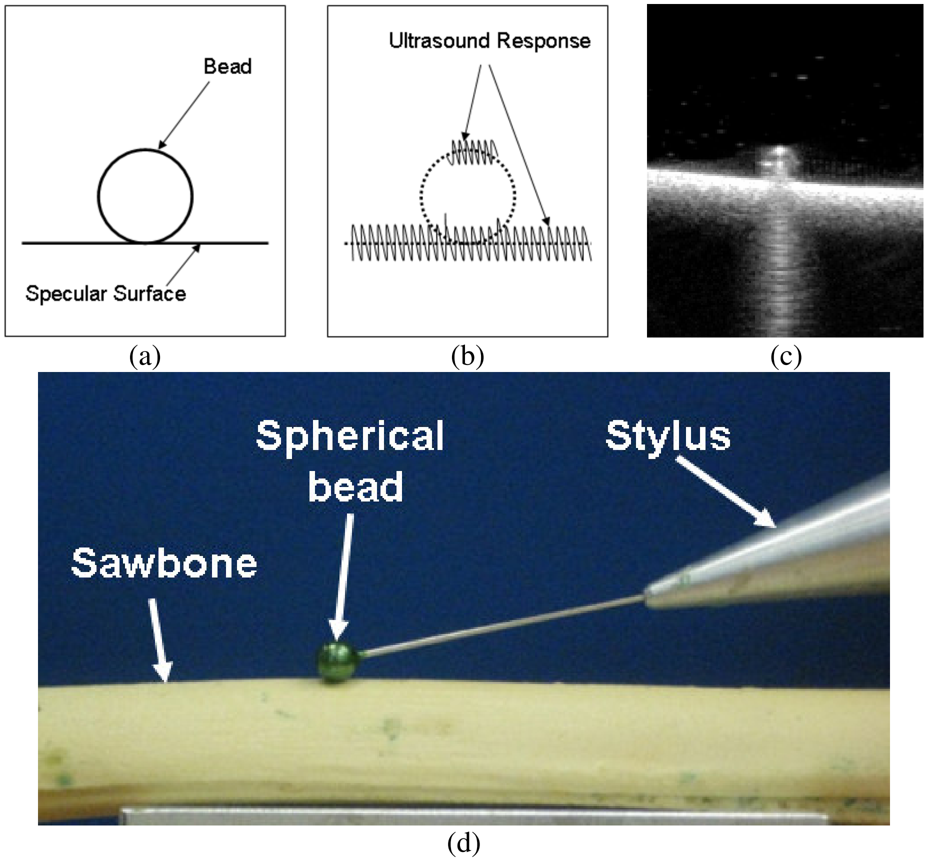

Fig.2.7 Bone surface localization experiment. (a) Sketch of a spherical bead on top of a specular surface (bone in this example). (b) Sketch showing the surface response thickness of bead top surface and specular surface (bone in this example) when imaged with US. (c) B-mode US image of a bead imaged inside a water tank. The feature extending to the bottom part of the image is due to the reverberation artifact which cause due to the multiple reflectins of the US signal from hard specular surfaces such as the bead top surface. (d)Picture showing the stylus with a spherical bead tip touching the top surface of the sawbone.

At each orientation and depth, the bead which was attached to the tip of the stylus (Fig. 2.7) was scanned at 15 different locations along the model surface. For each location we obtained 10 different US scans. To ensure that the bead was centred in the beam direction, the position of the stylus was adjusted until the clearest possible surface reflection was obtained.

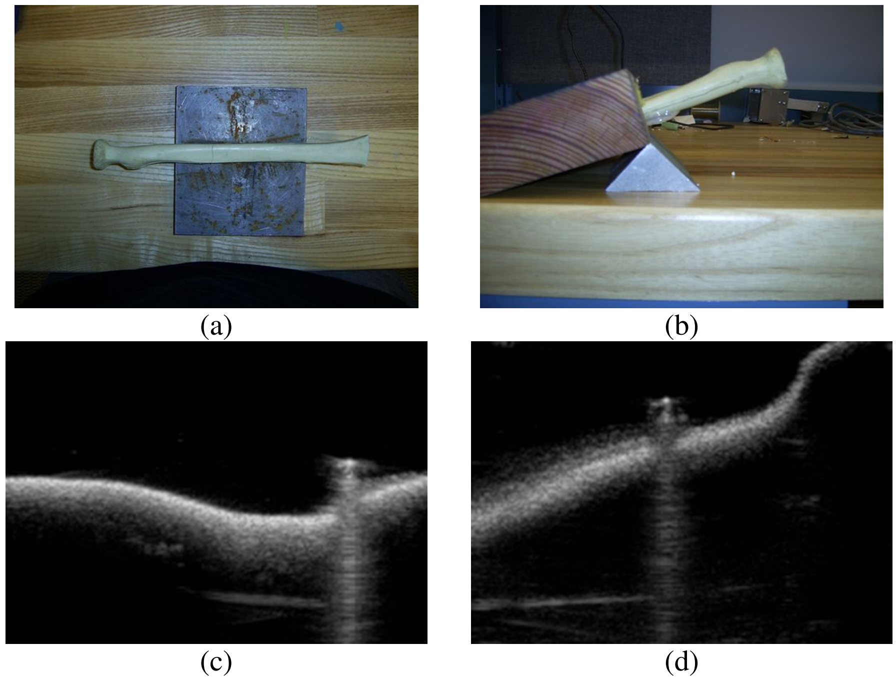

Fig.2.8 Experiment 1: Horizontal and angled cases. (a) Horizontal Sawbone. (b) Sawbone angled at 20°. (c) US image of horizontal case with tip of the stylus visible. (d) US image of the angled case with the tip of the stylus visible.

The location of the bright intensity response from the top of the bead tip, *f*, in the US image, and the location of the intensity response of the model surface obtained from the PS image, *b*, were then extracted as shown in Fig. 2.9 using an automated algorithm to reduce operator related variability.

First, a region of interest (ROI) was selected by the user around the bead top surface. A subpixel edge detection algorithm then automatically detected the top surface of the bead within the ROI by locating the position with the maximum vertical gradient. The same edge detection algorithm was also used to detect edges of the model surface in the *PS* image. The model surface localization error (in mm) was therefore defined as: $error = D - (b - f) * pixel\ length$, where D is the bead diameter. In the inclined orientation case, we corrected for the geometric error resulting from the bead not touching the surface along the vertical measurement direction (Fig. 2.9 (a)) as in (2.14):

$$\cos\alpha = \frac{D/2}{D/2 + error_\alpha} \Rightarrow error_\alpha = \frac{D/2}{\cos\alpha} - D/2 \qquad (2.14)$$

A 20° angle produced an error of 0.096mm, which was added to *f*. Some error may also arise from the squint angle of the transducer, but this error is assumed to be negligible for the range of bead diameters used in the tests. This error is less than 0.01mm for a squint angle of 2 degrees and less than 0.1mm for a squint angle of 10 degrees; the actual squint angle is assumed to be much less than 10 degrees.

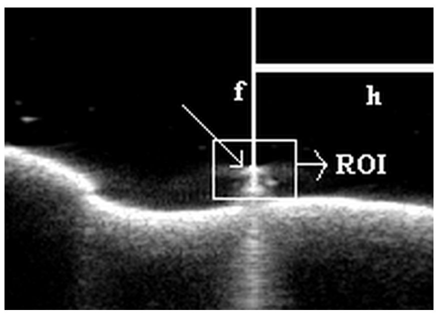

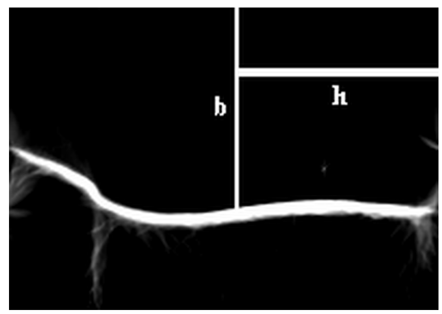

(a) (b)

Fig.2.9 Experiment 1: Bone surface localization measurements using a 3mm bead. (a) Original US image. (b) Corresponding *PS* feature image. For each vertical profile (at position *h*) the measurements *f* and *b* are made from US and *PS* images. *PS* measurements are considered accurate when *b* approaches *f*+3mm.

Our accuracy tests assumes that the sphere surface detected in the B-mode US image is in fact located at the top of the sphere (or at least at a small fixed offset) rather than at some interior or exterior point which depends on the radius of the sphere. To confirm the validity of our assumption, a separate validation step was conducted in which US images were acquired with a selection of *differently sized beads* (with 1.5mm, 3.2mm, 4.3mm and 6.3mm radius, respectively) glued against a metal block (Fig. 2.10 (b)) and immersed in water. B-mode US scans were obtained at three different depths (10 repetitions at each depth) with the same previously-described edge detection algorithm used to locate the top of each bead. The differences in depth measurements between the surfaces of all possible pairs of beads were compared against the actual known differences in bead diameter.

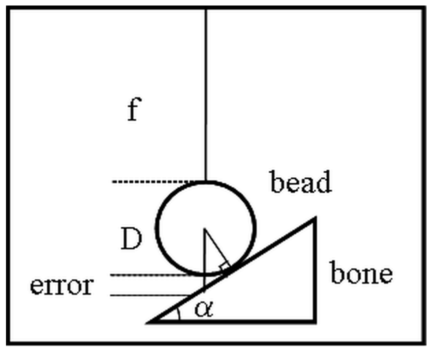

(a)

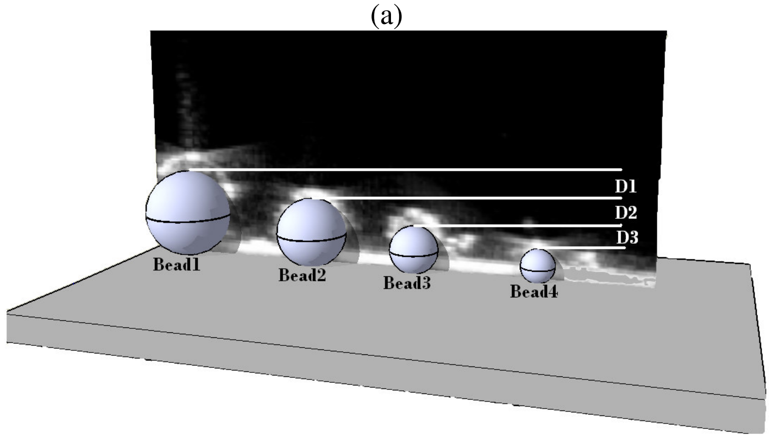

(b)

Fig.2.10 Testing different bead radii in experiment 1. (a) For cases where the bone surface is angled by α=20°, a geometric error is induced in the estimation of the bone surface because the bead does not touch the surface along the vertical measurement direction. This error is calculated and added to the measurements. (b) A series of US images were acquired with four beads of decreasing diameter. D1 is the difference in diameter between beads 1 and 2, D2 is the difference between beads 2 and 3, and D3 is the difference between beads 3 and 4. The appearance of the echo from the top surface of each bead should decrease by the difference in diameters to the next smaller bead.

Experiment 2-Accuracy Assessment of Bone Fracture Measurement

An important capability in an orthopaedic surgery system for fracture assessment is the ability to easily identify bone fragments and accurately assess their reduction. Our second experiment was thus designed to evaluate the accuracy of using the proposed *PS* features in measuring gaps between bone fragments.

The Sawbone model was cut into two parts with each part glued to the top surface of a metal block. Infrared emitting diodes were glued to the surface of one of the metal blocks to allow tracking of the displacements by an OPTOTRAK system. One block remained fixed while the other block was moved and clamped at different displacements and both vertical and horizontal displacements were measured (Fig. 2.11).

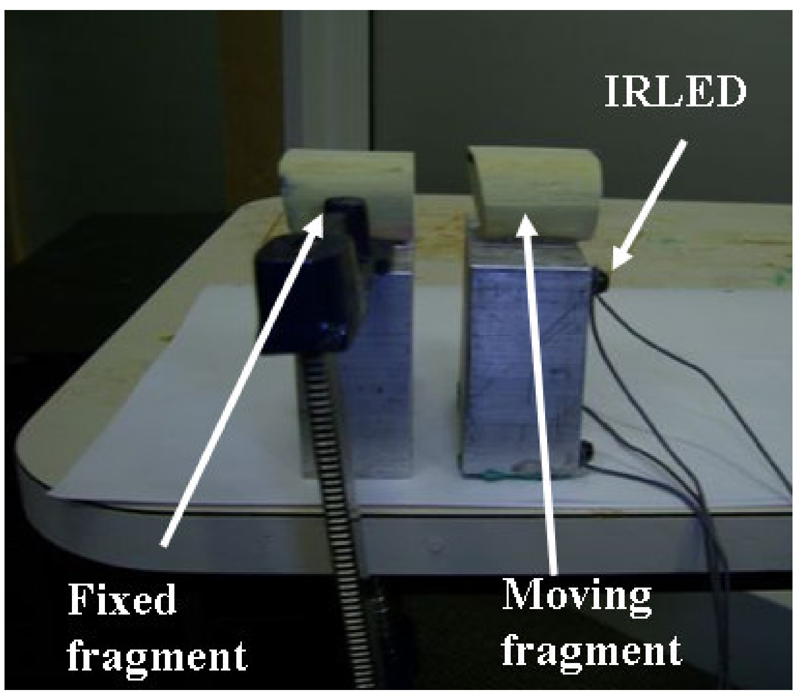

Fig.2. 11 Experimental setup for accuracy assessment of bone fracture measurement.

The OPTOTRAK, which was used to provide the gold standard displacement measurements, has a reported RMS accuracy of 0.1mm in the x and y (lateral) directions, and 0.15mm in the z (depth) direction at a distance of 2.5 meters. The range of displacements tested varied between ≈0.6mm-2.2mm. Continuous OPTOTRAK measurements verified that the displaced fractures remained stationary during US imaging. Tests were conducted first with standard coupling gel and then repeated with a 2cm thick slice of bovine muscle tissue overlaid on top of the fracture to simulate more realistic specimen conditions. The bovine tissue was obtained through a certified butcher following guidelines and notification of the UBC Animal Care and Biosafety Committee. A total of 10 scans were obtained for each displacement and the resulting measurements of the displacement from the *PS* image were compared with those measured by the OPTOTRAK system. The measurements in the image space were done by first applying the previously described sub-pixel edge detection (experiment 1) on a selected ROI around the fracture in the PS image and then measuring the distance between the detected edges on each side of the fragment. For horizontal displacements, this was performed by measuring the horizontal distance between the two closest edge pixels that lie along the gap (Fig. 2.12). The same method was used for measuring vertical displacements (Fig. 2.13). Measurement error was defined as the displacement measured from the *PS* image subtracted from the displacement obtained from the OPTOTRAK.

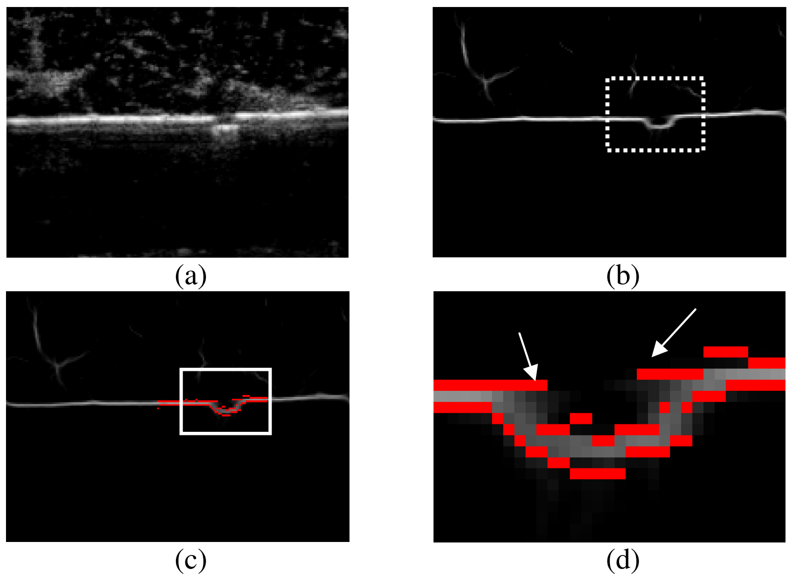

Fig.2.12 Experiment 2. Horizontal displacement of bone fragments. (a) US image with soft tissue overlaid on the Sawbone. (b) Corresponding PS image showing the ROI selected for the sub-pixel edge detection. (c) Edge pixels detected by the edge detection algorithm are shown in red. (d) Enlarged ROI. The horizontal gap betweeen the two fragments was calculated by measuring the horizontal distance between the last pixel shown in red in the right-left direction from the top bone surface (left arrow) and the last red pixel in the right-left direction from the top bone surface (right arrow).

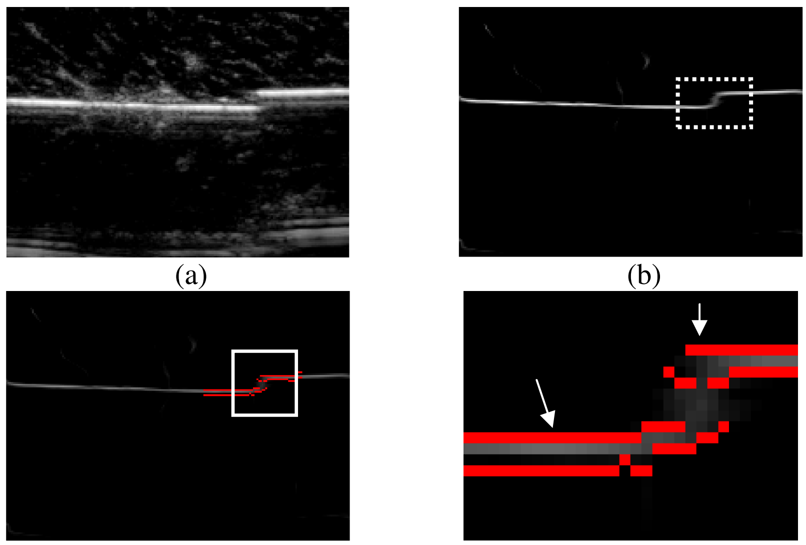
(a) (b)
(c) (d)

Fig.2.13 Experiment 2. Vertically displacement of bone fragments. (a) US image with soft tissue overlaid on the Sawbone. (b) Corresponding PS image showing the ROI selected for the sub-pixel edge detection. (c) Edge pixels detected by the edge detection algorithm are shown in red. (d) ROI. The vertical gap betweeen the two fragments was calculated by measuring the vertical distance between the first pixel shown in red in the top-down direction from the top bone surface on the left of the fracture (left arrow) and the first red pixel in the top-down direction from the top bone surface on the right of the fracture (right arrow).

Experiment 3 - Qualitative Evaluation Using In-Vivo Specimens

For qualitative evaluation of the proposed bone localization method, tests were performed in-vivo on the distal radius and ulna of a normal volunteer as well as on the Sawbone model overlaid with ~2.5 cm of bovine tissue. Since most previous work on bone localization in US used gradient or edge-based segmentation methods, we also applied gradient calculations and Canny edge detection to compare with the *PS* image results. The parameters of the gradient and Canny calculations were adjusted empirically for each image to give the best appearance. For the in-vivo study we have obtained 30 different US volumes.

2.3.2 Results

Implementation Details

For each experiment, the phase images were calculated as in (2.13) using empirically determined filter parameters. A set of scales (m=2) and orientations (N_r=6) with κ/ω_0=0.25 and a filter wavelength of $\lambda_{\min}$ =25 pixels were used which offered good spectral coverage and orientation resolution and produced good bone surface localization in the presence of speckle. The noise threshold parameter k was set to 8. Throughout the experiments, these values were *not* changed. During the construction of the angular component of the filter, σ_ϕ should be kept small in order to ensure good orientation resolution. On the other hand the angular component should contain an adequate range of frequencies to ensure its robustness to noise (setting s=1.2 ensured that this compromise was met).

Experiment 1- Bone Surface Localization

The processing time for the *PS* calculation for each 2D US image was approximately 0.5s on an Intel Pentium 4 PC (3.64 GHz, 2GB of RAM). Box and whisker plots of the localization errors from both US and *PS* images are shown in Fig. 2.14 for horizontal Sawbones and metal blocks. Fig.2.15 shows box and whisker plots for the angled case. The simpler surface geometry of the metal block produced smaller errors than the Sawbone for both cases.

The model surface estimated using the *PS* image tended to lie slightly interior to the bone on both models (metal block: mean= −0.28mm with STD= 0.27mm; Sawbone model: mean= −0.34mm with STD = 0.16mm relative to the gold standard estimate of 3mm distal to the edge of the sphere detected in the B-mode US image). The point of maximum gradient on the proximal edge was also a closer match to the gold standard estimate (Fig.2.16). The surface detected directly from the B-mode US image had no significant bias (mean = −0.11mm with STD = 0.2mm). We also found the PS localization accuracy results had statistical significance for Sawbone and metal block surfaces ($p>0.05$ Independent student t-test).

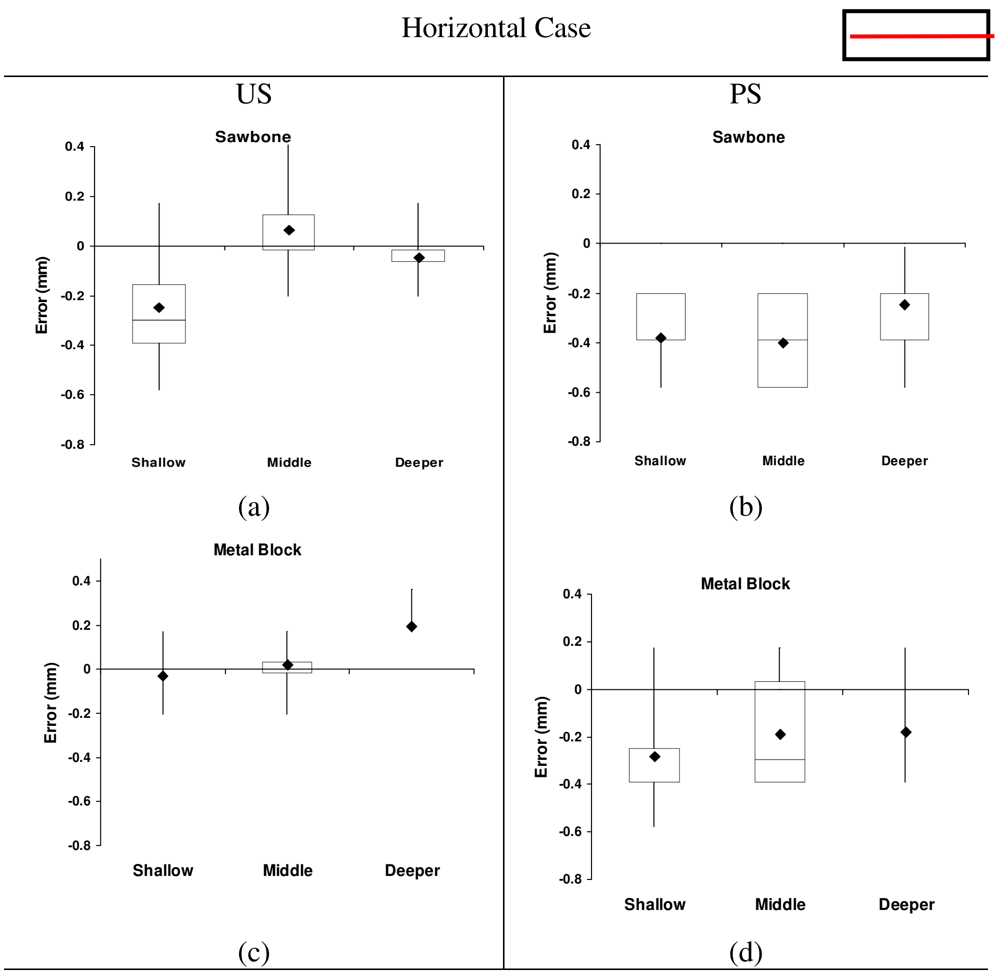

Fig.2.14. Experiment 1. Bone surface localization errors for a horizontal surface in a water bath. Errors are calculated as the difference between the edge-detector results and the results from the bead location. Tests are repeated for the phantom near the top, middle, and bottom of the US image. (a) US image used in edge-detection on a Sawbone. (b) PS image used in edge-detection on a Sawbone. (c) US image used in edge-detection on a flat metal block. (d) PS image used in edge-detection on a flat metal block. The black point represents the mean, and the box and whiskers represent the standard deviation and range of the data.

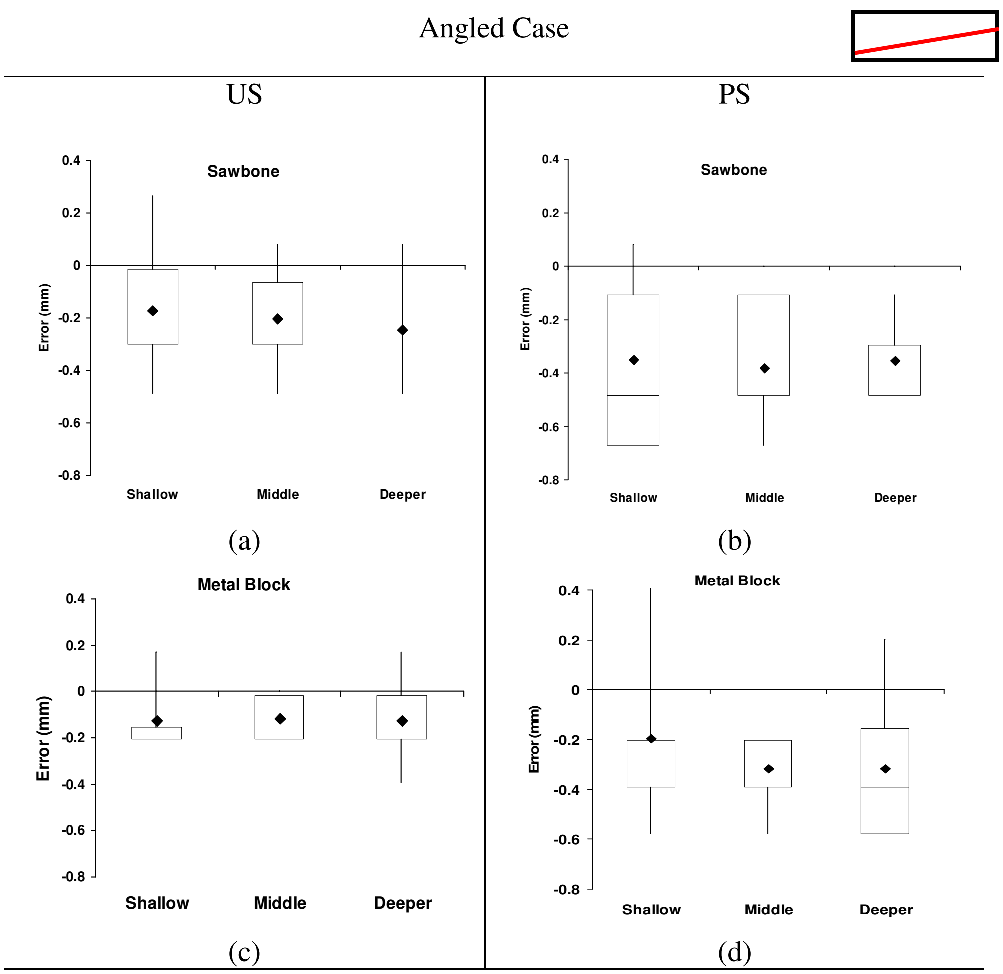

Fig.2.15 Experiment 1. Bone surface localization errors for a surface angled $\alpha=20^{o}$ in a water bath. Errors are calculated as the difference between the edge-detector results and the results from the bead location. Tests are repeated for the phantom near the top, middle, and bottom of the US image. (a) US image used in edge-detection on a Sawbone. (b) PS image used in edge-detection on a Sawbone. (c) US image used in edge-detection on a flat metal block. (d) PS image used in edge-detection on a flat metal block. The black point represents the mean, and the box and whiskers represent the standard deviation and range of the data.

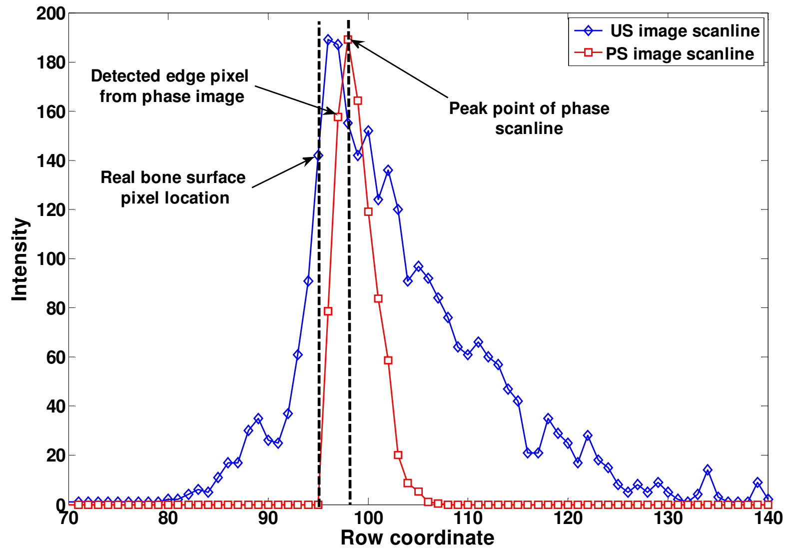

Fig.2.16 Sample scanline profile through the bone surface in the original US image (blue) and proposed *PS* (red) images. The two vertical dotted lines correspond to the pixel preceding the first positive intensity (line to the left) and the maximum intensity (line to the right) value of the line profiles. The real bone location lies close to the dotted line on the left, suggesting that the location where the gradient of *PS* is maximal corresponds to the true bone surfaces.

In both horizontal and inclined measurements, whether obtained from US or from *PS* images, the mean error was calculated based on measurements taken at 15 different bead locations for each depth setting. Hereafter we will report the highest mean error results of these three different depth settings as "maximum mean error". For the Sawbone model, the maximum mean error from US was 0.25 mm inside the Sawbone surface when the surface was horizontal and 0.26 mm when angled. The maximum mean error from *PS* was 0.40 mm inside the bone surface when horizontal and 0.38 mm when angled. These tests were performed in a water bath, so both US and *PS* show a high level of accuracy that is independent of the angle of the surface in this range and independent of the depth. It should be noted that the ability to detect the bone surface directly from US is relatively easy in a water bath but images of real tissue will contain significant artefacts. Edge detection in US is also more sensitive to parameter adjustment; the values used here to achieve the highest accuracy later proved unsuitable for in-vivo tests and had to be readjusted empirically. The *PS* results are less sensitive to parameter setting where the same parameter values were found suitable both for water tank and in-vivo tests. Figure 2.17 confirms that the top surface of the bead response does indeed drop by the difference in bead diameters for different beads. This suggests that the edge detector is identifying the top of the bead with at most a constant bias that is independent of bead diameter. No statistically significant difference was found between the actual differences of bead diameter and measured diameter for all locations in the image (paired student t-test, p=0.90).

Experiment 2 - Bone Fracture Displacement

Box and whisker plots of the errors from horizontal and vertical displacements are shown in Fig. 2.18 for both gel and soft tissue mediums. The errors in estimating displacements were consistently small, with maximum mean errors under 0.5 mm for all tests (here again "maximum mean error" indicates the mean error result that had the highest error among the introduced displacements). These results are especially encouraging for the potential use of *PS* in fracture assessment since the accuracy required in surgical navigation systems is typically in the range of 2-4mm [18].

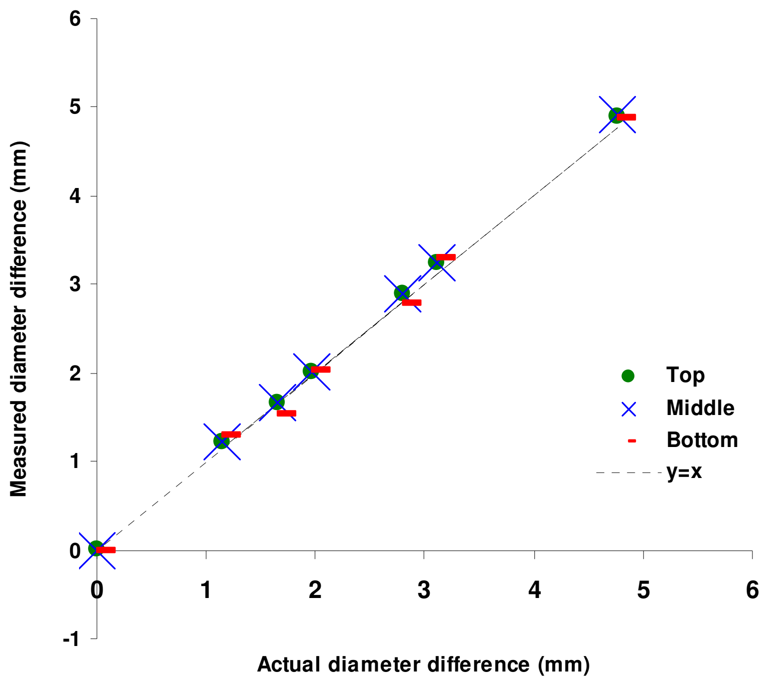

Fig.2.17 Experiment 1. Validation of bead measurements. If the edge measurements from the US images correspond to the top of the bead, then the difference in measurements from one bead to a smaller bead should be equal to the difference in the bead diameters. The measured differences between bead diameters is plotted against the actual differences in diameters. Tests were repeated for the bead near the top, middle and bottom of the image. The data fall close to the line y=x, indicating good agreement.

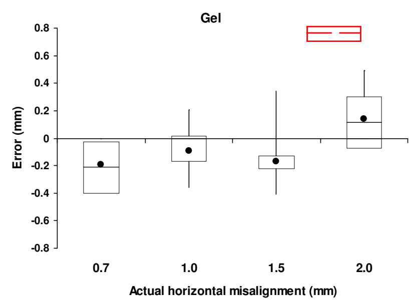

(a)

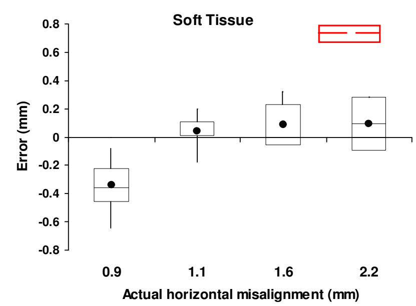

(b)

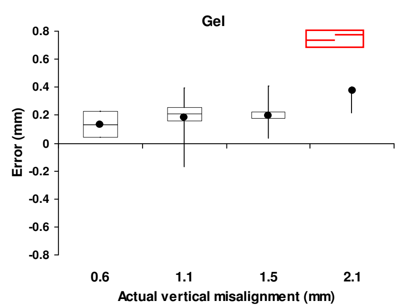

(c)

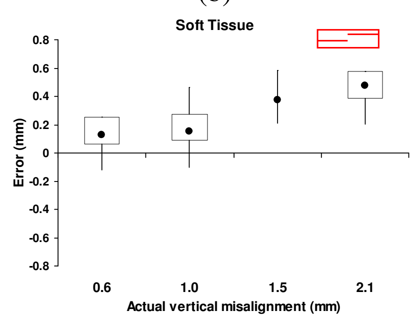

(d)

Fig.2.18 Horizontal and vertical displacement measurement errors from a fractured Sawbone for PS images only. 'Gel' indicates that the US transmission medium was coupling gel, and 'Soft Tissue' indicates that a layer of bovine muscle tissue was used. The error is defined as the difference between the measurements from PS and the OPTOTRAK. (a) Horizontal displacement with coupling gel. (b) Horizontal displacement with soft tissue. (a) Vertical displacement with coupling gel. (b) Vertical displacement with soft tissue.

Experiment 3 - Qualitative Results

Fig. 2.19 shows qualitative bone localization results on in-vivo scans of the human radius and ulna obtained using *PS* and compared to results of standard Canny and gradient images. For the gradient calculations, a 2D Gaussian with a standard deviation of two pixels for both directions was used for all scans. For the Canny edge detector, a threshold value of 90% and standard deviation of 2 pixels was used. These parameters were changed to 80% threshold value and a standard deviation of three pixels for the in-vivo scans to obtain good results with minimal artifacts.

As can be observed in Fig. 2.19, *PS* mostly captured continuous sections of the bone with little influence exhibited by soft-tissue interfaces which was not the case for the Canny and gradient images. Furthermore, while *PS* results were noticeably robust and stable, Canny filter results were highly dependent on the choice of parameters whereas gradient results were strongly influenced by speckle and soft tissue features. In a number of cases, the Canny edge detector extracted two surfaces, one above and one below the actual bone surface, due to the thick response of the bone reflection in US.

Figure 2.20 shows a stack of 2D PS images obtained by processing individual 2D slices from a 3D US scan. This result demonstrates how the proposed *PS* features can produce a 3D surface representation that is relatively continuous and robust in the presence of speckle, shadowing and other ultrasound-specific artifacts. The consistency of the surface produced by *PS* processing as it proceeds from scan to scan along a bone surface suggests the possibility of extending *PS* processing to 3D US imaging data.

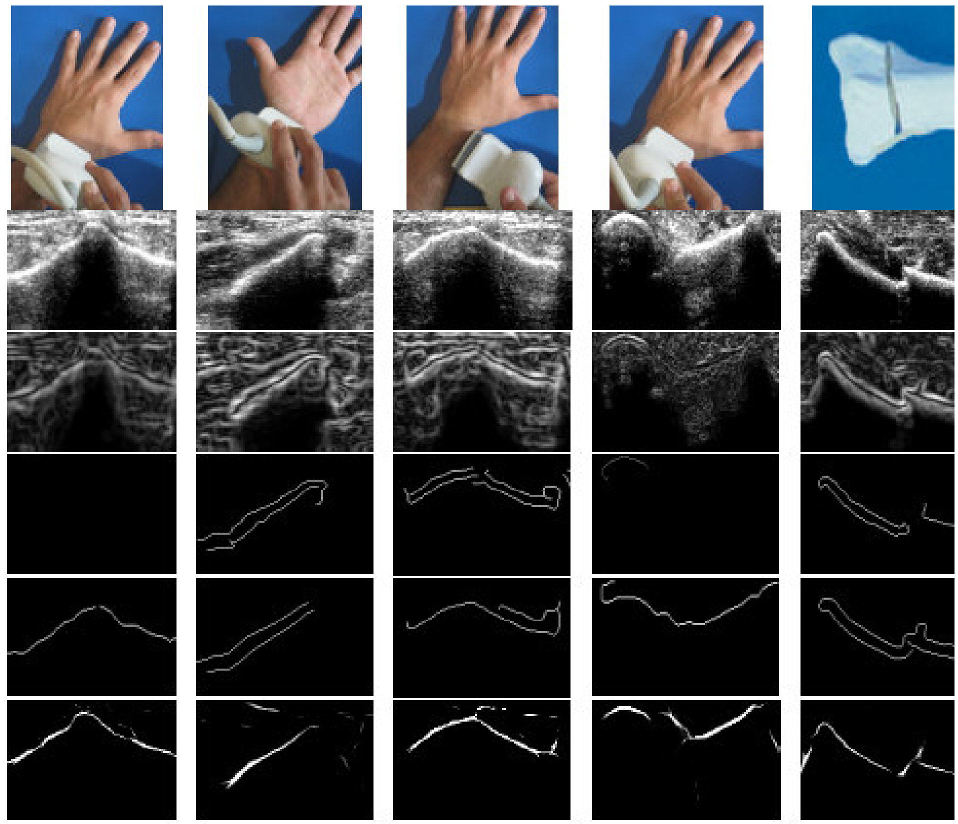

Fig.2.19 Qualitative results of the proposed bone localization method in experiment 3. In-vivo distal radius and ulna images of a normal volunteer and Sawbone imaged with bovine soft tissue overlaid (a) In-vivo scanning orientation, and Sawbone with two part fracture. (b) B-mode US image. (c) Gradient image obtained using 2D Gaussian with a standard deviation of two pixels for both directions. (d) Canny image with standard deviation of 2 pixels and 90% threshold value. (e) Canny image with standard deviation of 3 pixels and 80% threshold value. (f) Proposed *PS* image. Columns 1-3 show US images of a distal radius obtained at different probe positions. Column 4 shows an US image of the distal radius and ulna. Column 5 shows a Sawbone with two part fracture imaged with bovine soft tissue overlaid. Note how our proposed *PS* feature mainly localizes the bone boundaries with little visible influence from US image artifacts whereas gradient images are influenced strongly by speckle and soft tissue interfaces. Also note how the Canny edge detector extracts two surfaces, one above, and one below the actual bone, due to the thick response of the bone reflection in US. Rows (b) and (c) also show how sensitive the results are to the set parameters except in *PS* images which were obtained using the same parameter set in all images tested.

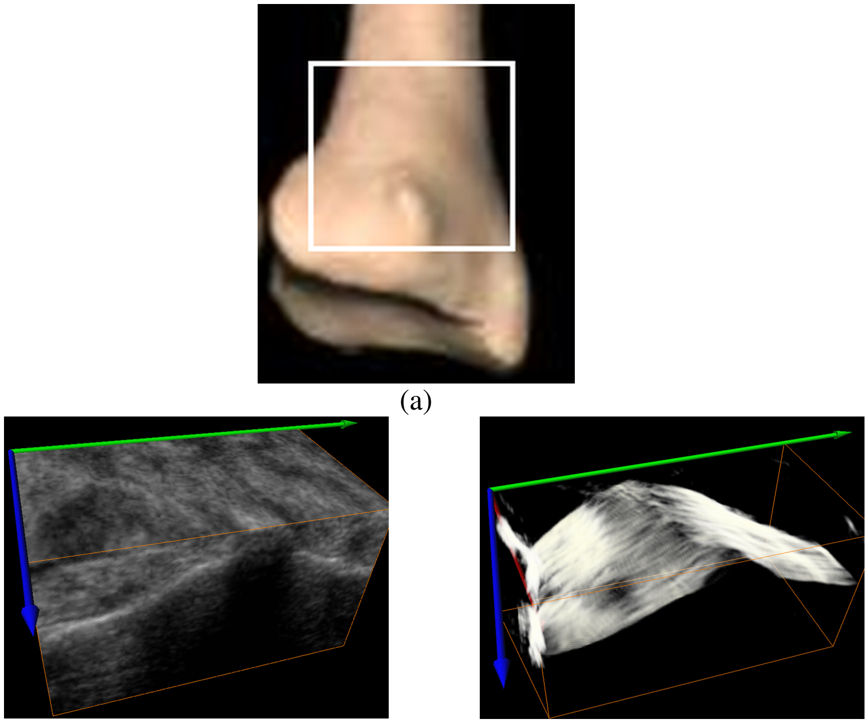

(a) (b) (c)

Fig.2.20 Qualitative results of the proposed bone localization method in experiment 3 where a stack of 2D images obtained by scanning an in-vivo distal radius with a 3D US probe was processed. (a) 3D anatomical sketch of a human radius. The scanned area is highlighted by the white rectangle. (b) 3D US volume of the scanned distal radius. (c) Corresponding 3D PS image which shows that the 2D algorithm (after processing individual 2D slices from a 3D volume) can produce relatively continues and clean bone surfaces with little speckle and US artifacts. This 3D test is only meant to show how repeatable the *PS* calculations are along a bone surface which suggests the possibility of extending *PS* processing to 3D US data.

2.4 Surgical Tool Localization from Ultrasound Using 2D Local Phase Features

Since our final aim is to develop a system for fracture reduction surgeries we are also interested in localizing surgical tools from US data. In current practice surgical tools such as K-wires are commonly used for fixation in orthopaedic fracture surgeries as a provisional fixation step prior to plating or as a definitive fixation. During the surgery in order to determine the drill trajectory of the surgical tool different 2D fluoroscopy images are taken from different directions. A lot of skill is required to visualize 3D anatomy based on information obtained from 2D scans and to properly perform the necessary surgical action accordingly. The surgeon must position the implant in one view, and then obtain additional images in other planes using trial and error placements of guide wires which increases the amount of radiation received. To overcome these limitations we tried to localize surgical instruments from US images using the proposed local phase symmetry approach.

In current orthopaedic surgery the surgical tools typically have narrow metallic surfaces which act as a strong reflector. Consequently, reverberation artefacts caused by these instruments aggravate the image quality and obscure the underlying bone surface making the localization of the bone surface difficult. Furthermore, at steep angles of the surgical tool the ultrasound beams are scattered causing problems during the accurate identification of the tool tip. Therefore, simultaneous identification of the bone surfaces and surgical tools is still a challenge due to the low signal to noise ratio in US data and the many artefacts present which complicate image interpretation.

Different methods have been proposed in order to improve the instrument imaging in US data. Ortmeier et al. [19] uses median filtering, adaptive thresholding and morphological operations to identify the head of the graspers made of various materials inside a water tank. The algorithm was tested in US images obtained from a water tank setup without the presence of soft tissue.

In a different study Novotny et al. [20] divides the 3D volume into discrete candidate volumes by using thresholding and connecting the neighboring voxels. Principle component analysis (PCA) was performed on each candidate. The longest and thinnest structure from the candidate US volumes was selected as the surgical tool. The experiments were conducted inside the water tank where the tool was incrementally moved toward a bovine tissue sample which was placed at the surface of the water tank. However in surgical situations the tool is in contact with the soft tissue which produces artefacts that obscure the instruments location and geometric detail. In his recent paper Novotny [21] also proposed to use a form of generalized Radon transform to search for long straight objects which was combined with the information obtained from a passive marker attached to the instrument shaft. The algorithm was tested with a water tank study and in-vivo animal study. For the tank study when the algorithm correctly identified the position of the passive markers the root mean square (RMS) error was 1.8mm. For the in-vivo study the maximum RMS was found 1.4mm.

Stoll et al. [22] used a line detection algorithm together with a passive marker attached to the tip of the instrument to locate the position and orientation of it from a single US image. The instrument was imaged inside the water tank and a mean error of 0.8mm was reported.

Linguraru et al. [23], proposed a statistical framework which consist of a combination of expectation maximization (EM), PCA and watershed transform (WT) algorithms. The algorithm requires expert segmented images to initialize the statistical distribution of the surgical tool and the surrounding soft tissue. This information is then used in the EM algorithm. The algorithm is tested in water tank settings and in-vivo interventions. The maximum segmentation error for in-vivo setting was 3.17 voxels.

In this part we extend the work that was explained in detail in sections 2.2 and 2.3 to scenarios involving K-wires which are commonly used for fixation during distal radius fracture surgeries as a provisional fixation step prior to plating or as definitive fixation. Following reduction and K-wire placement, the clinical scenario usually calls for intraoperative imaging (ionizing radiation fluoroscopy) to confirm the reduction and wire placement, a modality which we are aiming to replace.

2.4.1 Imaging and Experiments

To investigate the ability of our proposed 2D local phase method to localize surgical tools in US images, an experiment was conducted to assess the resolution of the tool localization relative to a simulated bone interface in both a water bath and in a more realistic tissue model; in both experiments, the surgical tool was a K-wire with a diameter of 1.6 mm. In the first part of the study, the bone was modeled using a flat metal block and the tissue was modeled using a water bath. In the second part of the study, the bone was modeled using a plastic bone model (Sawbone model #1018-3, Sawbones Inc., Vashon WA) and the tissue was modeled using a 2 cm thick piece of bovine muscle tissue. The wire, shown in Fig. 2.21, was fixed to a stylus which was tracked with an optical tracking system (OPTOTRAK 3020, NDI, Canada) which is accurate to approximately 0.1 mm in each cardinal direction. The optical tracking system measured the tool tip position with an RMS error of 0.12mm, so it can be considered the gold standard. The stylus was rigidly mounted onto a clamp which could be repositioned relative to the bone model's surface. The distance from the tool tip to the specular surface (Sawbone or metal block) was incrementally decreased by reducing the vertical distance while maintaining the horizontal position (Fig. 2.21.). After each position change we verified that the tool tip was in essentially the same position in the horizontal plane. The range of displacements in the vertical direction was 1.73mm to 6.39mm for the water medium and 2.01mm to 7.96mm for the bovine tissue medium. For each displacement we obtained 10 different scans.

In order to detect the tip of the K-wire, the US image was first processed using the local phase algorithm. Next, an edge detection algorithm, similar to the one used in section 2.3.2, was applied to the phase image in order to identify the inferior edge of the tool tip, which was defined as the pixel closest to the metal block's surface. The distance from this pixel to the metal block surface was recorded as the displacement in the image domain. Changes in this distance were compared to changes in vertical position obtained from the optical tracking system.

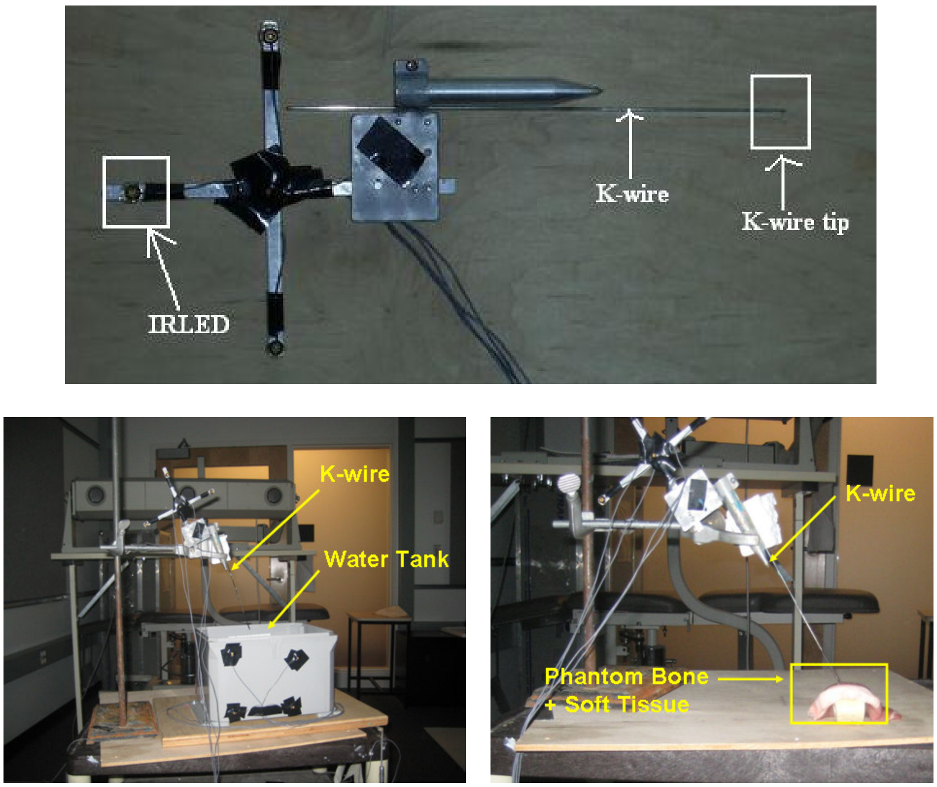

Fig.2.21 Surgical tool localization experimental setup. a) A K-wire with a diameter of 1.6 mm is shown attached to a tracked stylus that was used in the surgical tool localization experiment. (b) First part of the K-wire localization experiment where the imaging medium was water and the specular surface was modelled using a flat metal block. (c) Second part of the K-wire localization experiment where the was modeled using a plastic bone model (Sawbone model #1018-3, Sawbones Inc., Vashon WA) and the tissue was modeled using a 2 cm thick piece of bovine muscle tissue.

2.4.2 Results

The local phase algorithm is fully automatic and can process one slice in approximately 0.77s on an Intel Pentium 4 PC (3.64 GHz, 2GB of RAM). The tip of the K-wire was localized with a mean maximum localization error of 0.4mm when the tool was imaged inside the water tank. This number increased to 0.8mm when the K-wire was imaged inside the soft tissue (Fig. 2.22). Investigating Fig.2.22 we can see that the obtained results are encouraging for using local phase method for localizing surgical tools in a controlled environment. While the water tank study carefully characterized the accuracy of the method, it does not reflect the target conditions for the algorithm, detecting instruments within a soft tissue interface. However, the second study validated the effectiveness of the technique in a surgical setting and showed that the accuracy is still well below the required average accuracy which was reported to be typically in the range of 2-4mm for orthopaedic surgery [18].

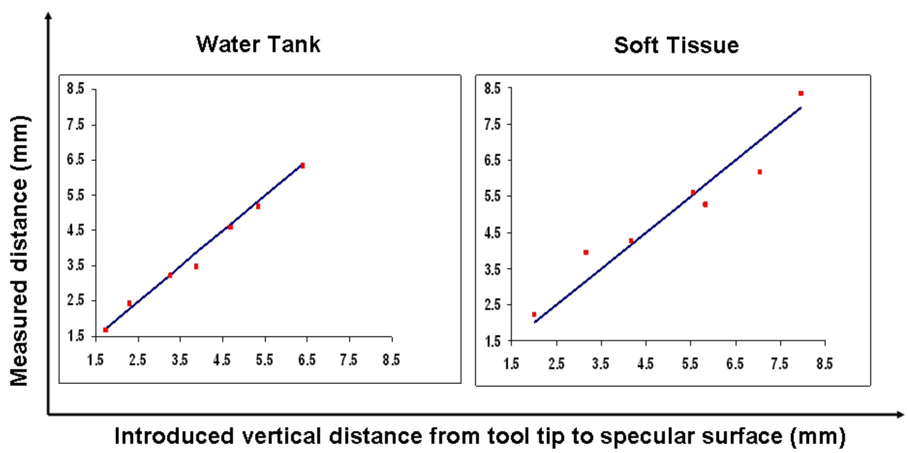

Fig.2.22 Quantitative results for the K-wire tracking experiment. Comparing the error results we can see that its more difficult to localize the K-wire tip for a soft tissue interface. However, the accuracy of the method is still under the required limits.

Qualitatively, the local phase algorithm produced clearer images of the bone surface and the K-wires than conventional ultrasound in all our experiments, especially when there was a soft tissue overlay, despite the decreased signal to noise ratio and increased imaging artifacts the soft tissue produces (see Fig. 2.23). Our results show that using the local phase information of ultrasound images is a promising approach for US guided CAOS applications.

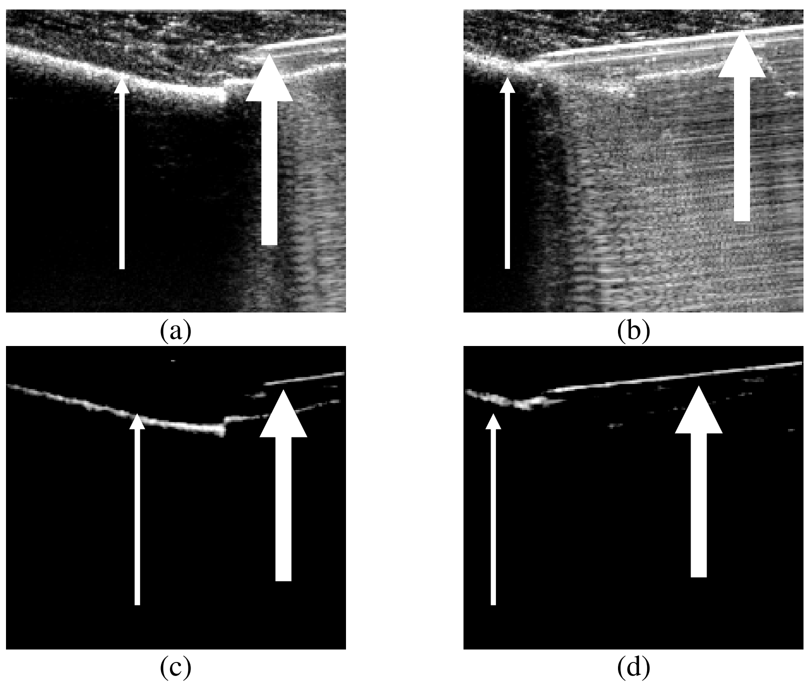

Fig.2.23 K-wire localization in ultrasound images: (a & b) conventional US images of the soft tissue overlaid on the bone model with a K-wire inserted into the soft tissue; (c & d) the corresponding local phase images. The thick arrows point to the K-wires in all of the images while the thin arrows point to the bone surface.

While it was clear in our experiments that identifying both the bone surface and K-wires is considerably more challenging with a model bone overlaid with soft tissue than in a simple water bath, the automatically-segmented surfaces were sufficiently clear and computed sufficiently quickly. Since the local phase algorithm can be performed essentially automatically, these results suggest that ultrasound can likely be used to track both surgical tools and bone surfaces in computer-assisted orthopaedic procedures such as fracture repairs.

2.5 Conclusion

Accurate localization of tissue/bone interfaces and surgical tools in US images is a challenging problem that continues to hamper US deployment in orthopaedic applications. This chapter presents a novel approach for automated and accurate bone segmentation and surgical tool localization from 2D US images based on local phase information. Phase symmetry extracted using 2D Log-Gabor filters was proposed as a robust image feature for accurate localization of bone surfaces. Quantitative validation demonstrated sub-millimetre localization accuracy in phantom studies. Phase information was also shown to be suitable for measuring small bone displacements, also with sub-millimetric accuracy, a very encouraging finding relevant to applications in fracture assessment and fixation.

In this chapter, the *PS* calculations are described but extension to clinical applications will require modifications of the algorithms for specific clinical tasks. Here, the *PS* feature was defined and the leading edge was extracted. An automatic algorithm may follow this approach that may require more specific definitions of the decision criteria used to identify the presence of bone or the extent or displacement of a fracture. Additional outlier rejection, incorporation of *a priori* anatomical information when available, pre-processing of the US images, and post-processing of the *PS* images are also likely to improve the accuracy and robustness of the algorithm.

Our preliminary results on in-vivo scans of the human distal radius and K-wire are very encouraging and demonstrate the power of the proposed method in extracting bone surfaces and surgical tools in practical applications in the presence of real soft-tissue interfaces. In the next chapter we extend this method to 3D designing 3D Log-Gabor filters and show that by incorporating the correlation between adjacent slices increases the success of the local phase based bone surface extraction.

2.6 References

[1] A.V. Oppenheim, J.S. Lim, "The importance of phase in signals", *Proc IEEE*, vol. 69, no. 5, pp. 529-541, 1981.

[2] M.C. Morrone, R.A. Owens, "Feature detection from local energy", *Pattern Recognition Letters*. Vol. 6, no. 5, pp. 303-313, 1987.

[3] M.G. Linguraru, M.A.G. Ballester, N.A. Ayache, "Multiscale feature detector for morphological analysis of the brain", *Proc Int. Conf. Med. Image Compt. Computer- Assisted Intervention*, vol. 2879, pp. 738-745, 2003.

[4] R.S.J Estepar, G.G. Washko, E.K. Silverman, J.J. Reilly, R. Kikinis, C.F. Westin, "Accurate airway wall estimation using phase congruency", *Proc Int. Conf. Med. Image Compt. Computer- Assisted Intervention*, vol. 4191, pp.125-134, 2006.

[5] L. O'Donnell, C.F. Westin, W.E.L. Grimson, J. Ruiz-Alzola, M.E. Shenton, R. Kikinis, "Phase based user steered image segmentation", *Proc Int. Conf. Med. Image Compt. Computer- Assisted Intervention*, vol.2208, pp.1022-1030, 2001.

[6] R. Dalvi, R. Abugharbieh, M. Pickering, P. Smith, "Registration of 2D to 3D joint mages using phase-based mutual information", *Proc. SPIE Medical Imaging*, pp. 1-9, February 2007.

[7] M. Hemmendorf, M.T. Andersson, T. Kronander, H. Knutsson, "Phase based multidimensional volume registration", *IEEE Transactions on Medical Imaging*, vol.21, no.12, pp.1536-1543, December 2002.

[8] M. Mellor, M. Brady, "Phase mutual information as a similarity measure for registration", *Medical Image Analysis*, vol. 9, no. 4, pp. 330-343, August 2005.

[9] V. Grau, A.J. Noble, "Adaptive multiscale ultrasound compounding using phase information", *Proc Int. Conf. Med. Image Compt. Computer- Assisted Intervention*, vol. 3749, pp.589-596, 2005.

[10] D. Boukerroui, A.J. Noble, M. Robini, M. Brady, “Enhancement of contrast regions in suboptimal ultrasound images with application to echocardiography”, *Ultrasound Med Biol*, vol. 27, no.12, pp.1583-1594, 2001.

[11] M. Mulet-Parada, A.J. Noble, “2D+T boundary detection in echocardiography”, *Medical Image Analysis*, vol.4, no.1, pp.21-30, 2000.

[12] G. Sanchez-Ortiz, J. Declerck, M. Mulet-Parada, A.J. Noble, “Automatic 3D echocardiographic image analysis”, *Proc Int. Conf. Med. Image Compt. Computer- Assisted Intervention*, vol.1935, pp. 687-696, 2000.

[13] X. Ye, A.J. Noble, “3D freehand echocardiography for automatic left ventricle reconstruction and analysis based on multiple acoustic windows”, *IEEE Trans on Medical Imaging*, vol. 21, no.9, pp.1051-1058, 2002.

[14] P.D. Kovesi, Invariant measures of image features from phase information, Ph.D. thesis, University of Western Australia, Australia, 1996.

[15] D. Boukerroui, A.J. Noble, M. Brad, “On the choice of band-pass quadrature filters”, *Journal of Mathematical Imaging and Vision*, vol.21, pp.53-80, 2004.

[16] P. Kovesi P, “Symmetry and asymmetry from local phase”, *Proc Tenth Australian Joint Conference on Artificial Intellegence*, pp185-190, 1997.

[17] P. Kovesi P, “Image features from phase congruency”, *Videre: A Journal of Computer Vision Research,* vol. 1, no.3, pp.1-26, 1999.

[18] R. Phillips, “The accuracy of surgical navigation for orthopaedic surgery”, *Current Orthopaedics*, vol. 21, no. 3, pp. 180-192, 2007.

[19] T. Ortmaier, M.A. Vitrani, G. Morel, S. Pinault, “Robust Real-Time Instrument Tracking in Ultrasound Images for Visual Servoing”, *Proc. SPIE Medical Imaging,* vol. 5750, pp. 170-177, 2005.

[20] P.M. Novotny, J.W. Cannon, R.D. Howe, “Tool localization 3D ultrasound ”, *Proc Int. Conf. Med. Image Compt. Computer- Assisted Intervention*, pp.969-970, 2003.

[21] P.M. Novotny, J.A. Stoll, N.V. Vasiley, P.J. Del Nido, P.E. Dupont, T.E. Zickler, R.D. Howe, "GPU based real time instrument tracking with three dimensional ultrasound", *Medical Image Analysis*, vol. 11, no.5,pp. 458-464, October 2007.

[22] J.A. Stoll, P.M. Novotny, R.D. Howe, P.E. Dupont, "Real time 3D ultrasound based servoing of surgical instruments", *Proc. IEEE International Conference on Robotics and Automation*, pp.613-618, 2006.

[23] M.G. Linguraru, N.V. Vasilyev, P.J. Del Nido, R.D. Howe, "Statistical segmentation of surgical instruments in 3D ultrasound images", *Ultrasound in Medicine and Biology*, vol. 33, no.9, pp.1428-1437, 2007.

Chapter 3
3D Local Phase Features for Bone Segmentation and Fracture Detection from 3D Ultrasound Data*

3.1 Introduction

Intra-operative visualization becomes more important with increasing use of minimal invasive operative techniques. In trauma and orthopaedic surgery, especially 3D visualization is in the centre of interest. Intra-operative visualization for fracture reduction and implant positioning in orthopaedic trauma surgery is classically based on two-dimensional imaging using routine X-ray or fluoroscopy. This technique however, lacks real time three-dimensional imaging capabilities. Unsatisfactory reconstruction results for joint fractures or incorrectly positioned screws are frequently discovered only on post-operative CT scans.

---

* A version of this chapter will be submitted for publication. I. Hacihaliloglu, R. Abugharbieh, A. Hodgson, R. Rohling. “3D Local Phase Features for Bone Segmentation and Fracture Detection from 3D US Data”.

With continuing developments in US technology, it has been recently demonstrated that 3D US can be efficiently and successfully used [1], [2] in a range of minimally invasive techniques in cardiac surgery [3], neurosurgery [4] and liver surgery [5]. Nevertheless, extraction of relevant anatomical information from US images continues to be very challenging because US images typically contain significant speckle and other artifacts that complicate image interpretation and automatic processing [6], [7]. Due to these difficulties, US has only been used intra-operatively in CAOS as a surface digitization tool in order to obtain patient-specific data rather than as an imaging modality [6], [8]-[12]. Although some research groups have had some success in automating bone segmentation from US images using image intensity and gradient information, these methods still remain highly influenced by image intensity variations and imaging artifacts and to date have been limited to 2D images [13]-[16]. The possibility of using 3D US as an alternative to fluoroscopy imaging for guiding basic surgical tasks and assessing fracture reduction in orthopaedic surgery has so far not been well studied. This possibility is explored in this chapter through the use of intensity-invariant 3D local image phase features to segment bone surfaces.

In chapter 2 we have proposed a method for automatic bone surface extraction from 2D US data using local phase features. However, 2D methods are inherently limited to cross-sectional analysis and do not take advantage of surface continuity between adjacent images (i.e., along the axis perpendicular to the scan plane direction). In this chapter we demonstrate that bone surfaces and fractures can be accurately localized using 3D local phase features computed *directly* from 3D US image volumes. We extend our original local phase based processing technique from 2D to 3D US using 3D Log-Gabor filters. Specifically, a 3D local phase symmetry measure is constructed that produces strong responses at bone surfaces and suppresses responses elsewhere.

3.1.1 Main Contributions

The main contributions of this chapter can be summarized as follows:

1. We extend our original local phase based bone surface extraction method to 3D.
2. We show that integrating the surface information along the axis perpendicular to the scan plane direction makes the proposed algorithm less sensitive to soft tissue artifacts and more sensitive to weak bone surface responses.
3. We improve the bone surface localization accuracy.
4. We validate the proposed method using carefully designed phantom, ex-vivo, in-vivo experiments.
5. We also use the proposed method in extracting surgical tools from 3D US volumes.

The remainder of this chapter is organized as follows. In Section 3.2 we describe the extension of our previous method to 3D using 3D Log-Gabor filter. Section 3.3 explains the laboratory experiments that were constructed in order to validate the method together with the obtained results. We also illustrate qualitative results in this section. Section 3.4 shows the application of the proposed method in localizing surgical tools from 3D US volumes. We finally draw our conclusion in section 3.5.

3.2 3D Local Phase Features

In this chapter, we extend our previous 2D adaptation of phase symmetry for US bone segmentation to 3D by using 3D Log-Gabor filters. The transfer function (*G)* of a 3D Log-Gabor filter in the frequency domain (3.1) is constructed as the product of two components: a one dimensional Log-Gabor function that controls the frequencies to which the filter responds and a rotational symmetric angular Gaussian function that controls the orientation selectivity of the filter [17]:

$$G(\omega,\phi,\theta)=\exp\left(\frac{(\log(\omega/\omega_0))^2}{2(\log(\kappa/\omega_0))}\right)\times\exp\left(-\frac{\alpha(\phi_i,\theta_i)^2}{2\sigma_\alpha^2}\right) \tag{3.1}$$

Here κ is a scaling factor used to determine the bandwidth of the filter in the radial direction, and ω_0 is the filter's center spatial frequency. To achieve constant shape-ratio filters, which are filters that are geometric scalings of a reference filter, the term κ/ω_0 must be kept constant. The angle between the direction of the filter, which is determined by the azimuth (ϕ) and elevation (θ) angles, and the position vector of a given point f in the frequency domain is given by $\alpha(\phi_i, \theta_i) = \arccos(f \bullet \nu_i / \|f\|)$ where $\nu_i = (\cos\phi_i \cos\theta_i , \cos\phi_i \sin\theta_i, \sin\phi_i)$ is a unit vector in the filter's direction. Here σ_α is the standard deviation of the Gaussian spreading function in the angular direction that describes the filter's angular selectivity. To obtain higher orientation selectivity, the angular function must become narrower.

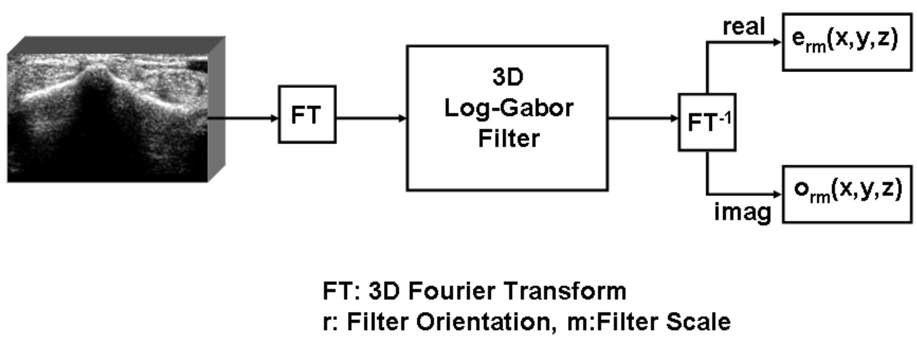

Fig.3.1 Flowchart for local phase analysis for a 3D volume. Here $e_{rm}(x,y,z)$ and $o_{rm}(x,y,z)$ denote the even and odd filter outputs, respectively, which are used during the construction of 3D phase symmetry metric given in equation (3.2).

The scaling of the radial Log-Gabor function is achieved by using different wavelengths that are based on multiples of a minimum wavelength, λ_{min}, which is a user-defined parameter. The relationship between the filter scale m, and the filter center frequency ω_0 is set as $\omega_0=2/\lambda_{min}\times(\delta)^{m-1}$ where δ is a scaling factor defined for computing the center frequencies of successive filters. Local phase analysis of a 3D image volume proceeds by convolving the image with the 3D Log Gabor filters (Fig.3.1).

Extending our previous work explained in chapter 2 where 2D phase symmetry was defined, we construct a 3D phase symmetry measure (3D PS), for different scales (m) and orientations (r) as in (3.2):

$$3DPS(x,y,z)=\frac{\sum_r\sum_m\left\lfloor\left[\left|e_{rm}(x,y,z)\right|-\left|o_{rm}(x,y,z)\right|\right]-T_r\right\rfloor}{\sum_r\sum_m\sqrt{e_{rm}^2(x,y,z)-o_{rm}^2(x,y,z)}+\varepsilon} \tag{3.2}$$

Here $\lfloor A \rfloor = \max(A,0)$, ε is a small number included to avoid division by zero, and T is a noise threshold calculated as a specified number (k) of standard deviations (σ) above the mean (μ) of the local energy distribution. Based on this, T is defined as: $T = \mu + k\sigma$ and the distribution is expected to be Rayleigh [18]. The response of the smallest scale filter is used for the calculation of μ and σ since it has the largest bandwidth and will give the strongest noise response. k can be tuned to provide a balance between the detected bone surface and speckle scale, though no principled basis for choosing this value has yet been described in the literature. Previous authors [18, 19, 20] have used values in the range of 3-5; we experimented with values beyond this range (up to about 12) but found that a value of 5 worked well.

3.2.1 Imaging and Experiments

US image acquisition was performed on a GE Voluson 730 Expert ultrasound machine (General Electric Healthcare, Waukesha, WI) with a 3D RSP5-12 transducer; this is a mechanized transducer in which a linear array transducer is swept through an arc range of 20° at a rate of 30 Hz. The reconstructed US volumes are of 199×119×60 voxel resolution (lateral×axial×elevational) with an isotropic voxel size of 0.19mm. Two different experiments were conducted to quantitatively evaluate the performance of the proposed 3D bone US segmentation method. In the experiments where bovine soft tissue was used as an imaging medium the tissue was obtained through a certified butcher following guidelines and notification of the UBC Animal Care and Biosafety Committee. The first experiment aimed at assessing the localization accuracy of the bone surface detection technique, while the second focused on assessing the accuracy of relative displacement measurements between bone fragments, as this is a clinically relevant task for which we are investigating the use of 3D US. A human left radius model and an ex vivo porcine fibula and tibia were used in our validation experiments. In order to quantify the bone localization accuracy, our segmented 3D PS surfaces were validated against two different 'gold standard' surfaces. The first gold standard reference was based on a stylus with a spherical bead tip placed at a variety of locations on the surface of a bone or bone model, in a manner similar to the method explained in Chapter 2 for 2D bone segmentation; the spherical bead tip produces a consistent and well-defined response a fixed distance from the bone that is independent of the orientation of the transducer relative to the underlying bone surface. The second gold standard measurements were based on CT imaging.

Stylus Validated Sawbone Experiment

Scans of a bone model (#1018-3, Sawbones Inc., Vashon WA) were acquired inside a water tank with the long axis of the bone aligned with the axis of the linear array of the mechanized transducer. This alignment produced the clearest depiction of the bone surface. Images of the Sawbone were obtained at varying depths (shallow: 0.9cm, middle: 1.5cm, deep: 3cm) by changing the transducer position inside the water tank. In addition, to test the accuracy of surface localization at different beam orientations relative to the bone surface, as might occur in clinical use, two different orientations for the Sawbone were tested – horizontal and inclined at 20° which we consider to be an upper limit for longitudinal angulations in the clinical situations for which we intend to use this imaging technique. For this reason angle values over 20° were not relevant. For each of these six transducer positions, a reference 3D US image was acquired and processed using our phase-symmetry algorithm. Following this, a stylus with a 3mm diameter spherical tip was sequentially placed at 30 locations along the bone surface (these points ranged over approximately 37.8 mm in length and 9.5 mm in width) and 10 different 3D US volumes were acquired for each tip placement. The tip produces a high-intensity response at the top surface which is known to be accurately correlated with an accuracy of 0.1mm (which was explained in detail in chapter 2) with the actual sphere surface. Since the physical diameter of the spherical tip is known, we use simple geometry to deduce the location of the actual bone surface (Fig. 3.2).

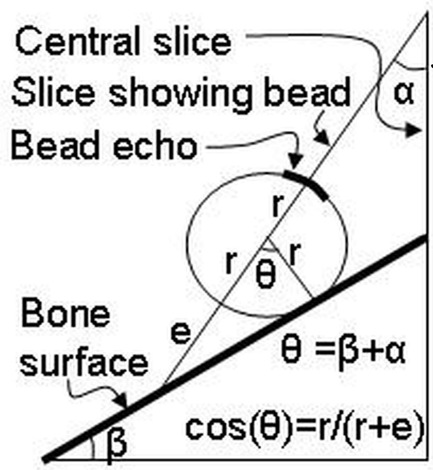

Fig.3.2 Using a stylus with a spherical bead tip as gold standard surface measurement for bone surface localization accuracy assessment. For cases where the bead was not aligned with the central slice of the volume, the location of the bone surface was calculated from the geometry of the angle of the plane showing the bead (α), the angle of the bone surface (β) and the radius of the bead (r).

The localization error at each point was defined to be the difference between the bone surface estimated using the PS image and the corresponding point calculated relative to the spherical tip. We also investigated the effect of the surface inclination and depth on the localization accuracy of the proposed method. Note that since mechanized 3D US transducers use a set of 2D images to reconstruct a volume, the effect of the finite beam thickness is implicitly incorporated into the volume data through the machine's reconstruction process.

Stylus Validated Porcine Experiment

To investigate the effect of more realistic soft tissue interfaces on our localization accuracy, we conducted an ex-vivo experiment on a porcine tibia and fibula. First, the soft tissue was removed of the bone and the same spherical-tipped stylus described above was placed against the bone. The removed soft tissue was then re-laid on top, leaving the tip underneath the tissue and touching the bone. A set of 3D scans were then acquired with the bead positioned at 30 different locations along the bone surface (again these points covered a range of 3.78 cm in length and 0.95 cm in width). The error calculation proceeded in the same manner described earlier.

CT-based Validation

We performed a more comprehensive surface accuracy assessment using a CT scan as a reference. For this study, we built a novel phantom by placing an *ex vivo* bovine femur specimen inside an open-topped plexiglass cylindrical tube (Fig. 3.3). Twenty eight markers (1mm diameter steel balls) were added to the construct with fourteen beads placed on each side of the bone (longitudinally), spaced at equal axial intervals over a distance of 75 mm. We obtained US scans of this specimen where the captured volumes contained 16 fiducials (8 on each side) spanning a region of 37.8mm. To hold the specimen and fiducials securely in place during both CT and US scanning, the tube was filled with a polyvinyl chloride gel (Super Soft Plastic, M-F Manufacturing, Texas, USA).

3D US scans were acquired of the phantom resulting in images of 199×119×60 (lateral×axial×elevational) voxels at an isotropic resolution of 0.19mm. Since the speed of sound differed in the soft tissue from that in the gel, the portion of the bone positioned below the gel appeared displaced relative to the rest of the bone (i.e. that positioned under the soft tissue). We therefore applied a simple correction for that difference in the speed of sound. This adjustment brought the fiducials back into their correct position relative to the bone which is necessary prior to registration to the corresponding CT image.

The same specimen was also scanned in the axial plane using a high-resolution CT machine (HR-pQCT, XtremeCT, Scanco Medical, Switzerland) resulting in a 512×512×324 voxels image with an isotropic resolution of 0.25mm. Registration of the CT dataset to 3D US volume was then performed using the AMIRA software (TGS, San Diego, USA). A landmark-based rigid registration algorithm transformed the input image (CT dataset) by applying a rigid transformation that minimized the sum of the squared distances between the corresponding fiducial points captured in both datasets. The accuracy of the registration was measured by calculating the fiducial registration error (FRE).

Following CT-US registration, bone surfaces were extracted from the CT scan by Otsu thresholding [21] which we used to define the gold standard surface. In order to investigate the effect of the thresholding method on the resulting gold standard bone surface from CT, we also tested seven different automatic threshold selection methods [22]-[28]. Since the US images captured the top surface of the bone surface, only the upper transition in the vertical direction was extracted from the CT dataset to generate a corresponding bone surface.

In order to compare our 3D gold standard CT surface to the 3D US-extracted surface localized using our phase-based processing method, a signed distance map was computed around the CT bone surface. Each non-zero value in the phase-processed US image was then mapped to its corresponding location in the CT image so as to identify the signed distance value associated with that location. This produced a set of intensity/distance pairs. High intensity values confined to a zone near zero distance indicate a highly accurate US surface localization. The surface matching error was thus defined by the average signed distance values corresponding to the maximum phase intensity value along the vertical direction of the 3D phase symmetry image. Our described surface localization accuracy assessment was repeated for 15 different volumes obtained from the same specimen in order to minimize any errors introduced during the manual fiducial landmark selection process.

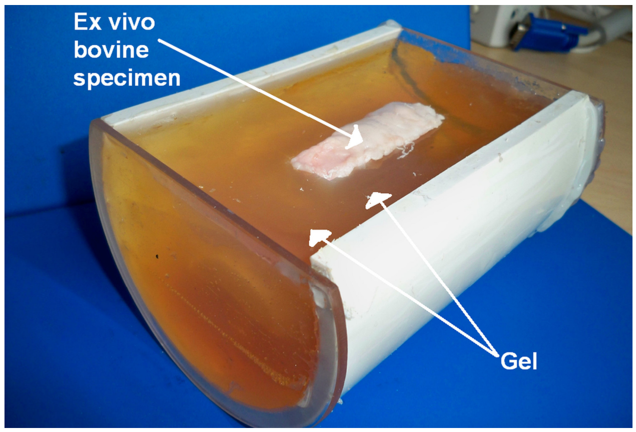

(a)

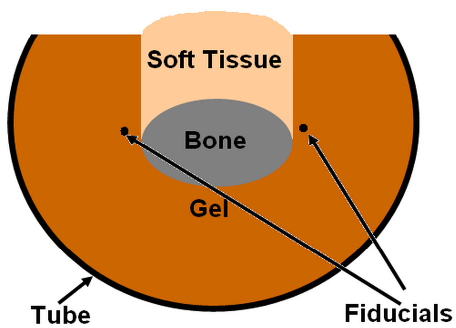

(b)

Fig.3.3 Using CT as a gold standard surface measurement for bone surface localization accuracy assessment. (a) Our constructed phantom comprised of an ex vivo bovine femur specimen inside an open-topped plexiglass cylindrical tube filled with polyvinyl chloride gel. (b) Diagram depicting a 2D axial cut of the constructed phantom showing the fiducials inserted into the gel.

Fracture Misalignment Experiment

In order to assess the capability of our proposed 3D phase symmetry technique to detect small gaps between bone fragments in 3D US data, which is relevant to using 3D US in fracture reduction applications, we created a simulated fracture using a Sawbones model (#1018-3, Sawbones Inc., Vashon WA) and applied a series of displacements to the two fragments ranging between 0.6 to 2.2 mm in the vertical and horizontal directions. The displacement values were chosen to be similar to the range of bone fracture separations which our consulting orthopedic surgeons advised they would need to resolve in order to perfect an intra-articular fracture reduction. An optical tracking system (OPTOTRAK 3020, Northern Digital Inc., Waterloo, ON, Canada) with a localization accuracy of 0.1 mm provided the gold standard displacement measurement of the fracture fragments. Tests were conducted first with standard coupling gel alone and then repeated with a 2-cm thick slice of bovine muscle tissue overlaid on top of the fracture to simulate more realistic specimen conditions. This experiment is similar to our original 2D study, however, in this current experiment, we measured displacements along the top edges of the fracture boundaries on each slice of the 3D phase volume in which they appeared, rather than using only a single imaging plane as we did in chapter 2. Since fracture reduction is a 3D problem we believe that integrating displacement information from multiple slices provides a more accurate assessment of the reduction. Ten US volumes were obtained for each displacement. The displacements estimated from each of the US volumes were then compared to the known applied displacement.

Qualitative Validation Experiments

In this experiment, we performed several qualitative evaluation tests using in-vivo scans of a human distal radius and pelvis, and from ex-vivo scans of a porcine tibia and fibula using the high frequency (RSP5-12) 3D transducer. Furthermore, we also show qualitative results of the 3D local phase surfaces extracted from US volumes obtained using a low frequency transducer (RAB4-8P) with a greater penetration depth, but lower axial resolution We compared the 3D surfaces obtained from our proposed 3D PS based method (i.e. where processing was applied directly on the entire 3D US volume) to our previously reported 2D PS method (where processing was applied to individual 2D US slices that were subsequently stitched together to form a surface). We also repeated similar tests on a fractured Sawbone model (#1018-3, Sawbones Inc., Vashon WA) imaged with an overlay of a 2-cm thick bovine tissue. For in-vivo studies 30 different US volumes were investigated using the proposed method.

Implementation Details

The proposed method was implemented in MATLAB (The Mathworks Inc., Natick, MA, USA) and run on an Intel Pentium 4 PC (3.64 GHz, 2GB of RAM)**.** After investigating results from various 1D scanline profiles of a distal radius and pelvis, scanned in-vivo, with a pair of quadrature filters at different scales, selecting a single scale (m=1) with a large wavelength (λ_{min}= 25 pixels) resulted in very well localized bone surface phase features. In the CT-validated porcine experiment we extracted 3D PS images using multiscale analysis with scale values of m=2,3 by selecting a scaling factor of δ=3 in order to investigate the effect of multi-scale analysis to surface localization accuracy. A value of κ/ω_0 =0.25 provided good surface localization in the presence of speckle. For the angular component, we empirically determined, based on experimentation with models of the human distal radius and pelvis, that it was possible to get good orientation resolution while containing an adequate range of frequencies by selecting an angular bandwidth value σ_α=14.3°. The filter bank used in this work used 15 different (α) 3D filter orientations. The noise threshold parameter k was set to 5. The selected filter parameters were kept the same in all experiments.

3.2.2 Results

Stylus-Validated Sawbone Experiment

For both the horizontal and inclined specimens, the mean PS error was calculated from the measurements taken at the 30 different bead locations for each depth setting. The mean errors at the different scanning depths ranged from 0.40 to 0.62 mm (biased towards the inside of the bone surface) with standard deviations of approximately 0.25 mm. There was no significant influence on these results of surface inclination angle when comparing the fiducial localization errors for the same depth setting (p values > 0.05 except in the shallow depth setting p=0.01, see Table 1). If the imaged surface had an inclination, the error results obtained from all the depth settings had no significant difference (except shallow-middle depth setting p=0.06 using t-test) (Table 3.1). The processing time was approximately 43s for each 3D volume.

Table 3.1Quantitative results for bone surface localization accuracy assessment using stylus with a spherical bead tip as gold standard measurement for 3D PS method. Number of measurements (different stylus positions) used for calculating the mean error is n=30 for each volume.

Surface Inclination: *Horizontal*		
Depth Setting	Mean Error (mm)	Std (mm)
Shallow	-0.54	0.27
Middle	-0.62	0.24
Deep	-0.42	0.22
Surface Inclination: *20° inclined*		
Depth Setting	Mean Error (mm)	Std (mm)
Shallow	-0.40	0.22
Middle	-0.53	0.26
Deep	-0.45	0.23

Std: Standard deviation

Stylus-Validated Porcine Experiment

The mean localization error was 0.44mm (STD 0.16mm) inside the bone surface response. This was similar to the Sawbone error values, which demonstrates the ability of the proposed 3D method to accurately detect bone surfaces even in the presence of significant artefacts due to the presence of soft tissue.

CT-Validated Bovine Experiment

The fiducial registration error for the 15 different US volumes averaged to 0.18mm (Std: 0.31mm) (Table 3.2). The average localization error was the lowest with a mean value of 0.18mm (Std:0.31mm) using a single scale compared to 2 scales (0.21mm), or 3 scales (0.23mm) for the proposed 3D method. Multi-scale analysis added additional computation time during the calculation of 3D PS image (Table 3.2). Comparing the 2D PS results (0.31mm Std: 0.61mm) given in Table 3.2, we can see that extending the local- phase analysis to 3D resulted in an 42% increased accuracy of the bone surface localization. The local phase bone surfaces extracted using 2D PS and 3D PS method were significantly different (all p values were < 0.05).

The effect of using different automatic threshold selection algorithms on the extracted gold standard CT surface was in the range of 0.04mm to 0.1mm. The distribution of phase intensity values with their corresponding signed distance values obtained from volume 5 by processing it with 2D PS method and the proposed 3D PS method are shown in Fig.3.4. Investigating these two figures we can see that the proposed 3D method is less sensitive to typical US image artifacts and most of the intensity distribution is concentrated close to the zero signed distance region.

Table 3.2 Quantitative results for bone surface localization accuracy assessment using CT scan as the gold standard measurement. Number of measurements used for calculating the mean is n=11940. For FRE this number is n=16.

		2D phase symmetry		3D phase symmetry					
		Two Scales		Single Scale Run time: 43sec		Two Scales Run time: 90sec		Three Scales Run time: 150sec	
US Vol.	FRE (mm)	ME (mm)	Std (mm)	ME (mm)	Std (mm)	ME (mm)	Std (mm)	ME (mm)	Std (mm)
1	0.28	0.52	1.02	0.24	0.44	0.31	0.37	0.36	0.36
2	0.33	0.56	0.39	0.47	0.33	0.43	0.29	0.44	0.32
3	0.21	0.42	0.58	0.33	0.21	0.36	0.20	0.41	0.19
4	0.36	0.36	0.98	0.25	0.71	0.21	0.16	0.23	0.16
5	0.22	0.46	1.02	0.21	0.52	0.31	0.44	0.32	0.40
6	0.24	0.38	0.92	0.06	0.54	0.16	0.46	0.19	0.47
7	0.26	0.20	0.26	0.16	0.22	0.18	0.23	0.19	0.25
8	0.28	0.53	0.37	0.42	0.30	0.52	0.29	0.57	0.28
9	0.30	0.58	0.37	0.48	0.28	0.52	0.29	0.51	0.29
10	0.28	0.28	0.79	0.23	0.17	0.27	0.16	0.27	0.16
11	0.22	0.24	0.48	0.23	0.30	0.24	0.31	0.27	0.31
12	0.25	0.12	0.24	0.07	0.22	0.11	0.2	0.14	0.22
13	0.31	0.33	1.97	-0.06	0.17	-0.04	0.74	-0.10	0.20
14	0.34	-0.32	0.20	-0.38	0.18	-0.36	0.16	-0.37	0.19
15	0.34	0.05	0.15	0.03	0.14	0.05	0.16	0.06	0.16
Avr.	**0.28**	**0.31**	**0.64**	**0.18**	**0.31**	**0.21**	**0.29**	**0.23**	**0.26**

Vol.: Volume, Avr.: Average, ME.: Mean Error, Std: Standard deviation, FRE: Fiducial registration error.

Fracture Misalignment Experiment

The PS images permitted accurate assessment of both horizontal and vertical displacements, although vertical displacements were more accurately resolved than horizontal ones (0.51 mm vs. 0.66 mm) (Fig. 3.5). There was no significant effect of imaging medium, gel vs. soft tissue, on these accuracies except for the 0.6mm and 1.5mm vertical displacements where the p value was less than 0.05. Furthermore, there was no significant dependence (all p-values <0.05) of the accuracy of displacement measures on the degree of displacement except when the introduced fracture displacement was 0.6mm in vertical direction (p=0.07 using t-test) when the imaging medium was soft tissue (Fig. 3.5).

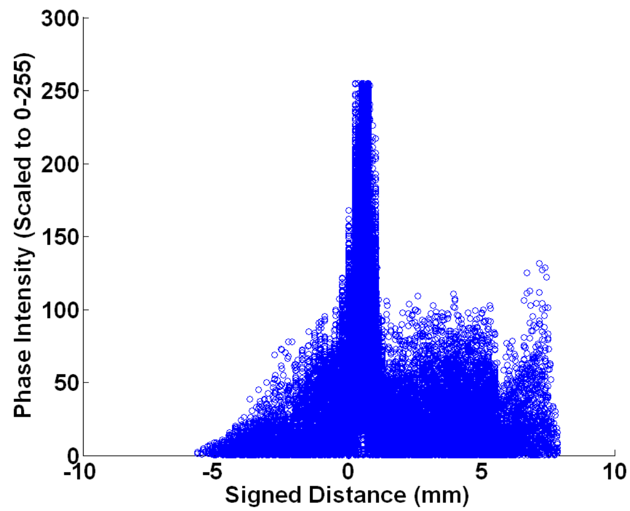

(a)

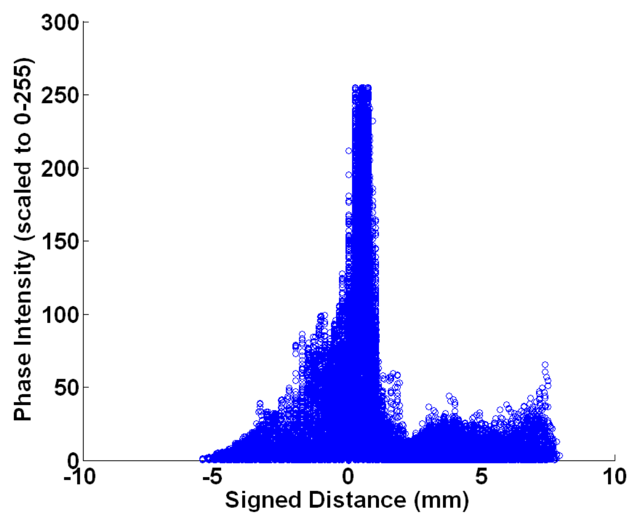

(b)

Fig.3.4 Signed distance plots for CT validated bovine experiment for volume 5. (a) Signed distance (mm) vs intensity plot using 2D PS method, (b) Signed distance (mm) vs intensity plot for the proposed 3D PS method demonstrating how the proposed 3D method is less sensitive to typical US artifacts.

Vertical Fracture Displacement

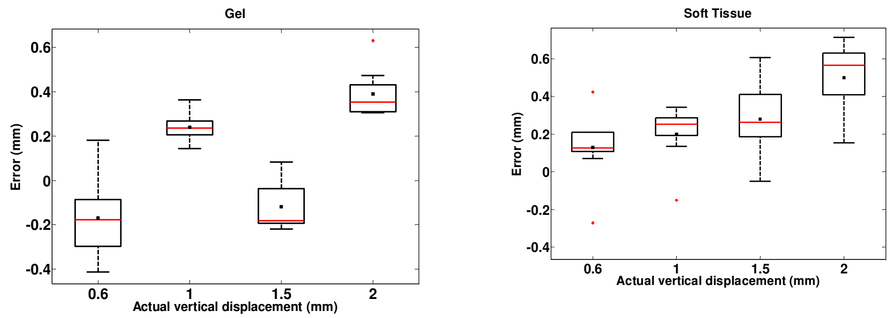

(a) (b)

Horizontal Fracture Displacement

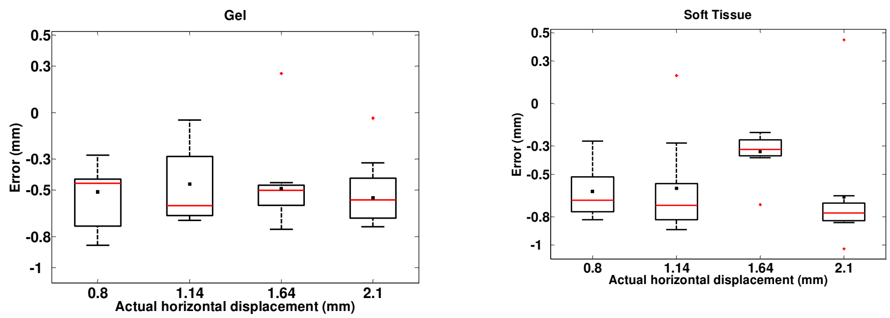

(c) (d)

Fig.3.5 Fracture misalignment results imaged through gel (left column) or a layer of bovine soft tissue (right column). The black point represents the mean, the red horizontal line shows the median and the box and whiskers represent the standard deviation and range of the data.

Qualitative Results

Figs 3.6, 3.7 and 3.8 show 3D phase symmetry images of an in-vivo human distal radius, an in-vivo human pelvis, and an ex-vivo pig leg, respectively. Comparing columns (b) and (c) of Figs. 3.6, 3.7 and 3.8 it can be seen that the 3D version of the phase symmetry images is markedly smoother than the 2D version (where each slice is treated independently) due to the fact that our proposed 3D method takes into account the information in the elevational direction as well. Furthermore, the 3D phase surfaces from Fig. 3.6 (column (b) bottom image) and Fig. 3.6 (column (b) bottom image) show that the proposed method is able to extract bone features even when a low frequency transducer (with lower resolution, which produces a weaker bone feature response) is used. Finally, it can be seen that fracture displacements can be clearly visualized in 3D phase symmetry images (Fig. 3.9). Fig. 3.9 also shows that the proposed method is able to extract a connected smooth surface even when the bone surface response is weak due to shadowing from muscle and fascia interfaces above the bone surface. In contrast, the 2D method is more severely affected by this overlying tissue and shows a small gap on the extracted bone surface (Fig. 3.9).

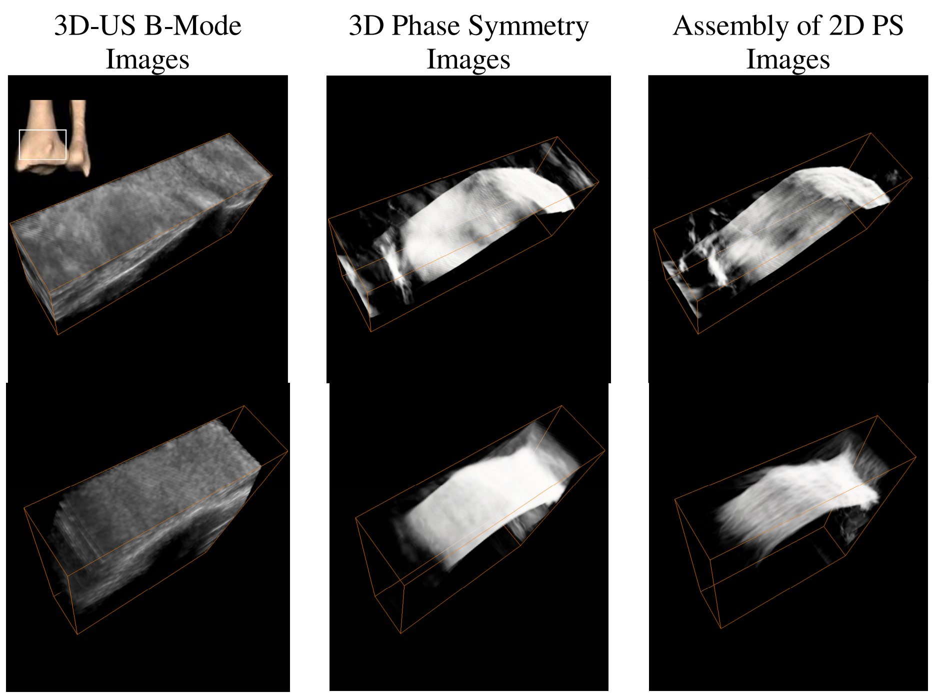

(a) (b) (c)

Fig.3.6 Qualitative results for in-vivo human distal radius scans. 3D mode US volumes obtained using 3D 5-12 MHz transducer (top) and 3D 4-8MHz transducer (bottom). The top left image also shows a 3D anatomical sketch of a human radius where the scanned area is highlighted by the white rectangle.

3D-US B-Mode Images | 3D Phase Symmetry Images | Assembly of 2D PS Images

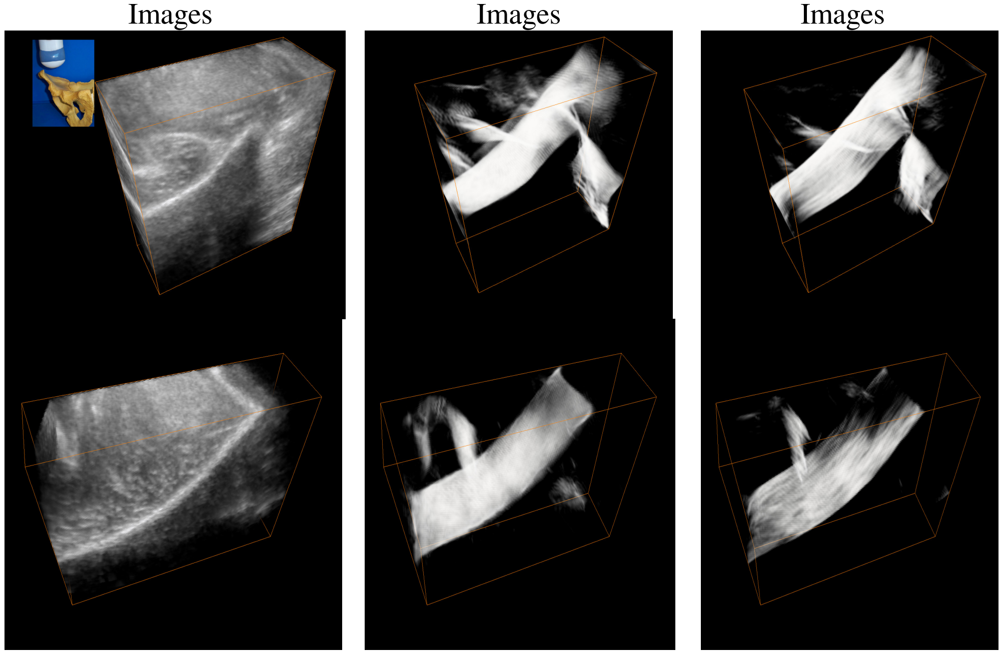

(a) (b) (c)

Fig.3.7 Qualitative results for in-vivo human pelvis scans. 3D US volumes obtained using 3D 5-12 MHz transducer (top) and 3D 4-8 MHz transducer (bottom). Top left image also shows a 3D anatomical sketch of a human pelvis with a 3D transducer showing the scanned area.

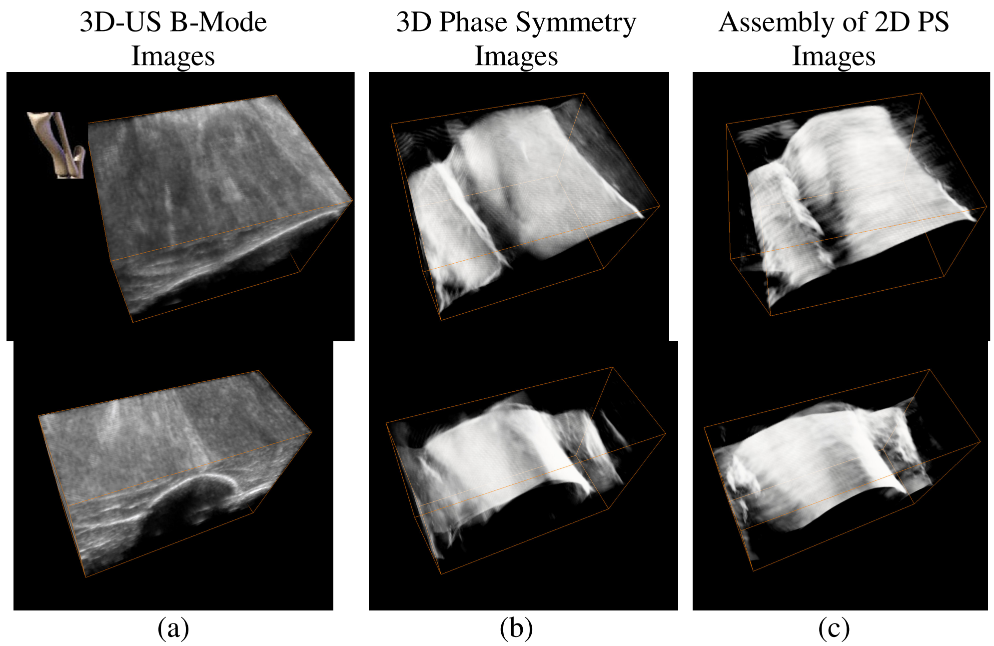

Fig.3.8 Qualitative results for ex-vivo pig leg scans. 3D US volumes of tibia and fibula (top) and tibia (bottom) obtained using 3D 5-12 MHz transducer. Top left image also shows a 3D anatomical sketch of a pig leg tibia and fibula bones.

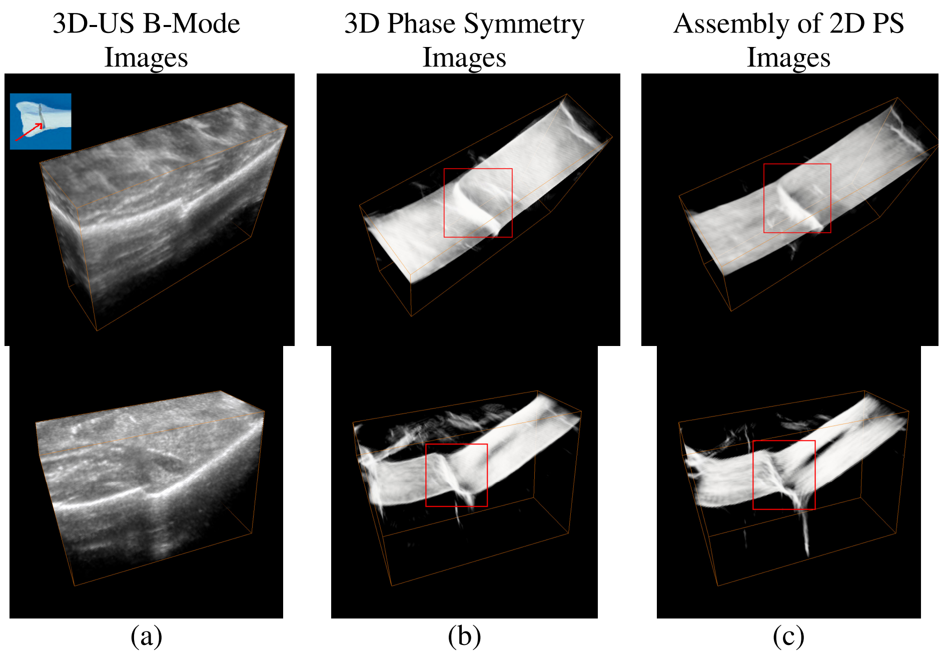

Fig.3.9 Qualitative results for fractured Sawbones model imaged with soft tissue overlaid. 3D US volumes of fractured Sawbones model (top) and same Sawbone where fractured pieces are displaced differently (bottom) obtained using a 3D 5-12 MHz transducer. The top left image also shows a 3D anatomical sketch of the scanned Sawbone with the fracture indicated by a red arrow. The red rectangles highlight the location of the fracture. Again the detected fracture is shown inside the red rectangle.

3.3 Surgical Tool Localization using 3D Local Phase Features

In this part we extend the work that was explained in detail in section 2.4 to 3D using the proposed 3D local phase symmetry method explained in this chapter. In non-ultrasound-based applications of local phase filtering, the outputs of the various filter responses are normally combined to produce a single feature map. However, we have observed that due to the directional characteristics of ultrasound, orientations perpendicular to the specular surface (K-wire or bone) tend to produce stronger responses to the surgical tool surfaces, while other orientations are more sensitive to ultrasound data artifacts. Therefore, instead of combining all filter responses, we relied on prior knowledge of the ultrasound image formation to combine the filter responses that provided the strongest echoes from the surgical tool. Finally, we applied thresholding to the 3D volume to extract the strong bone feature responses from the remaining weaker features.

3.3.1 Imaging and Experiments

The same experimental setup explained in section 2.4.1 was used as well. Therefore we refer the reader to the appropriate section for detailed explanation of the conducted experiment. The main difference from the previous setup was during the calculation of the error which is explained next. Rather than using the central slice we used all the slices where the K-wire tip was visible and averaged the error results obtained using the error calculation method explained in section 2.4.1.

3.3.2 Results

The tip of the K-wire was localized with a mean maximum localization error of 0.6mm when the tool was imaged inside the water tank. This number increased to 0.9mm when the K-wire was imaged inside the soft tissue (Fig. 3.10).

Fig. 3.11 shows that the 3D Log-Gabor filter successfully extracts 3D features corresponding to the surgical tool and the bone surface and it strongly attenuates US artifacts. There was remarkable separation of the K-wire from the bone surface and soft tissue, especially given the near-invisibility of the K-wire on the standard B-mode image.

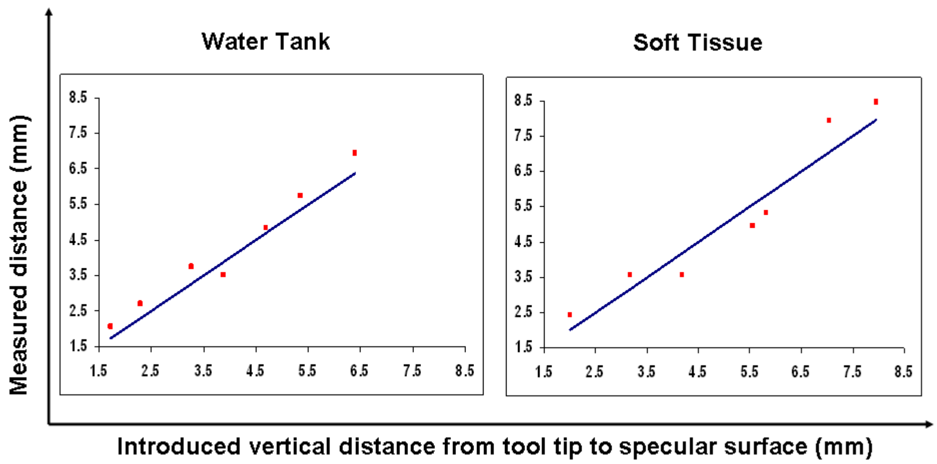

Fig.3.10 Quantitative results for the 3D K-wire tracking experiment. Comparing the error results we can see that its more difficult to localize the K-wire tip for a soft tissue interface.

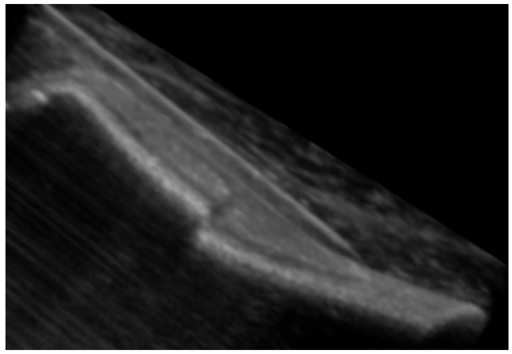

(a)

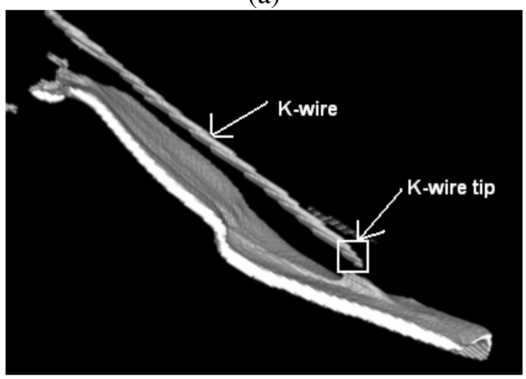

(b)

Fig.3.11 Surgical toll localization qualitative results. (a) 3D B-mode US volume of the soft tissue overlaid on the bone model with a K-wire inserted into the soft tissue. Note significant US artifacts and relative invisibility of K-wire, (b) corresponding thresholded 3D local phase volume showing the K-wire extracted clearly from soft tissue and other US artifacts.

3.4 Conclusion

We proposed a novel approach for accurate and fully automatic extraction of bone surfaces and surgical tools directly from 3D ultrasound volumes based on 3D local phase symmetry image features calculated using 3D Log-Gabor filters. The proposed method is an extension of the method explained in chapter 2 for 2D bone segmentation in US to 3D enabling the extraction of more accurate bone surfaces. Integrating the surface information along the axis perpendicular to the scan plane direction makes the proposed algorithm less sensitive to soft tissue artifacts and more sensitive to weak bone surface responses.

Using carefully designed experiments, we demonstrated how bone surface localization error could be decreased down to 42% of the error levels obtained with the earlier 2D PS bone localization method by incorporating the image's third dimension. The proposed bone surface localization accuracy was extensively and rigorously assessed using phantom bone models and ex-vivo porcine specimens. Quantitative results demonstrated a maximum mean error of 0.44 mm and a low standard deviation across the sampled points of only 0.16 mm. These errors were relatively independent of the depth of the bone interface and of the inclination of the transducer relative to the bone surface. Furthermore, the 3D phase method resulted in high localization accuracy even when the US beam was not perfectly perpendicular to the bone surface. Horizontal and vertical displacements between model bone fragments were also accurately measured with a maximum mean error under 0.6 mm.

The quantitative and qualitative results presented in this work were obtained using single-scale analysis. Although the method is amenable to multi-scale analysis, we have observed that the use of extra scales did not affect the accuracy results; however, it adds extra computation time. Nevertheless, we anticipate that multi-scale analysis will likely be useful in clinical situations when weak bone surface responses are expected due to swollen soft tissue. We plan to further investigate this issue in future clinical studies.

Our bone localization accuracy results (0.18-0.6 mm) were comparable to the best results reported by other groups, in particular, Foroughi et al. [14] and Kowal et al. [15] who showed mean errors in the range of 0.3-0.6 mm. Previously reported results, however, were obtained from 2D US studies in which the transducer was optimally aligned relative to the bone surface by a trained sonographer in order to achieve the best surface response. In addition, both of the cited previous studies incorporated bone surface connectivity information as part of their proposed framework which will likely fail when the imaged bone surface involves a fractured region and will thus limit the applicability of these methods to track fractures. In contrast, our proposed method performs very well with arbitrary probe orientations eliminating the need for a trained sonographer and is also able to handle fractured bone segments and gaps.

The average time to obtain a 3D US volume is an order of magnitude lower than acquiring a 3D fluoroscopy scan (about 10 s vs 120 s) [29], and we have shown that the phase symmetry processing time in a high-level programming environment (MATLAB) is about a third of the fluoroscopy acquisition time (43 s vs 120 s); we anticipate that we would be able to reduce this processing time significantly by implementing our algorithm in a lower-level language and optimizing the coding. This short acquisition and processing time would make 3D US especially attractive for use in orthopaedic fracture reduction surgeries where multiple scans are frequently needed to confirm the reduction.

We also showed that surgical tools such as K-wires could also be successfully extracted. 3D generalization of the local phase filter can produce remarkably clear images of the surgical tool positioned above a simulated bone surface.

Potential limitations of 3D US in orthopaedic surgery are related primarily to difficulties in obtaining a scan under typical operative conditions and to limited availability of 3D US machines. With regard to the first issue, US imaging typically requires the use of a coupling gel between the transducer and the patient; in a trauma situation, the patient may have an open wound above the bone, which could potentially interfere with the ability to place the US transducer in a reasonable position. We are currently conducting a clinical study to assess the potential opportunities and limitations of 3D US on an orthopaedic trauma service. The first results of our clinical study are explained in chapter 5. With regard to limited availability of 3D US machines, we expect that the number of such machines will increase in the future. Another limitation of the proposed method is the limited field of view of the US which could be problematic during the assessment of long bone fractures and might require volume stitching. This could introduce additional sources of error including speed of sound variations, refraction, miscalibration of the position tracker and non-constant tissue compression. Previous research by our group has already investigated methods for stitching 3D US volumes obtained from mechanical 3D transducers used in this study. However, quantification of the proposed method, using stitched 3D volumes or 3D volumes obtained using 2D tracked freehand transducers, remains an open question which we are aiming to answer in the future. Finally, parameter selection such as orientations, bandwidth, scale were so far done empirically by investigating different outputs of the 3D Log-Gabor filter. This will be further investigated in chapter 4 of this thesis work.

Our reported results are very encouraging and suggest a strong potential for success in using local phase processed images for bone localization and fracture assessment since the average accuracy required for such applications is typically in the range of 2-4mm [30]. A comparison of in-vivo scans of the human distal radius and pelvis showed that a true 3D analysis produced a noticeably smoother image of the bone surface than previously reported 2D analysis. We expect that such 3D processing will be of special importance during the assessment of fractures where good accuracy is needed to avoid malunions. Furthermore, since there is no need to align the imaging plane with the anatomical area of interest, evaluation of the fractured area can likely be performed more rapidly

3.5 References

[1] J.W. Cannon, J.A. Stoll, I.S. Salgo, H.B. Knowles, R.D. Howe, P.E. Dupont, G.R. Marx, P.J. del Nido, "Real time three dimensional ultrasound for guiding surgical tasks", *Journal of Computer Aided Surgery*, vol. 8, pp. 82-90, 2003.

[2] A. Fenster, D.B. Downey, "Three dimensional ultrasound", in *Annual Review of Biomedical Eng.*, vol. 2, pp. 457-475, 200.

[3] Y. Suematsu, G.R. Marx, J. K. Triedman, T. Mihaljevic, B.N. Mora, S. Takamoto, P. delNido, " Three dimensional echocardiography guided atrial septectomy: an experimental study", *Journal of Thoracic and Cardiovascular Surgery*, vol. 128, pp. 53-59, 2004.

[4] T.A.N. Hernes, F. Lindseth, T. Selbekk, A. Wollf, O.V. Solberg, E. Harg, O.M. Rygh, G.A. Tangen, I. Rasmussen, S. Augdal, F. Couweleers, G. Unsgaard, " Computer-assisted 3D ultrasound-guided neurosurgery: technological contributions, including multimodal registration and advanced display, demonstrating future perspectives", *The International Journal of Medical Robotics and Computer Assisted Surgery*, vol. 2, pp.45 – 59, 2006.

[5] T. Lange, S. Eulenstain, M. Hunerbein, P.M. Schlag, H. Lamecker, "Vessel based non-rigid registration of MR/CT and 3D ultrasound for navigation in liver surgery", *Journal of Computer Aided Surgery* ,vol. 8, pp. 228-240, 2003.

[6] B. Brendel, S. Winter, A. Rick, M. Stockheim, H. Ermert, "Registration of 3D CT and ultrasound datasets of the spine using bone structures", *Journal of Computer Aided Surgery*, vol. 7, pp.146-55, 2002.

[7] A.K. Jain and R.H. Taylor, "Understanding bone responses in B-mode ultrasound images and automatic bone surface extraction using a bayesian probabilistic framework", *in Proc. SPIE Medical Imaging*, vol. 5733, pp. 131-142, 2004.

[8] D.V. Amin, T. Kanade, A.M. Digioia, B. Jaramaz, “Ultrasound registration of the bone surface for surgical navigation”, *Journal of Computer Aided Surgery*, vol. 8, pp.1-16, 2003.

[9] M. Beek, M. Abolmaesumi, S. Luenam, R.E. Ellis, R.W. Sellens, D.R. Pichora, “Validation of a new surgical procedure for percutaneous scaphoid fixation using intra-operative ultrasound”, *Medical Image Analysis*, vol. 12, pp. 152-162, 2008.

[10] D.C. Barratt, C.S.K. Chan, P.J. Edwards, P.G. Penney, M. Slomczykowski, T.J. Carter, D.J. Hawkes, “Instantiation and registration of statistical shape models of the femur and pelvis using 3D ultrasound imaging”, *Medical Image Analysis*, vol. 12, pp.358-374, 2008.

[11] G.P. Penney, D.C. Barratt, C.S.K Chan, M. Slomczykowski, T.J. Carter, P.J. Edwards, D.J. Hawkes,”Cadaver validation of intensity-based ultrasound to CT registration”, *Medical Image Analysis*, vol. 10, pp. 385-395, 2006.

[12] J. Tonetti, L. Carrat, S. Blendea, P. Merloz, J. Troccaz, S. Lavallee, J.P. Chirossel, “Clinical results of percutaneous pelvic surgery: Computer assisted surgery using ultrasound compared to standard fluoroscopy”, *Journal of Computer Aided Surgery*, vol. 6, pp.204-211, 2001.

[13] V. Daanen, J. Tonetti, J. Troccaz, “A fully automated method for the delineation of osseous interface in ultrasound images”, *in. Proc Int. Conf. Med. Image Compt. Computer- Assisted Intervention,* vol. 3216, pp. 549-557, 2004.

[14] P. Foroughi, E. Bocto, M.J. Swatrz, R.H. Taylor, G. Fichtinger, “Ultrasound bone segmentation using dynamic programming”, *in Proc. of IEEE Ultrasonics Syposium*, 2007, pp. 2523-2526.

[15] J. Kowal, C. Amstutz, F. Langlotz, H. Talib, M.G. Ballester, “Automated bone contour detection in ultrasound B-mode images for minimally invasive registration in computer assisted surgery an in vitro evaluation”,

The International Journal of Medical Robotics and Computer Assisted Surgery, vol. 3, pp. 341-348, 2007.

[16] A. Kryvanos, ”Computer assisted surgery for fracture reduction and deformity correction of the pelvis and long bones”, PhD thesis. University of Mannheim, Germany, 2002.

[17] R. Dosil, X.M. Pardo, X.R. Fernandez-Vidal, “Data driven synthesis of composite feature detectors for 3D image analysis”, *Journal of Image and Vision Computing*, vol. 24, pp. 225-238, 2006.

[18] P. Kovesi, “Image features from phase congruency”, Videre: A Journal of Computer Vision Research, vol. 1, pp. 1-26, 1999

[19] P. Kovesi, “Image features from phase congruency”, Videre: A Journal of Computer Vision Research, vol. 1, pp. 1-26, 1999.

[20] M. Mulet-Parada and A.J. Noble, “2D+T boundary detection in echocardiography”, *Medical Image Analysis*, vol. 4, pp. 21-30, 2000.

[21] N. Otsu, "A threshold selection method from gray-level histogram," *IEEE Transactions on Systems, Man, and Cybernetics*, vol. 9, pp. 62-66, 1979.

[22] J. M. S. Prewitt and M. L. Mendelsohn, "The analysis of cell images," *in Annals of the New York Academy of Sciences*, vol. 128, pp. 1035-1053, 1966.

[23] W. Tsai, "Moment-preserving thresholding: a new approach," *Computer Vision, Graphics, and Image Processing*, vol. 29, pp. 377-393, 1985.

[24] J. N. Kapur, P. K. Sahoo, and A. K. C. Wong, "A new method for gray-level picture thresholding using the entropy of the histogram," *Computer Vision, Graphics, and Image Processing*, vol. 29, pp. 273-285, 1985.

[25] J. M. S. Prewitt and M. L. Mendelsohn, "The analysis of cell images," *in Annals of the New York Academy of Sciences*, vol. 128, pp. 1035-1053, 1966.

[26] A. P. Dempster, N. M. Laird, and D. B. Rubin, "Maximum likelihood from incomplete data via the EM algorithm," *Journal of the Royal Statistical Society, Series B*, vol. 39, pp. 1-38, 1977.

[27] J. Kittler and J. Illingworth, "Minimum error thresholding," *Pattern Recognition*, vol. 19, pp. 41-47, 1986.

[28] C. A. Glasbey, "An analysis of histogram-based thresholding algorithms," *CVGIP: Graphical Models and Image Processing*, vol. 55, pp. 532-537, 1993.

[29] J. Geerling, S. Zech, M. Citak, K. Knobloch, M. Frink, T. Hufner, C. Krettek, M. Richter, ”Evaluation of distal fibula position after closed reduction and syndesmotic screw placement with intraoperative three dimensional imaging (ISO-C-3D)”, *Fuß &Sprunggelenk*, vol. 5, pp.254-261, 2007.

[30] R. Phillips, “The accuracy of surgical navigation for orthopaedic surgery”, *Current Orthopaedics*, vol. 21, pp. 180-192, 2007.

Chapter 4 Data-Driven Parameterization for Automatic Bone Localization in Ultrasound Using Log-Gabor Filter Based Phase Features*

4.1 Introduction

In chapters 2 and 3 we have shown for the first time that bone surfaces could be extracted automatically and with sufficient accuracy from 2D and 3D US data using local phase features. Although local phase measures can be quite successful in extracting important image features, they remain somewhat sensitive to the underlying filter parameters used. Previous approaches using

---

* A version of this chapter will be submitted for publication. I. Hacihaliloglu, R. Abugharbieh, A. Hodgson, R. Rohling. "Data-Driven Parameterization for Automatic Bone Localization in Ultrasound Using Log-Gabor Filter Based Phase Feature".

local phase relied on empirical selection of appropriate filter parameters, which was typically performed by trial and error and ad hoc investigation of filter outputs on samples of US images depicting a certain anatomical area of interest ([1, 2, 3, 4]).Once acceptable filter parameters were found, they were typically fixed for subsequent application to new data. The difficulty in relating correct parameter choices to the properties of the image and image-processing task has thus inhibited more widespread use of phase-based techniques. Specifically, in ultrasound image processing, the effect of each parameter, as well as the effects of their interaction remains unclear. In this work, we present a novel method for automatic selection of the scale, bandwidth, orientation and angular bandwidth parameters of a Log-Gabor filter based phase symmetry (PS) measure in US images, specifically in the context of bone surface localization. The proposed approach incorporates the use of principal curvature computed from the Hessian matrix and directional filter banks in a phase scale-space framework. Our technique relies on contextual information obtained solely from image content.

4.1.1 Main Contributions

The main contributions of this chapter can be summarized as follows:

1. We show the importance of correct filter parameter selection in the extraction of local phase features and develop a method to automatically select 2D Log-Gabor filter parameters to extract bone surfaces from US data.
2. We validate the proposed method with carefully designed in-vitro experiments and demonstrate 35% improvement in accuracy of bone surface localization compared to empirically set parameterization results [1, 2].
3. We compare the proposed method with the filter parameters obtained through an exhaustive search procedure which gave the best

localization accuracy results and show that the proposed method achieves similar filter parameters.

The remainder of this chapter is organized as follows. In Section 4.2 we give a brief introduction to Log-Gabor filter and discuss the important parameters that need to be optimized for extracting bone surfaces from US data. Section 4.3 presents the proposed data-driven filter parameterization approach. Experimental setup for quantitative validation is explained in section 4.4. Qualitative and quantitative results are given in section 4.5 and finally we present our conclusions in section 4.6.

4.2 Review of Log-Gabor Filter Based Analysis of Bone in Ultrasound

In chapters 2 and 3 we have presented a local phase-based method for extracting ridge-like features, similar to those that occur at soft tissue/bone interfaces, using a PS measure. Here, we propose an improvement to such an approach by presenting complete automation of the parameter selection process. In this chapter the focus is on extraction of ridge-like features but could be extended to other feature types.

A ridge can be thought of as a one dimensional curve representing an axis of local symmetry. It is well known that symmetric features can be easily extracted using local phase information [3]. Local phase of a one dimensional (1D) signal can be obtained by convolving the signal with a pair of band-pass quadrature filters (an odd filter and an even filter). Using the two filters in quadrature enables the calculation of signal amplitude and phase at a particular scale (spatial frequency) at a given spatial location. One choice of quadrature filters is the 2D Log-Gabor filter, $R(\omega,\omega_0)$, which can be constructed with an arbitrary bandwidth. In order to obtain simultaneous localization of spatial and frequency information, analysis of the signal must be done over a narrow range (scale) of frequencies at different locations in the signal. This can be achieved by constructing a filter bank using a set of quadrature filters created from rescalings of the Log-Gabor filter.

This analysis can be extended into two dimensions (2D) where a filter tuned to a particular orientation ϕ_0 in the frequency domain (ω) is constructed by masking a radial Log-Gabor function ($R(\omega,\omega_0)$) with an angular Gaussian ($G(\phi,\phi_0)$) tuned to ϕ_0:

$$G(\omega,\phi) = R(\omega,\omega_0)\times G(\phi,\phi_0) = \exp(\frac{(\log(\omega/\omega_0))^2}{2(\log(\kappa/\omega_0))})\times\exp(\frac{(\phi-\phi_0)^2}{2\sigma_\phi}) \qquad 4.1$$

Here κ is the standard deviation of the filter in the radial direction and ω_0 is the filter's center spatial frequency. The term κ/ω_0 is related to the bandwidth (β) of the filter with β= -2 $(\ln 2/2)^{(-0.5)}$ $\ln(\kappa/\omega_0)$ [2].

The scaling of the radial Log-Gabor function is achieved by using different wavelengths that are based on multiples of a minimum wavelength, $\lambda_{\min}$, which is a user-defined parameter. The relationship between the filter scale m, and the filter center frequency ω_0 is set as $\omega_0=1/\lambda_{\min}\times(\delta)^{m-1}$ where δ is a scaling factor defined for computing the center frequencies of successive filters. $\sigma_\phi=\Delta\phi/s$ defines the angular bandwidth $\Delta\Omega = 2\,\sigma_\phi\,(2\log 2)^{-05}$ where $\Delta\phi$ is the angular separation between neighbouring orientations and is defined as $\Delta\phi$=180°/N_r, and N_r denotes the total number of orientations used. The parameter s is the standard deviation of the Gaussian spreading function in the angular direction that describes the filter's angular selectivity. To obtain higher orientation selectivity, the angular function must become narrower. Steering of the filter is achieved by changing its angle (ϕ_0). After investigating different filter outputs empiricially we have found that selecting 2 scales and 6 orientations (0°-150° with 30° increments) with σ_ϕ=25°, κ/ω_0=0.25, δ=3 and a filter wavelength of $\lambda_{\min}$ =25 pixels offered good spectral coverage and orientation resolution and produced good bone surface localization in the presence of speckle. The obtained results using these filter parameters were presented in chapter 2. An example of a 2D Log-Gabor filter is given in Fig.4.1.

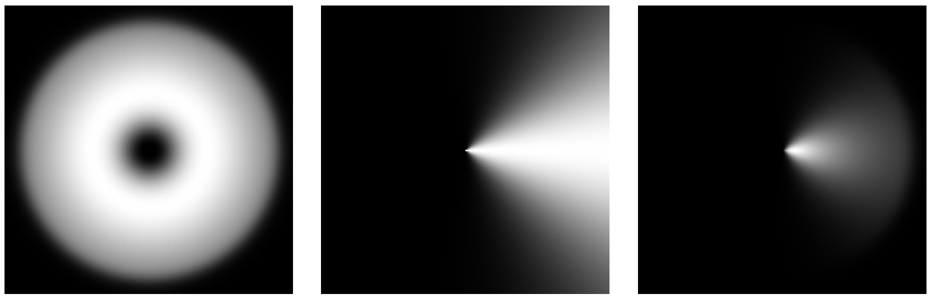

(a) (b) (c)

Fig.4.1 An example of a 2D Log-Gabor filter with λ_{min} =25, δ =3, ϕ_0=0°, σ_ϕ=30°, κ/ω_0=0.25, s=1. (a) Log-Gabor component $R(\omega,\omega_0)$ of the filter, (b) Angular Gaussian component $G(\phi,\phi_0)$ of the filter, (c) product of the two components which represents the 2D Log-Gabor filter in the frequency domain.

4.3 Proposed Data Driven Filter Parameterization

The design of the Gabor filter bank relies on the proper selection of a set of filter parameters: bandwidth (β), scale (λ_{min}), angular bandwidth ($\Delta\Omega$) and orientation (ϕ_0). The possible combinations of these various parameters directly affect the filter's ability to accurately extract local phase image features. In the following sections, we analyze the Log-Gabor filter response in detail and present a data-driven approach for contextual selection of its main parameters. Our approach first optimizes the bandwidth parameter according to image acquisition properties. We then optimize for the scale parameter based on a set of initial filter orientations extracted through analysis of bone surface orientation information from the B-mode US image. We finally optimize for the orientations and angular bandwidth parameters. The flowchart of the proposed framework is given in Fig.4.2.

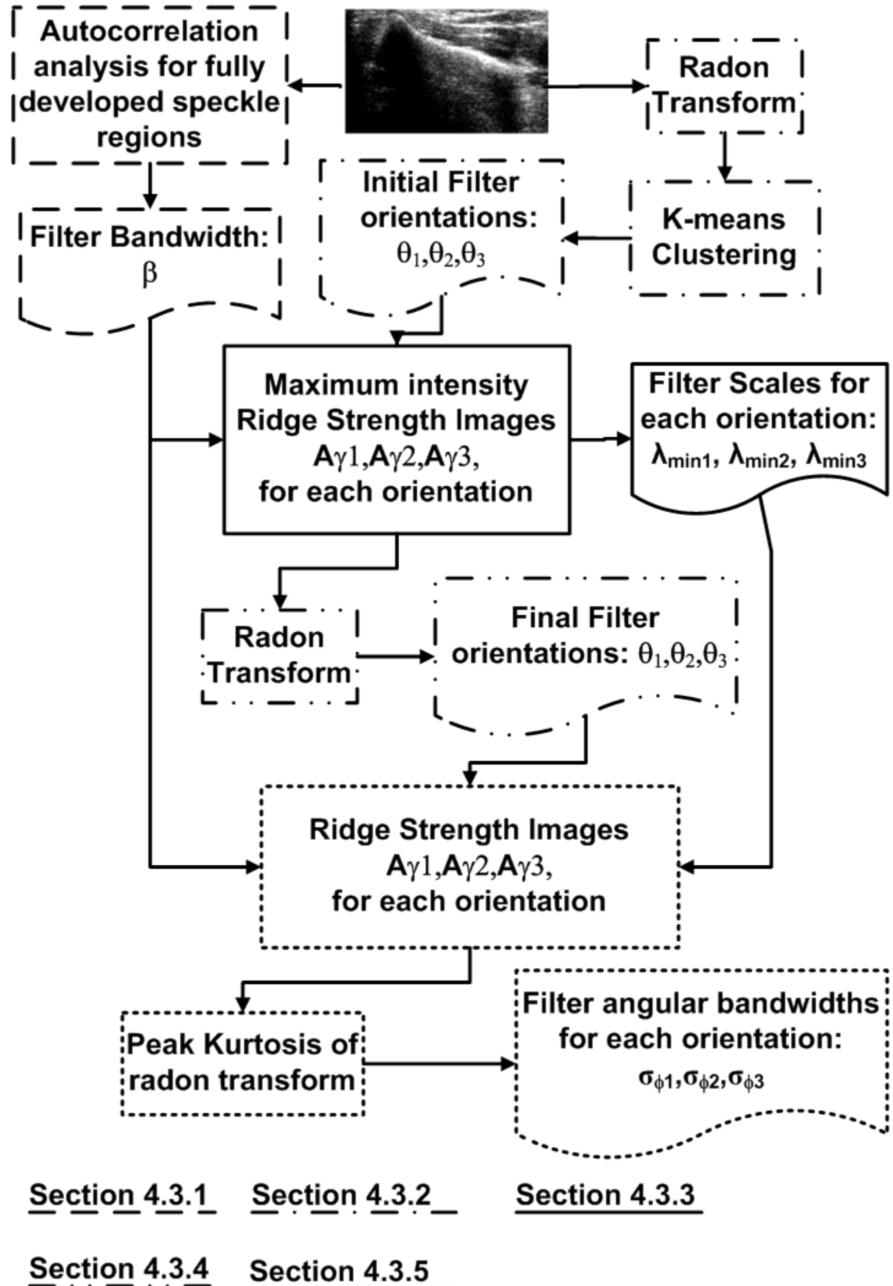

Fig.4.2 Flowchart of the proposed data driven parameterization of Log-Gabor filter for bone surface localization from B-mode US images. Each section of the proposed framework is shown with a different line pattern.

4.3.1 Filter Bandwidth Selection

The proper filter bandwidth ($\beta=-2\ (2/\ln 2)^{(-0.5)}\ln(\kappa/\omega_0)$) in the radial direction is related to both the spatial extent of the speckle and boundary responses in the image. Therefore, we first estimate the image speckle size by selecting a set of images covering a range of depths acquired by the US transducer used in the imaging (in our experiments, the transducer's center ultrasound frequency = 7.5 MHz, image depth setting ranged between 1.9cm-7.2cm). By analysing a region with fully developed speckle from each image, we compute the autocorrelation of each region, and extract the full-width at half-maximum (FWHM) value of these autocorrelations which we then use as a measure of the speckle size [5]. We compute the ratio, κ/ω_0, for each image using:

$$\kappa/\omega_0 = \exp(-\frac{1}{4}\sqrt{2\times ln(2)}\times FWHM \times r) \qquad (4.2)$$

where r is the pixel size in mm. We average the κ/ω_0 ratio over the set (in our case 25) different B-mode US test images. The resultant average is then set as the filter bandwidth. Note that selecting a bandwidth significantly greater than this value (i.e. selecting a smaller value for κ/ω_0) will result in a filter that fails to separate small scale speckle features from larger scale boundary responses. On the other hand, selecting a significantly lower bandwidth will reduce the accuracy of the boundary detection and cause blurring of the detected bone boundary (Fig.4.3).

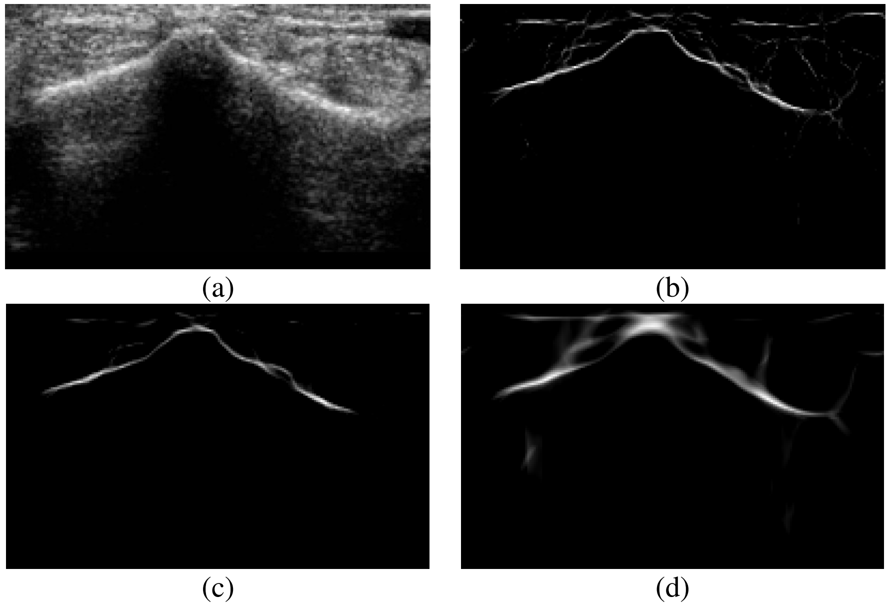

Fig.4.3 Effect of filter bandwidth selection on local phase based bone detection. (a) in-vivo B-mode US image of human distal radius, (b) – (d) PS images obtained using κ/ω_0 values of 0.05, 0.24, and 0.55 respectively. (b) illustrates unintended speckle detection at high bandwidths and (d) illustrates bone boundary blurring at low bandwidths while (c) reflects the effect of selecting an appropriate bandwidth where the PS captured continuous sections of the bone with little influence exhibited by soft-tissue interfaces and speckle.

4.3.2 Initial Filter Orientation Selection

The orientation of the Log Gabor filter is controlled by the angular Gaussian function ($G(\phi,\phi_0)$). During the calculation of the PS metric, the filter is directed at a number of orientations. Commonly, six orientations are employed to cover the entire angular range (0°-180° with 30° increments) with the responses subsequently averaged [1, 2, 4]. However, given the highly directional nature of ultrasound bone image data, integration of the responses from all these different filter orientations in fact largely degrades the PS response due to the inclusion of many non-relevant filter orientations. Noting that the strongest ridge features appear when the filter orientation is perpendicular to the bone surface (Fig. 4.4), identifying and combining filter angles which produce strong responses will therefore likely enhance feature extraction (Fig. 4.5).

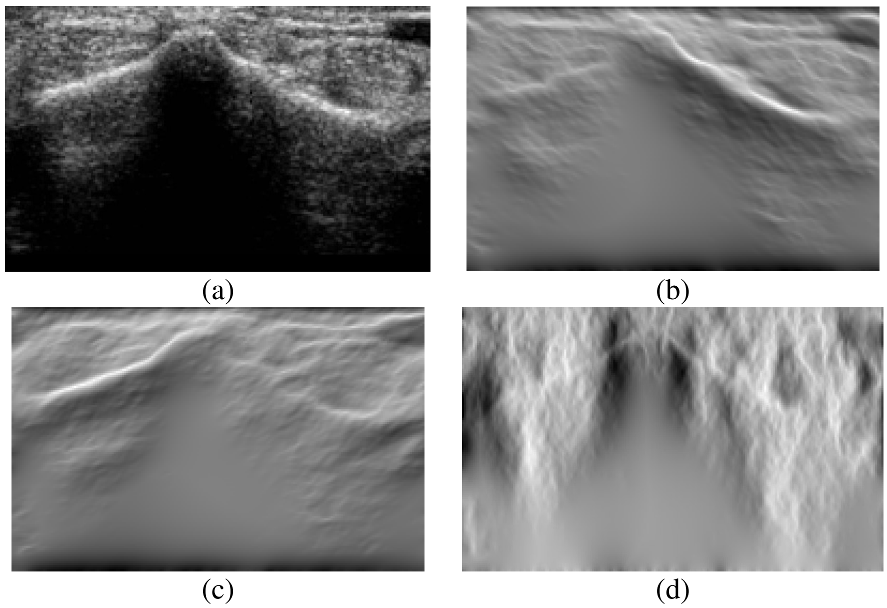

Fig.4.4 Effects of filter orientation selection. (a) B-mode US of in-vivo distal radius, (b) filter response at ϕ=60°, (c) filter response at ϕ=120°, (d) filter response at ϕ=0°. All images were produced at a fixed filter scale of λ_{min} =25 and κ/ω_0 =0.25.

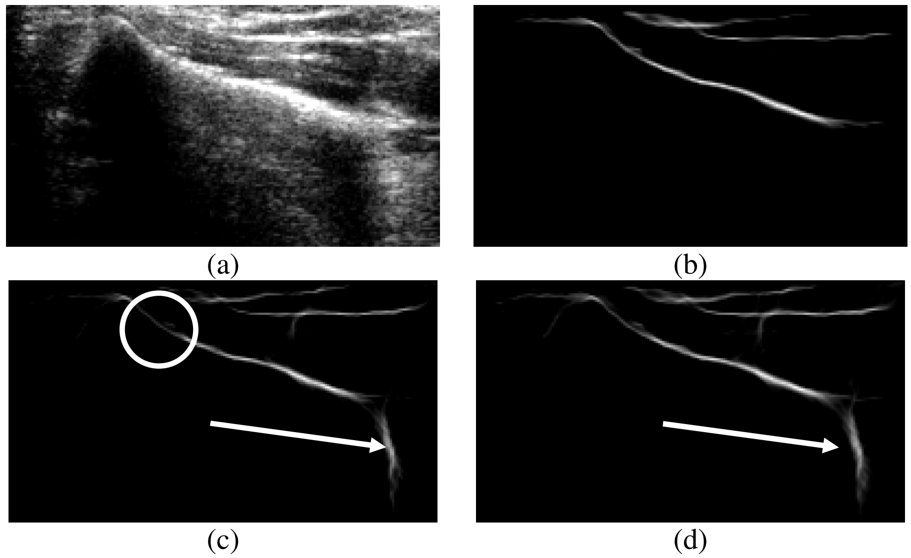

Fig.4.5 Effect of varying the number of orientations used. (a) B-mode US image of in-vivo human distal radius. (b) PS image using 3 orientations (58° 74° 89°), (b) PS image using 6 orientations (0°-150° with 30° increments), (c) PS image using 10 orientations (0°-270° with 30° increments). The white arrows point out extracted phase features that are not bone surfaces (i.e. artefacts of combining orientations that are not close to perpendicular to the bone surface during the calculation of PS). The white circle points to a location of a degraded bone surface due to the inclusion of less informative orientations with weaker bone responses.

Bone surfaces in B-mode US images typically appear as elongated line-like objects with a higher intensity compared to the other image features. The same in fact applies to the corresponding PS images. Therefore, integration along a bony feature produces a higher intensity value than doing the integration along a non-bony feature. Using this simple fact, we employ the radon transform (RT) in order to detect the orientation of such line-like structures. To automatically define meaningful starting angles for our filter, we initially cluster the RT (obtained from the B-mode US image) image using k-means clustering (Fig. 4.6).

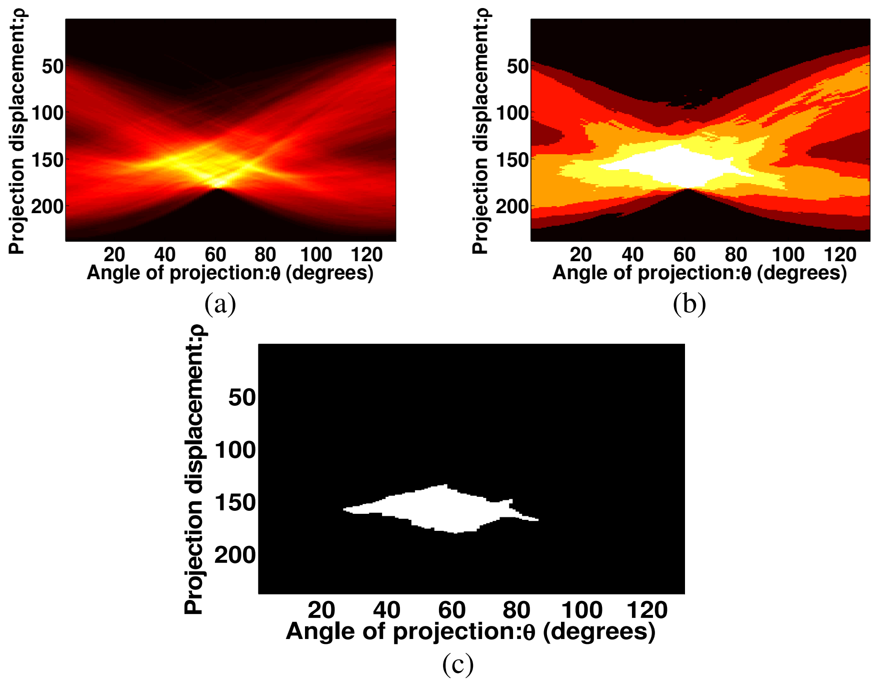

Fig.4.6 Filter orientation selection step. (a) RT of B-mode US image in Fig.4.3 (a), (b) k-mean clustered RT of (a), (c) the cluster corresponding to the highest RT values. The three initial angles deduced from this cluster are 66°, 88° and 106°. Detailed explanation on how these three angles were calculated is given in the below paragraph.

The projection angles corresponding to the peak values of the RT reflect the angles that are perpendicular to the high intensity features, bone surfaces in our case. Those angles are therefore used for initializing the orientations of the Log-Gabor filter. Three initial filter angles are selected, which we choose from the cluster that corresponds to the peak values of the RT (Fig. 4.6. (c)). Specifically, the mean value of the projection angles corresponding to the RT values in that chosen cluster and two additional angles set at ±1 standard deviation within the thresholded region are used. These three initial angles are used as the initial filter angle parameters during the calculation of the filter scale as will be explained in section 4.3.3.

4.3.3 Filter Scale Selection

Local image PS is computed by convolving the image with a number of scaled Log-Gabor filters. Each scaling is designed to pick out particular features of the image being analyzed with results typically integrated over multiple scales (in addition to multiple orientations) [2]. Since boundaries are extracted by analyzing the PS measure over a range of scales, correct scale selection is of major importance. When using very small scales, the filters become highly sensitive to speckle. Selecting larger scales blurs the extracted bone features. Simply integrating different filter scales for PS calculations is typically insufficient as it results in PS images that either extract speckle or blurs the detected features (in our case bone boundaries), as demonstrated in Fig.4.7.

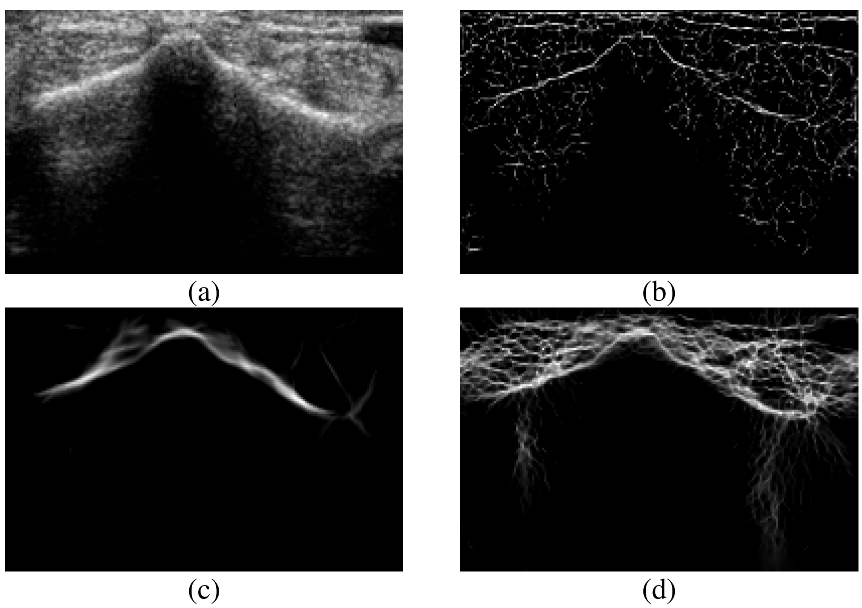

Fig.4.7 Effects of filter scale selection. (a) Original B-mode US image of in-vivo distal radius, (b) PS obtained using a scale value of λ_{min} =2, (c) PS obtained using a scale value of λ_{min} =88, (d) PS obtained by combining the results of both scales (2 and 88).

Line enhancing filters based on multiscale eigenvalue analysis of the Hessian matrix have been commonly used to extract vessel-like structures in 2D and 3D medical images [6]. The scale selection approach we present in this chapter is inspired by these studies where we use the Log-Gabor filter response as the input to the Hessian matrix defined as in (4.3):

$$H = \begin{bmatrix} L_{xx} & L_{xy} \\ L_{yx} & L_{yy} \end{bmatrix}, \text{with } L_{ab} = \frac{\partial^2 L}{\partial a \partial b} \tag{4.3}$$

L is an image obtained by convolving the US image with a Log-Gabor filter at a particular scale. Here, the subscripts x and y represent spatial derivatives in the x and y directions. At this stage, the orientation of the Log-Gabor filter during the scale setting step is set to the initial filter angle calculated from the B-mode US image as outlined in section 4.3.2. We calculate a ridge strength measure, $A_\gamma=t^{2\gamma}((L_{xx}-L_{yy})^2+4L_{xy}^2)$, which is the square of the γ normalized eigenvalue difference, and t is the scale of the filter ($t=\lambda_{min}$) [7]; see Fig. 4.8. This metric in our context measures the 'ridgeness content' of an image, since our main interest here is in localizing bone contours, which generally appear as ridges in US images. The optimal scale is thus defined as the one corresponding to the maximal ridgeness content in the Gabor filtered image. In order to define the optimum global filter scale, which highlights the most significant ridge content in the image, we analyze the intensity distribution of A_γ over all possible scales (e.g. ranging from 2-150 in our experiments). We then select the scale where the sum of the intensities achieves a maximum value as the optimal filter scale (Fig.4.8 (d)). This is based on the observation that at the optimal scale the response of the filter will produce a sharp ridge feature aligned with the bone surface, whereas significantly different scales will result either in detection of speckle or blurred bone surfaces which will reduce the intensity sum (Fig. 4.8 (a)–(c)). This analysis is repeated for each orientation separately.

(a)

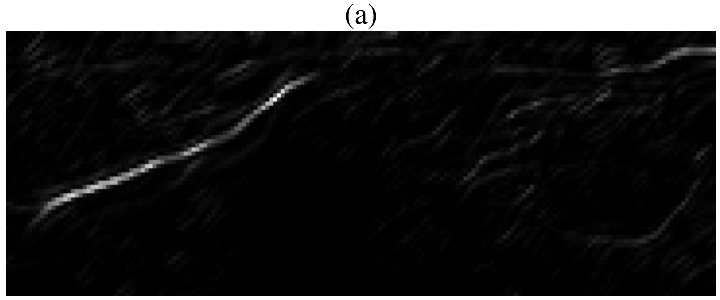

(b)

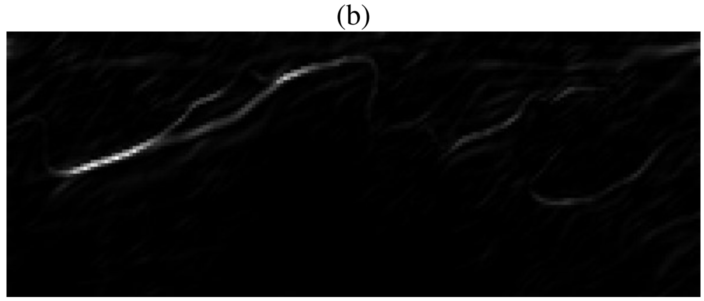

(c)

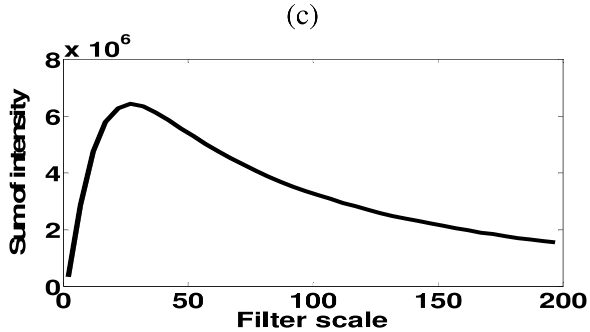

(d)

Fig.4.8 Effects of filter bandwidth selection. A_γ ridge strength obtained from B-mode US image in Fig.4.3 (a) for a fixed filter orientation (140°) and scale (a) λ_{min}=10, (b) λ_{min}=35, (c) λ_{min}=140. Investigating (a)-(c) we see that the bone ridge content in (b) is the strongest and the most continuous. (d) Filter scale versus sum of intensity values of A_γ.

4.3.4 Final Filter Orientation Selection

In order to select the final filter orientations, the RT is re-calculated for the ridge strength image A_γ as obtained using the scale calculated in section 4.3.3. Figure 4.9 shows the calculated RT of the A_γ for the initial angles of 66° and 106° as an example. Noting that the RT has high intensity locations indicating the presence of line-like structures in the image, the maximum value of the RT simply indicates the main orientation of the bone, since it has the strongest filter response, and is thus used to set the final filter orientation. Figure 4.9 (c) and (d) show an example where the angles corresponding to the peak occur at 62° and 115°, hence the initial angles set as per section 4.3.2 are corrected based on these new calculated angles. We would like to note that this analysis is done for all the three initial filter angles obtained from section 4.3.2. In Fig. 4.9 we only show two angles.

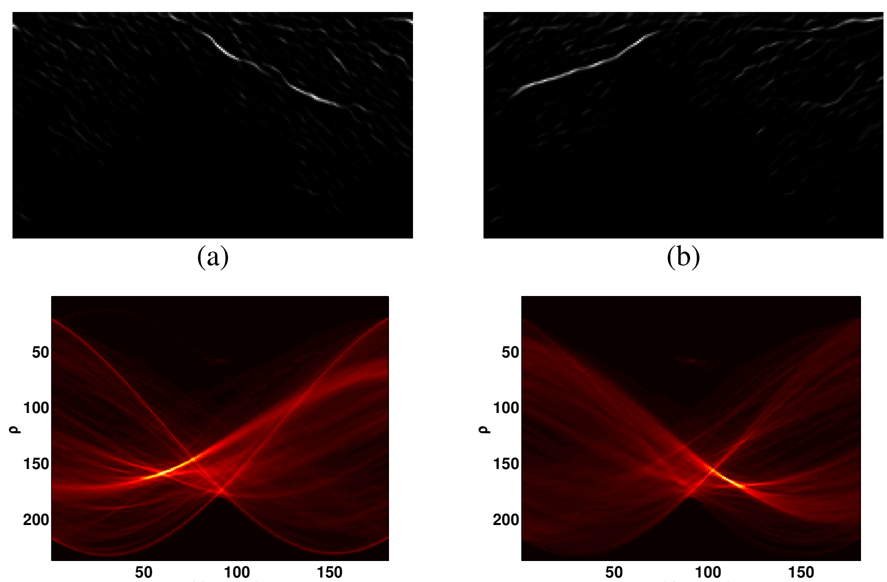

(a) (b) (c) (d)

Fig.4.9 Filter orientation selection. (a) & (b): A_γ obtained using the initial filter angle (a) ϕ=66° and(b) ϕ=106° which are calculated from the RT of the B-mode image Fig.4.3, (c) & (d) RT of (a) & (b) showing new peaks at 62° and 115°, respectively. The two initial orientation of the filter is thus fine-tuned to 62° and 115°.

4.3.5 Filter Angular Bandwidth Selection

The angular bandwidth parameter, $\sigma_{\o}= \pi/(No/k)$, corresponds to the standard deviation of the Gaussian spreading function in the angular direction and describes the filter's angular selectivity. Here No is the number of filter orientations and "k" is the constant that is used to define the filter angular bandwidth, which is a user defined parameter. Investigating the example in Fig. 4.10, we can see how at large angular bandwidths, the Log-Gabor filter acts as a smoothing filter without being sensitive to any orientation. On the other hand, for small angular bandwidths, the filter acts like a line detector degrading the curvature of the bone surface as it becomes less sensitive to curvature making the extracted features look like short line segments. Therefore, using the same analysis we used in our filter scale selection process would not be suitable to set $\sigma_{\o}$ since the intensity distribution of A_{γ} over all possible angular bandwidths will give a peak at very large angular bandwidths. An example for his situation is given in Fig. 4.11 (a) where selecting the peak value of the angular bandwidth versus sum of intensity values of A_{γ} plot corresponds to a filter response shown in Fig.4.10 (a).

Based on these observations, we thus analyze the kurtosis of the RT of A_{γ} over different angular bandwidth values. Higher kurtosis means more of the variance is due to infrequent extreme deviations (A_{γ} image with uniform black background with sharp high intensity bone boundary), as opposed to frequent modestly-sized deviations (A_{γ} image with uniform black background degraded with speckle/ soft tissue interfaces or short line segments with different intensity values). We select the bandwidth corresponding to the peak kurtosis value (Fig.4.11 (b)). During this stage, the A_{γ} images used are obtained using the optimum filter scale as calculated in section 4.3.3.

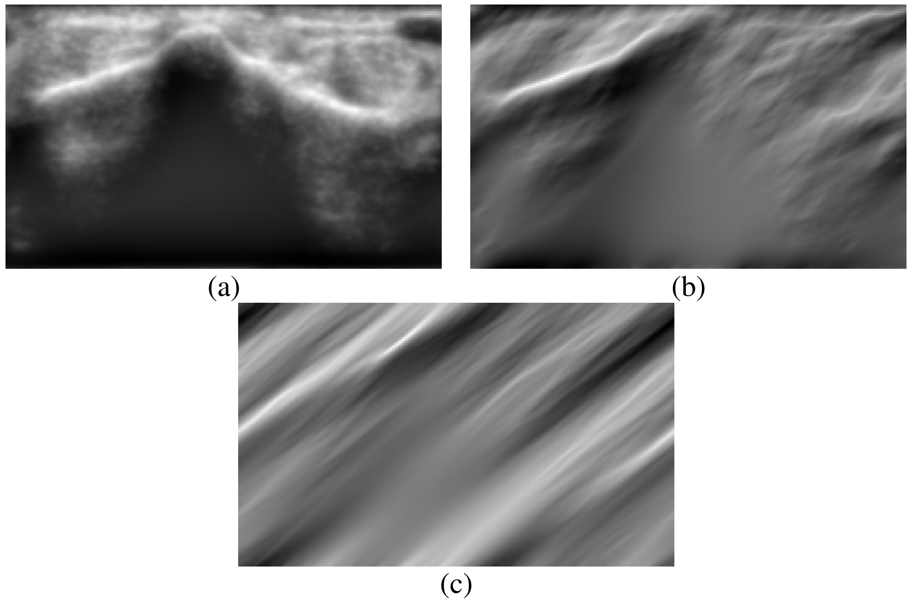

Fig.4.10 Effect of varying angular bandwidth on the Log-Gabor filter output for filter orientation 115°. (a), (b) and (c) are Log-Gabor filter outputs obtained using angular bandwidth values of σ_{ϕ}=120°, σ_{ϕ} =30°, σ_{ϕ}=7.5° respectively.

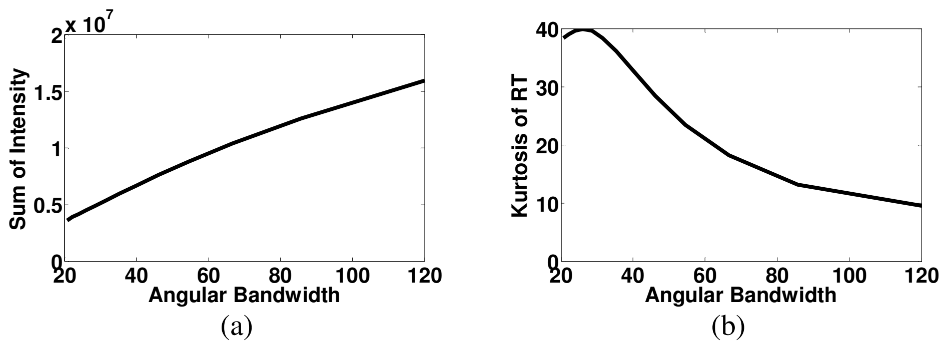

Fig.4.11 Angular bandwidth selection step. (a) Filter angular bandwidth versus sum of intensity values of A_{γ}. (b) Filter angular bandwidth versus kurtosis of RT obtained from calculating the RT of A_{γ}.

4.4 Experimental Setup for Quantitative Validation

The same experimental setup explained in chapter 3 section 3.2.1 was used for quantitative validation of the proposed method. Therefore, we will not go into the detailed explanation of the constructed phantom and the scanning process and refer the reader to the appropriate section for the details. The gold standard surface was again provided from the obtained CT scan. The main difference of the surface validation experiment from the previously explained one is the extraction of the bone surfaces from US scans using the PS method which is explained next.

The PS images were obtained using the 2D Log-Gabor filter which is designed with the filter parameters obtained using the proposed framework. In order to compare the localization accuracy with our previous method, explained in chapter 2, we also obtained PS images with the Log-Gabor filter designed using filter parameters (given in chapter 2) which were empirically selected by investigating different filter outputs. The error calculations were calculated the same way as explained in chapter 3 section 3.2.1. This surface localization accuracy assessment was repeated for 15 different volumes obtained from the same specimen by processing each 2D slice of the US volume and averaging the results.

In order to show that the proposed method is less sensitive to typical US artifacts and soft tissue interfaces we also calculated the signed distance values corresponding to all PS intensity values rather than the maximum PS intensity in the vertical direction as was done for surface localization accuracy assessment. This analysis was again repeated by processing each 2D slice of the 3D US volume and averaging the results.

Finally, we have also performed an exhaustive search parameter selection procedure in order to compare these parameters and the localization accuracy achieved using these parameters with the parameters/accuracy found by using the proposed method. The ranges of parameters that have been tested are given in Table 4.1. PS images were extracted using all the possible parameter combinations and calculating the previously explained signed distance error metric. The optimum parameters were chosen as the ones that gave the lowest mean error.

Table 4.1 The ranges of the filter parameters that were used as an input to the exhaustive search algorithm.

Parameters	Start Value	Increment	End Value
Filter Bandwidth (κ/ω_0)	0.1	0.1	0.6
Filter Scale (λ_{min})	2	1	100
Number of Filter Orientation (*No*)	1	1	6
Filter Angular Bandwidth constant (*k*)	0.2	0.1	3

4.5 Results

The proposed method was implemented in MATLAB (The Mathworks Inc., Natick, MA, USA). The extra added time of the proposed framework to the previously reported 2D PS method (0.5sec) is 6sec. For our data, the filter bandwidth was calculated to be 0.24 by using the proposed method in section 4.3.1. During the scale selection process the γ value was set to 0.75 since this was reported to be optimal value for ridge feature detection [7]. For filter orientation we chose to work with three angles since choosing greater than three orientations had an insignificant effect on the results.

4.5.1 Quantitative Results

The distribution of intensity values with their corresponding signed distance values obtained from one B-mode US image volume by processing each individual 2D slice are shown in Fig. 4.12. The figure also shows the corresponding results obtained from PS images calculated using the best empirically-set parameters and the PS image calculated using the proposed parameter-optimized approach.

Investigating these figures and Table 4.2 we can see that in both of the PS images, the concentration of the intensity values away from the zero signed distance value is much less compared to the B-mode US image intensity distribution which highlights the ability of the PS method in extracting bone surfaces without being affected by the US image artifacts. It can be easily noted how the PS obtained using the optimized parameters is much less sensitive to typical US artifacts or soft tissue interfaces compared to the PS obtained using the empirically-set parameters (Table 4.2).

The average surface matching mean error was 0.51 mm (Std: 1.46mm) with the best empirically-set parameters compared to 0.33mm (Std: 0.71mm) for our proposed automatically-set parameters. Choosing two scales for the empirical method decreases the surface matching mean error to 0.41mm (Std: 1.16mm) but introduces more outlier points away from the zero signed distance indicating an increase in the detection of US artifacts (Table 4.2 and 4.3).

For future applications the statistical distribution of signed distance values inside regions A and B (Fig. 4.12) could be used as a potential image quality metric since we would like to minimize the distribution inside these regions.

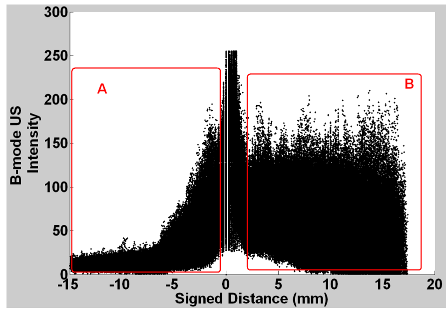

(a)

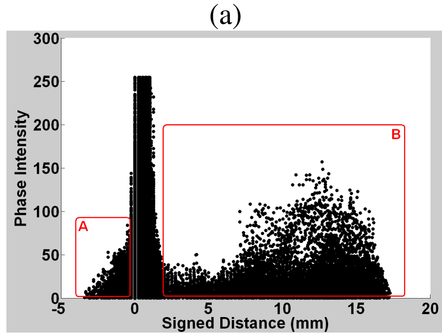

(b)

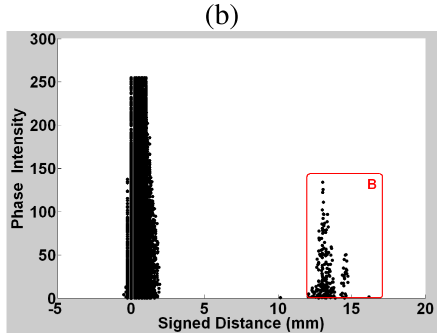

(c)

Fig.4.12 Signed distance plots obtained from our quantitative validation experiment. (a) Signed distance (mm) versus B-mode US image intensity, (b) Signed distance (mm) versus phase intensity obtained from phase symmetry method with the best empirically set parameters using two scales, (c) Signed distance (mm) versus phase intensity obtained from our proposed optimized parameter phase symmetry method. Signed distance/intensity pairs inside the red rectangular boxes B reflect features corresponding to soft tissue interface or speckle noise. Signed distance/intensity pairs inside the red rectangular boxes A are features corresponding to shadowing artefact, speckle noise or thick bone response. Comparing these rectangles we can see that with the proposed parameter optimization algorithm the PS method becomes less sensitive to typical US artifacts.

Table 4.2 Quantitative results for bone surface localization accuracy assessment comparing empirical PS with the proposed parameter tuned PS. The results represent the average signed distance values that correspond to all phase intensity values of a 3D US volume.

	Empirical PS				Parameter Tuned PS	
US Vol.	One scale		Two scales		One scale	
	ME (mm)	std (mm)	ME (mm)	std (mm)	ME (mm)	std (mm)
1	1.67	3.91	3.32	4.70	0.77	2.17
2	2.03	4.56	3.87	5.21	1.98	4.21
3	2.54	4.91	3.46	5.48	0.91	2.74
4	1.84	4.12	3.19	4.74	1.2	3.15
5	3.1	4.17	4.20	4.85	2.44	3.47
6	3.07	4.60	4.28	5.09	2.6	4.11
7	2.62	3.95	3.85	4.97	2.35	3.91
8	2.52	4.48	4.49	5.30	2.85	4.88
9	2.33	4.06	3.74	5.03	2.26	3.94
10	2.03	4.05	3.07	4.84	1.7	3.5
11	2.13	4.09	3.39	4.98	2.61	4.43
12	1.78	4.26	2.71	4.72	1.54	3.66
13	0.95	4.01	2.84	4.94	0.22	2.18
14	2.65	4.70	4.29	5.32	3.97	5.07
15	0.97	4.07	2.92	4.98	0.23	2.50
Average	**2.14**	**4.26**	**3.58**	**5.01**	**1.84**	**3.59**

Vol.:Volume; std : Standard Deviation; ME: Mean Error

Table 4.3 Quantitative results for bone surface localization accuracy assessment comparing empirical PS with the proposed parameter tuned PS.

	Empirical PS				Parameter Tuned PS	
US Vol.	One scale		Two scales		One scale	
	ME (mm)	std (mm)	ME (mm)	std (mm)	ME (mm)	std (mm)
1	0.83	1.81	0.79	1.79	0.67	1.14
2	0.75	2.23	0.66	1.89	0.51	1.42
3	1.25	2.92	0.96	2.34	0.65	1.35
4	0.65	1.69	0.63	1.87	0.50	1.45
5	0.69	1.26	0.76	1.28	0.62	0.34
6	0.25	0.54	0.31	0.90	0.30	0.64
7	0.57	0.50	0.60	0.53	0.59	0.54
8	0.83	1.47	0.47	0.96	0.40	0.28
9	0.57	0.95	0.58	0.62	0.44	0.27
10	0.19	0.95	0.15	0.52	0.14	0.35
11	0.29	0.96	0.28	0.53	0.27	0.55
12	0.96	2.31	0.76	1.84	0.66	1.35
13	-0.35	1.39	-0.46	0.59	-0.40	0.15
14	0.69	1.64	0.15	0.82	0.12	0.65
15	-0.40	1.38	-0.46	0.97	-0.50	0.17
Average	**0.51**	**1.46**	**0.41**	**1.16**	**0.33**	**0.71**

Vol.:Volume; std : Standard Deviation; ME: Mean Error

Investigating Table 4.4 we can see that the filter parameters from the proposed method are very close the filter parameters obtained from the exhaustive search method. One of the main advantages of the proposed method is that the orientation selection procedure is based on the information obtained from the image content which makes the algorithm more robust to typical US artifact. Furthermore, filter scale and angular bandwidth is also adaptive with orientation. On the other hand in the original method the filter angles, filter scale (λ_{min}), and filter angular bandwidth are always fixed which will result in the extraction of non bone surfaces as well. The average localization accuracy obtained from the exhaustive search method was 0.24mm (Std: 1.06mm). However, we would like to mention that the exhaustive search method requires one day per slice where the proposed method only takes 6 sec per slice. Therefore, in this paper we are not targeting an optimization method since this would not be feasible in a clinical environment where speed is of major importance.

4.5.2 Qualitative Results

Figures 4.13-4.15 show a qualitative comparison of PS images of an in vivo human distal radius (Fig. 4.13 and 4.14) and pelvis (Fig.4.15) obtained with the proposed optimized Gabor filter parameters and contrasted to the best values we could empirically set. Note how the local phase images obtained empirically using 2 scales extracted more US artifacts and resulted in a thicker bone boundary due the unsuitable scale combination. Moreover, integrating the zero angle as one of the filter orientations caused the detection of unwanted features on the sides of the bone surface (white arrows). Decreasing the filter scale to 1 in the empirical case caused gaps in the extracted bone surfaces (white circles). Our surface results on the other hand, which used optimized filter parameters, were consistently sharper with reduced unwanted features on the bone sides and with no gaps in the detected surfaces. Figure 4.16 shows further supporting qualitative examples where scans of a fractured ex-vivo porcine tibia fibula specimen were acquired. Note how the proposed method again produced a cleaner identification of the bone fracture.

Table 4.4 Quantitative results comparing the filter parameters obtained using the exhaustive search method to the proposed method. The results represent the average signed distance values that correspond to maximum phase intensity values in vertical direction of a 3D US volume.

US Vol.		κ/ω_0	λ_{min}	*No*	*k*
1	ES	0.4	69	4 (30°, 45°, 90°,135°)	3
	PO	0.25	55, 45, 65	3 (72°,92°,112°)	2.2, 2.5, 1.89
2	ES	0.4	60	3 (60°, 90°,120°)	3
	PO	0.25	49, 52, 65	3 (72°,94°,116°)	2.2, 1.56, 2.1
3	ES	0.4	60	3 (60°, 90°,120°)	3
	PO	0.25	55, 66, 65	3 (88°,98°,107°)	2.2, 2.2, 2.4
4	ES	0.3	65	3 (60°, 90°,120°)	3
	PO	0.25	48, 66, 56	3 (96°,105°,114°)	2.1, 2.2, 2.3
5	ES	0.5	47	4 (30°, 45°, 90°,135°)	2
	PO	0.25	52, 61, 56	3 (85°,101°,118°)	2.1, 2.3, 1.95
6	ES	0.4	67	4 (30°, 45°, 90°,135°)	2.7
	PO	0.25	49, 52, 65	3 (87°,103°,120°)	2.1, 2.2, 2.4
7	ES	0.4	72	3 (60°, 90°,120°)	3
	PO	0.25	58, 62, 65	3 (62°,91°,120°)	2.3, 2.6, 2.4
8	ES	0.5	67	3 (60°, 90°,120°)	0.5
	PO	0.25	51, 53, 69	3 (78°,96°,116°)	2.6, 2.3, 2.1
9	ES	0.6	62	4 (30°, 45°, 90°,135°)	3
	PO	0.25	65, 55, 72	3 (84°,101°,118°)	2.3, 2, 2.4
10	ES	0.4	72	3 (60°, 90°,120°)	3
	PO	0.25	52, 63, 72	3 (78°,94°,110°)	2.1, 2.2, 2.3

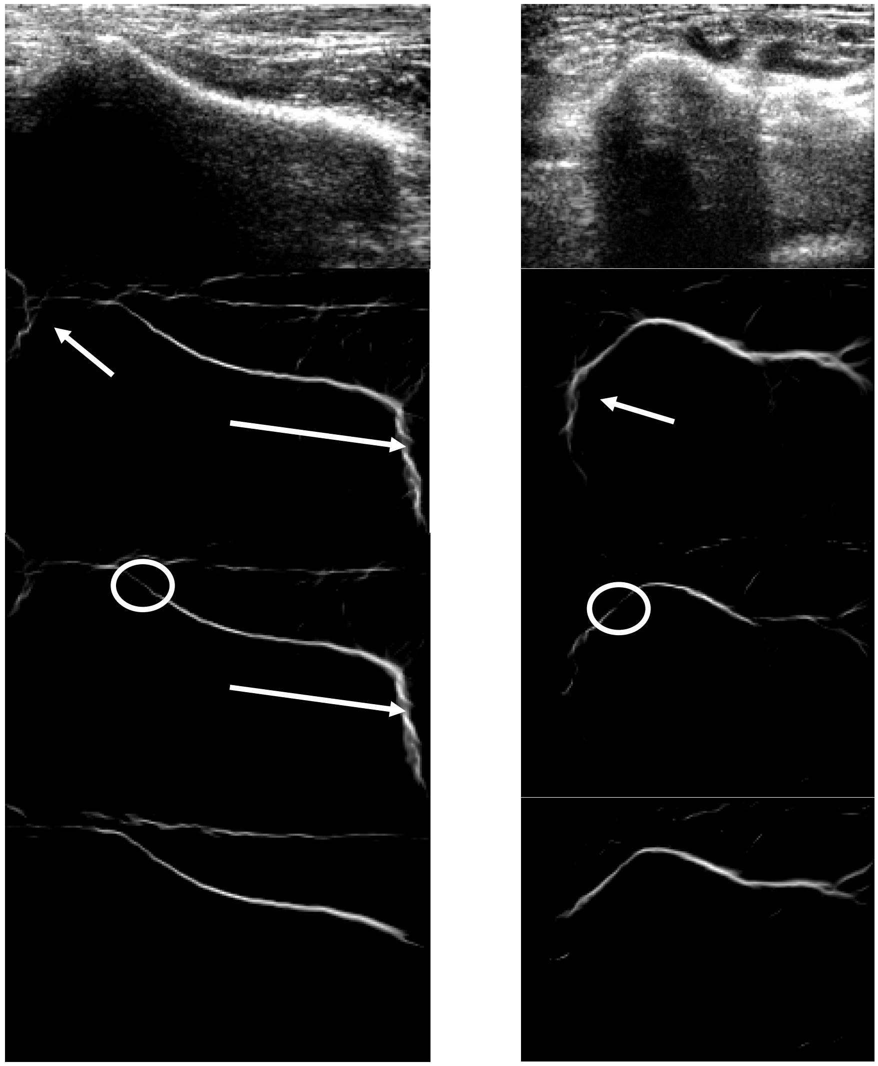

(a) (b)

Fig.4. 13 Qualitative results on in-vivo human distal radius data where the imaging depth was 3.5cm. (a)US image obtained by positioning the US transducer in volar plane, (b) US image obtained by positioning the US transducer in dorsal plane. From top to bottom: B-mode US image, PS image obtained using empirical filter parameters with 2 scales, PS image obtained using empirical filter parameters with one scale, proposed data-driven PS image. White arrows point out some extracted phase features that are not bone surfaces due to combining orientations that are not perpendicular to the bone surface during the calculation of PS. The white circles highlights example locations of a degraded bone surface due to the inclusion of less informative orientations with weaker bone responses.

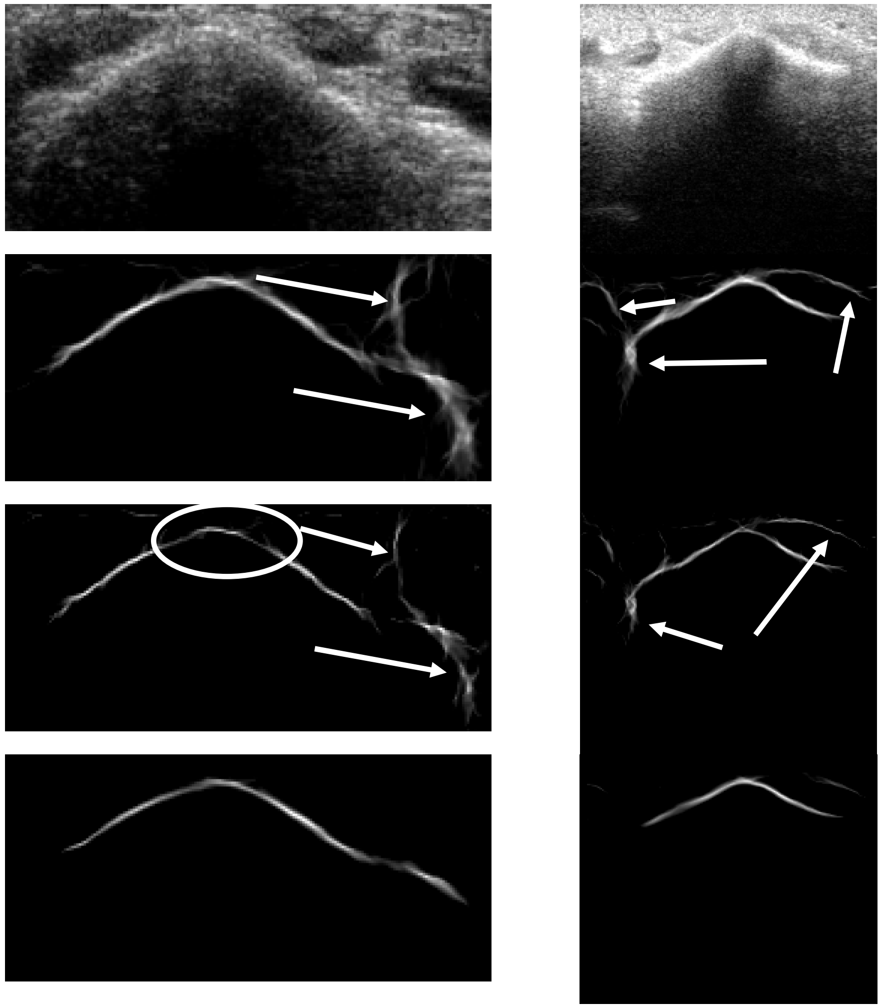

(a) (b)

Fig.4. 14 Qualitative results on in-vivo human distal radius data where (a)the imaging depth was 1.9 cm (left B-mode image), (b) 4.5cm (right B-mode image). From top to bottom: B-mode US image, PS image obtained using empirical filter parameters with 2 scales, PS image obtained using empirical filter parameters with one scale, proposed data-driven PS image. White arrows point out some extracted phase features that are not bone surfaces due to combining orientations that are not perpendicular to the bone surface during the calculation of PS. The white circles highlights example locations of a degraded bone surface due to the inclusion of less informative orientations with weaker bone responses.

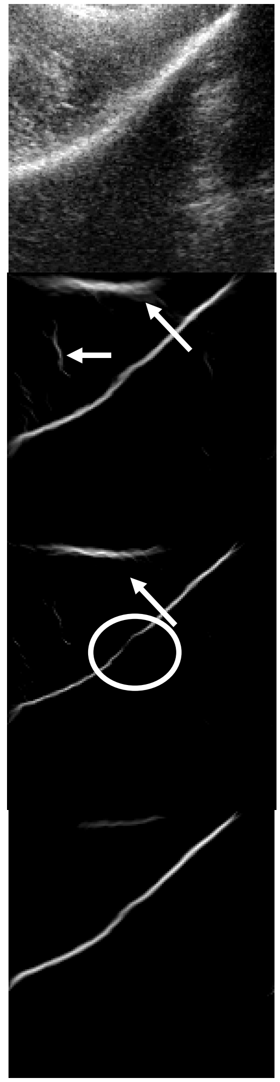

Fig.4. 15 Qualitative results on in-vivo human pelvis where the imaging depth was 4.9cm. From top to bottom: B-mode US image, PS image obtained using empirical filter parameters with 2 scales, PS image obtained using empirical filter parameters with one scale, proposed data-driven PS image. White arrows point out some extracted phase features that are not bone surfaces due to combining orientations that are not perpendicular to the bone surface during the calculation of PS. The white circles highlights example locations of a degraded bone surface due to the inclusion of less informative orientations with weaker bone responses.

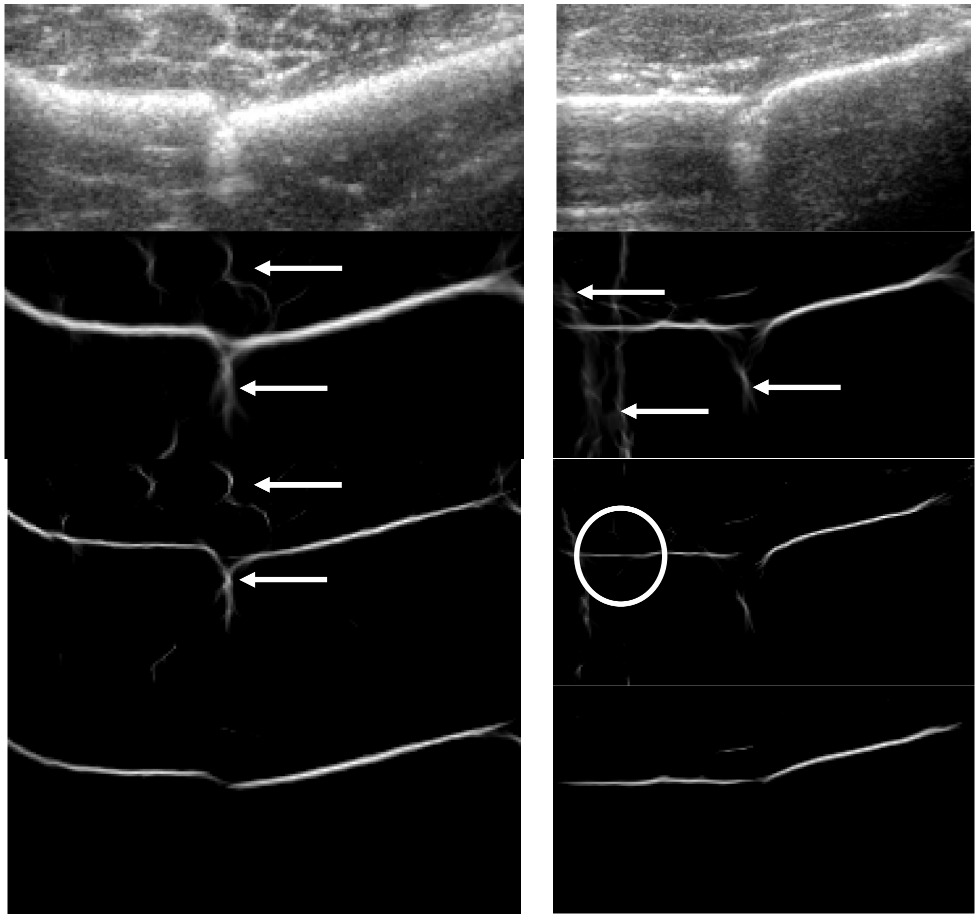

(a) (b)

Fig.4. 16 Qualitative results on fractured ex-vivo porcine tibia fibula specimen showing two different fractures (a) and (b). From top to bottom: B-mode US image, PS image obtained using empirical filter parameters with 2 scales, PS image obtained using empirical filter parameters with one scale, proposed data-driven PS image. White arrows point out some extracted phase features that are not bone surfaces due to combining orientations that are not perpendicular to the bone surface during the calculation of PS. The white circles highlights example locations of a degraded bone surface due to the inclusion of less informative orientations with weaker bone responses.

4.6 Discussion and Conclusion

We believe that this scale and orientation adaptation approach addresses the key weaknesses of the previously published local phase based image enhancement methods [2]. In particular, the combination of automatic scale selection method with a very simple orientation optimization module was shown to produce qualitatively and quantitatively improved results. It should be noted that the previous local phase based feature extraction algorithms [2] are likely to enhance speckle regions and soft tissue interfaces as well as bone surfaces since they do not provide an explicit mechanism for distinguishing between these features, whereas the proposed data driven approach handles this situation by means of the ridgeness measure for automatic scale selection and orientation optimization with the RT.

Qualitative results obtained from in-vivo and ex-vivo scans and demonstrated the critical importance of selecting the correct scales and orientations in local phase based US processing. Quantitative results were also presented on a specially constructed bone phantom where the gold standard surface of the bone was established through CT imaging. An improvement of close to 0.18mm in bone localization accuracy was observed. Furthermore, our adaptive parameter selection approach produces close to a 50% decrease in the variability and in the reduction of worst case scenario (i.e., the standard deviation of the bone surface localization error for the proposed method (0.71mm) is almost half of the empirical PS (1.46mm) method) compared to empirical and exhaustive search methods. In US based computer assisted orthopaedic surgery (CAOS) systems, inaccuracies may arise from various sources such as US-CT registration, tracking of surgical instruments, and localization of the surgical tool tips. Therefore an improvement in bone surface extraction from US data will play an important role in all US based CAOS systems, which will in turn improve the total accuracy of the system which, for a number of applications in orthopaedic surgery will need to be in the range of 2-4mm [8].

Though local image phase information has previously been successfully applied for extracting US image features, none of the prior studies investigated the effects of parameter setting on the extracted features nor provided guidelines on how proper selection could be achieved. Some authors left this as an open question for future development, while others tried to address it in an ad hoc manner, by investigating the filter outputs on samples of US imaged depicting a certain anatomical area of interest. In this chapter, we proposed a novel approach for automatic data-driven selection of the scale, bandwidth and orientation of Log-Gabor filters for calculating phase symmetry responses in bone US.

To determine the filter bandwidth, US images with fully developed speckle were analyzed and the image speckle size was measured by calculating the autocorrelation function. For scale selection, we used a ridgeness content measure obtained from the Hessian matrix eigenvalues and investigated the information content extracted at different scales. This measure was adopted since a line profile across a bone surface in an US response typically depicts a ridge-like rather than a step or ramp-like edge at the bone boundaries [2]. This metric could be changed to a step edge response which is a common feature in echocardiography US images seen at the epicardial, the endocardial and pericardial boundaries [4]. For orientation selection, the appearance of bone surfaces was incorporated within our framework where a RT obtained from the image ridgeness content measure was used to deduce the optimal angles of the directional filter. This orientation optimization approach would be also useful during the extraction of K-wires, commonly used for fixation during distal radius fracture surgeries as a provisional fixation step prior to plating or as definitive fixation, as well as possibly other surgical instruments used during cardiac surgeries from US images [9, 10]. Because bone surfaces in US images typically appear as elongated line-like features, the RT which was used in this study is the traditional RT where the integration of intensity values is performed along a line. This could be easily extended to a generalized RT where the integration could be performed on a curve which would be more suitable during enhancing curved features from US images.

Our qualitative and quantitative results demonstrate how the proposed framework for automatic filter parameter selection captures essential aspects of US image feature enhancement based on local phase information, which would be of interest to developers of US based computer aided intervention systems.

Future work will include the extension of this automatic parameter selection method to 3D and a clinical study where the proposed method will be tested on scans obtained from patients with distal radius and pelvis fractures.

4.7 References

[1] I. Hacihaliloglu, R. Abugharbieh, A.J. Hodgson, R.N. Rohling, "Enhancement of bone surface visualization from 3D ultrasound based on local phase information", *Proc. IEEE Ultrasonics Symposium*, pp. 21-24, 2006.

[2] I. Hacihaliloglu, R. Abugharbieh, A. Hodgson, R.N. Rohling, "Bone Surface Localization in Ultrasound Using Image Phase Based Features", *Ultrasound in Medicine and Biology*,vol.35, no. 9, pp. 1475-1487, 2009.

[3] P. Kovesi P, "Symmetry and asymmetry from local phase", *Proc Tenth Australian Joint Conference on Artificial Intellegence*, pp.185-190, 1997.

[4] M. Mulet-Parada, A.J. Noble, "2D+T boundary detection in echocardiography", *Medical Image Analysis*, vol.4, no.1, pp.21-30, 2000.

[5] R.F. Wagner, S.W. Smith, J.M. Sandrik, H. Lopez, "Statistics of Speckle in Ultrasound B-Scans", *IEEE Trans on Sonics and Ultrasonics*, pp.156-163, 1983.

[6] A. Frangi, W. Niessen, K. Vincken, M. Viergever, "Multiscale vessel enhancement filtering", *Proc Int. Conf. Med. Image Compt. Computer-Assisted Intervention*, vol.1496, pp. 130–137, 1998.

[7] T. Lindeberg, "Edge detection and ridge detection with automatic scale selection", *International Journal of Computer Vision*, pp, 117-154, 1998.

[8] R. Phillips, "The accuracy of surgical navigation for orthopaedic surgery", *Current Orthopaedics*, vol. 21, no. 3, pp. 180-192, 2007.

[9] I. Hacihaliloglu, R. Abugharbieh, A. Hodgson, R.N. Rohling, P. O'Brien , P. Guy P, "Distal radius and K-wire localization in 3D ultrasound using local phase information", *Proc of the 7th Annual Meeting of CAOS International CAOS*, pp.572-575, 2007.

[10] M.G. Linguraru, N.V. Vasilyev, P.J. Del Nido, R.D. Howe, "Statistical segmentation of surgical instruments in 3D ultrasound images", *Ultrasound in Medicine and Biology*, vol. 33, no.9, pp.1428-1437, 2007.

Chapter 5
Clinical Evaluation and Validation*

5.1 Introduction

In previous chapters we have shown for the first time that local phase features provide useful information for automatic and accurate extraction of bone surfaces and fractures from 2D and 3D US image data. In this chapter we present our first clinical results with three studies to assess the feasibility of the proposed methods.

5.2 Current Distal Radius and Pelvis Reduction Procedure

Close cooperation with orthopaedic surgeons is an absolute necessity for the proper design and realization of a successful CAOS system. The cooperation for this work was motivated by a necessity of the computer assistance in distal radius and pelvic fracture identification and fracture reduction assessment. As was mentioned in chapter 1, traditional approaches are facing many problems ranging from navigation to lack of real-time 3D surface information. Furthermore, current orthopaedic surgery relies on the use of imaging modalities that operate on X-rays which causes serious radiation exposure to the patient and surgical team.

---

* A version of this chapter will be submitted for publication. I. Hacihaliloglu, R. Abugharbieh, A. Hodgson, R. Rohling, P.Guy. “Local Phase Features of Ultrasound Images for Orthopaedic Surgery: First Clinical Results”.

To extract detailed information about the procedures currently followed by orthopedic surgeons for fracture reduction and address the problems, we attended numerous distal radius and pelvic fracture surgeries (Fig.5.1) at the Vancouver General Hospital (VGH), and worked closely with two orthopaedic surgeons; Drs. Peter O'Brien and Pierre Guy. A typical flowchart for the preoperative treatment and intra-operative reduction procedure used is given in Fig 5.2.

Generally, X-ray scans are obtained in order to validate the initial fracture reduction and to identify the basic anatomic structures. The treatment method is then chosen. A range of operative and non-operative treatment options are recommended based on injury and patient characteristics. In today's practice, methods for distal radius fracture fixation are based on either cast immobilization, percutaneous pinning, external fixation, internal fixation with plates, or combination treatments, while pelvic fractures are either managed non-operatively with protected mobilization or with internal and external fixation devices following reduction (realignment) of the fracture fragments.

Our aim is to eliminate the difficulties encountered during the conventional 2D fluoroscopy based orthopaedic surgeries and open new minimally invasive treatment options. Therefore, the work presented in this thesis is part of a larger project to develop a three dimensional (3D) US based computer assisted orthopaedic surgery (CAOS) system for fracture reduction assessment. The envisioned system is given in Fig.5.3.

In the next sections we present our first clinical results using the proposed methods to identify fractures from B-mode images. We would like to mention 3 cases will be presented in the following chapters as pilot cases which are the first cases within a clinical study that will continue beyond this Thesis. The scanning studies performed in the previous chapters were obtained under controlled laboratory environments with optimum scanning conditions. With these three prospective case studies we hope demonstrate that similar results could also be obtained under clinical environments. Furthermore, we anticipate that with these three studies we will determine the potential benefits of the proposed methods and what limitations are faced during the actual scanning procedure. Finally, we hope to learn useful information about which type of fractures are easy to identify and which types are causing limitations during the scanning and localization procedure.

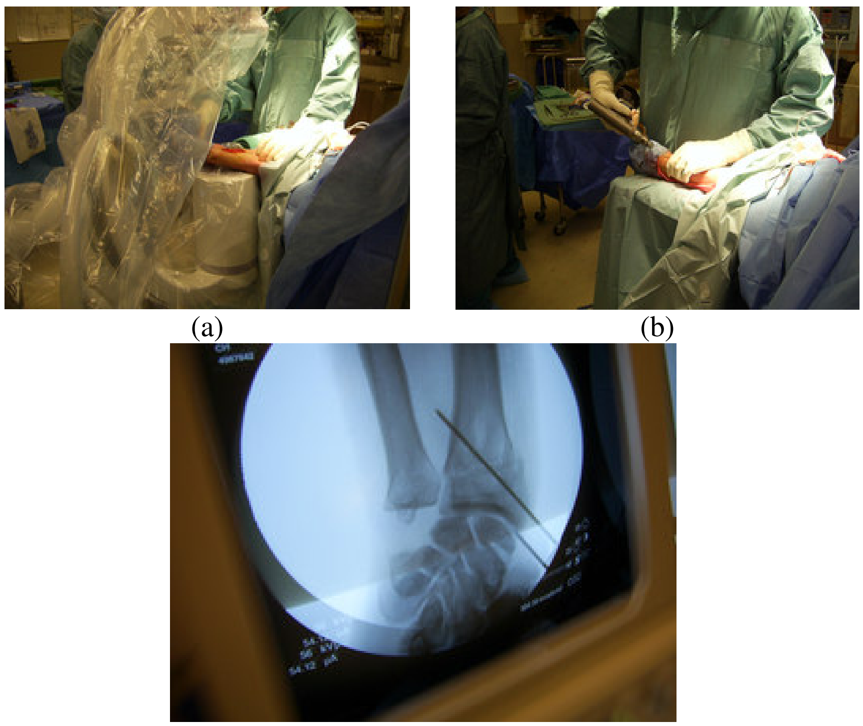

(a) (b) (c)

Fig.5. 1 Distal radius surgery at the Vancouver General Hospital. (a) 2D fluoroscopy shot during surgery, (b) drilling the K-wire, (c) 2D fluoroscopy showing the position of the K-wire inside the bone.

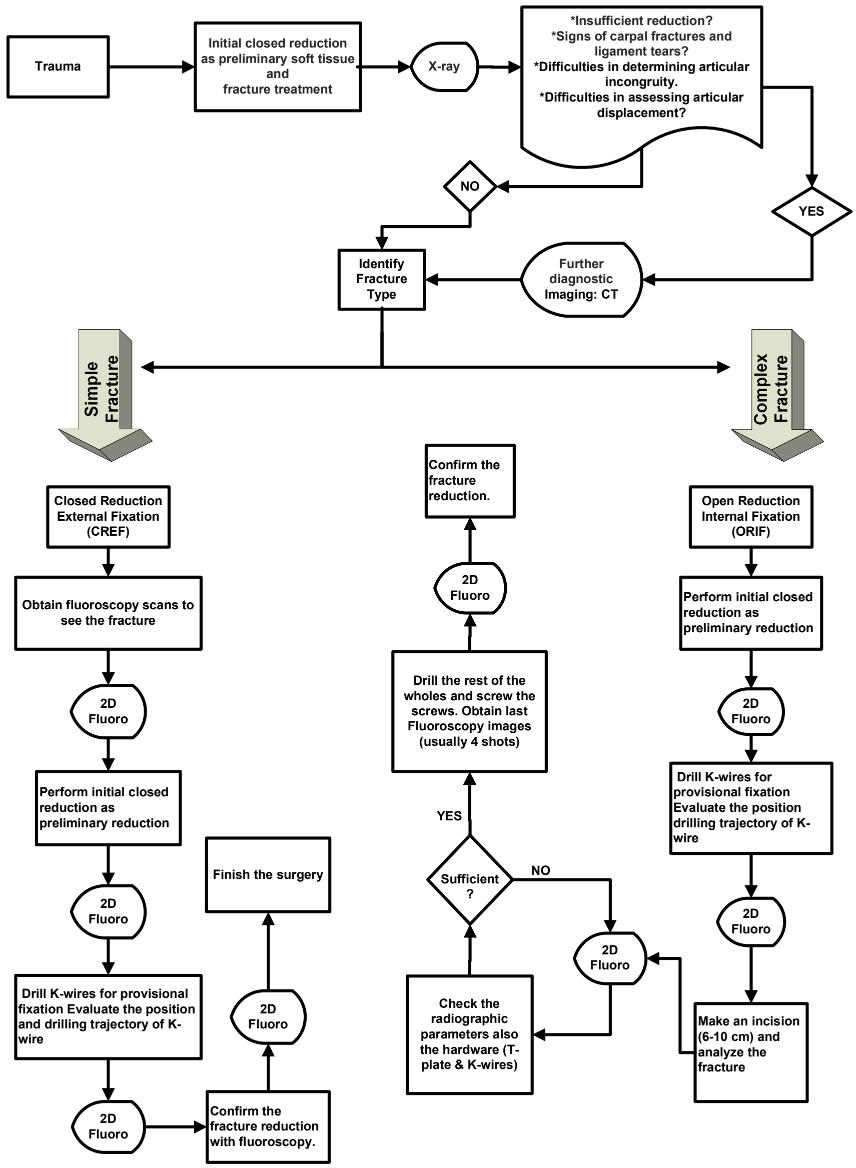

Fig.5.2 Flowchart of typical preoperative treatment and intra-operative reduction of distal radius fracture surgery followed by our clinical partners at the VGH orthopedic surgery department.

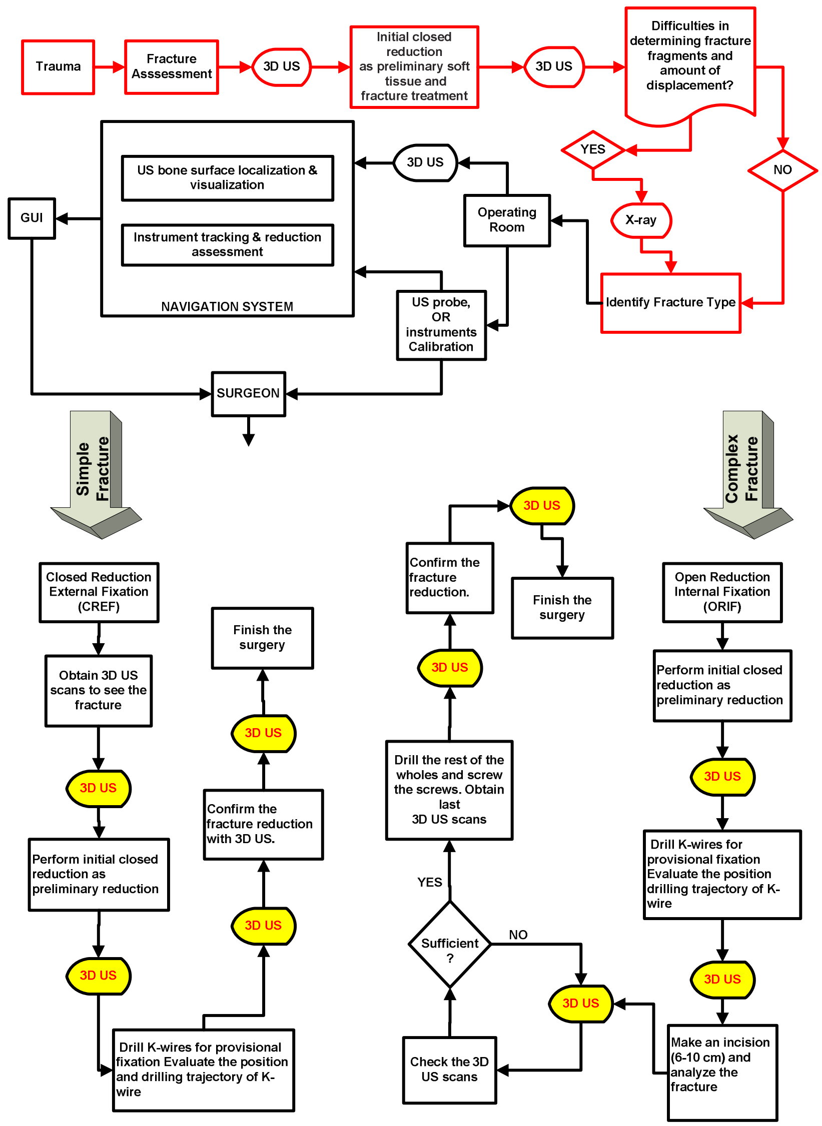

Fig.5.3 Proposed 3D US based fracture reduction assessment CAOS system framework. Red boxes show the pre-operative actions and the black boxes represent the intra-operative actions

5.3 Bone Fracture Assessment Using 3D Ultrasound: A Pilot Study

To validate the proposed US based CAOS system US scans were obtained from patients who arrived to the emergency department with a distal radius or pelvic ring fracture. Enrollment in this pilot study was limited to 20 patients who have already been diagnosed with a fracture in this area and who have been referred to the Orthopedic Trauma team at VGH for consultation and treatment. The patient was already undergone a standard investigation procedure, which involved anatomical investigation by the surgeon and obtaining X-ray scans and CT scan. Once the area (wrist or pelvis) was confirmed to involve a fracture requiring further care (surgery), the patient was informed about the study and invited to participate. Informed consent for the use of 3D US were obtained. The time allowed for the patient to make a decision after he/she was informed about the study was limited to 2 hours.

Inclusion criteria for the study were:

- Patients presenting to VGH Emergency Room with a diagnosis of distal radius or pelvis fracture, who are referred to the orthopaedic Trauma team.

Exclusion criteria for the study were:

- Patients with skin conditions, skin breakdown, or allergy which precludes the use of ultrasound gel.
- Patients who have sustained a previous pelvis or distal radius fracture.
- Patients unable to provide informed consent.

5.3.1 Data Collection and Qualitative Validation

All US examinations in this clinical study were performed with a commercially available real-time scanner (Voluson 730, GE Healthcare, Waukesha, WI) with a 3D RSP5-12 transducer. This is a mechanized probe where a linear array transducer is swept through an arc range of 20°. During the scanning standard US coupling gel was placed on the skin over the positions for the dorsal, volar, and radial sections (Fig.5.3). In total 15 different US volumes were acquired. The gold standard comparison was provided by the 3D surfaces extracted from the pre-operative CT scans. The analysis was done by assessing the "fitness" of US derived surfaces to the gold standard which was achieved using the same procedure explained chapter 3-Section 3.2.1 and chapter 4-Section 4.4. US image was matched to the CT surface by matching selected anatomical landmarks (note: in previous ex vivo bovine study, we used implanted fiducials to perform the registration, but fiducials could not be used in this clinical study) and computing the rigid body transformation. In order to minimize the user variability due to anatomical landmark selection the registration procedure was repeated 10 times.

(a) (b) (c)

Fig.5.4 Pictures showing the scanning position of the US transducer. (a)dorsal, (b) volar, (c) radial sections.

5.4 Results

5.4.1 Case 1

The patient was presented to the emergency department with right wrist pain. The fracture was identified as a right distal dorsal radius cortex fracture. Figures 5.5 and 5.6 are showing the conventional X-ray scans and gold standard CT scans respectively.

Fig 5.7 shows the corresponding US images for case study 1. Distinct presentation of homogeneous, strong, bright reflective echoes with dorsal acoustic shadowing was the characteristic feature of the bone border in all patients. A longitudinal examination across the fracture site revealed a clear disruption of the continuous reflection of the radius; furthermore, the displacement between the fracture fragments and the angle formed by the fracture fragments could be observed easily in every case. The PS images obtained using the methods explained in chapter 2 and chapter 4 are shown in Fig. 5.7 (b) and (c) respectively. Investigating Fig. 5.7 (b) we can se that the proposed method extracts bone surfaces without being affected too much by the typical US artifacts. However, due to the empirical filter parameter selection and without tuning the filter orientations to the specific bone appearance the method also extract soft tissue interfaces which are not part of the bone surface. Using the method provided in chapter 4 we can see that using the optimized filter parameters the extracted bone surfaces were consistently sharper with reduced soft tissue interfaces and unwanted features. Comparisons of the extracted PS surfaces with the gold standard CT surface are given in Fig. 5.8. Finally we show 3D surfaces extracted using the proposed methods in Fig. 5.9 and Fig. 5.10.

(a)

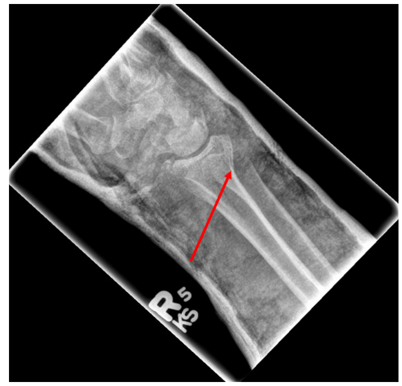

(b)

Fig.5.5 Case study 1 conventional X-ray images. (a) Anterior posterior view on post attempted reduction, (b) Lateral view on post attempted reduction. Red arrows point out to the location of fracture.

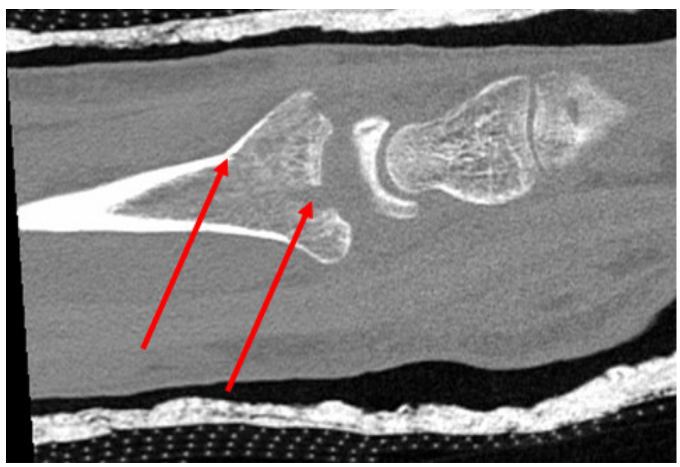

(a)

Fig.5.6 Case study 1 gold standard 2D CT slice. (a)Sagittal 2D CT slice. Red arrows point to the location of fracture.

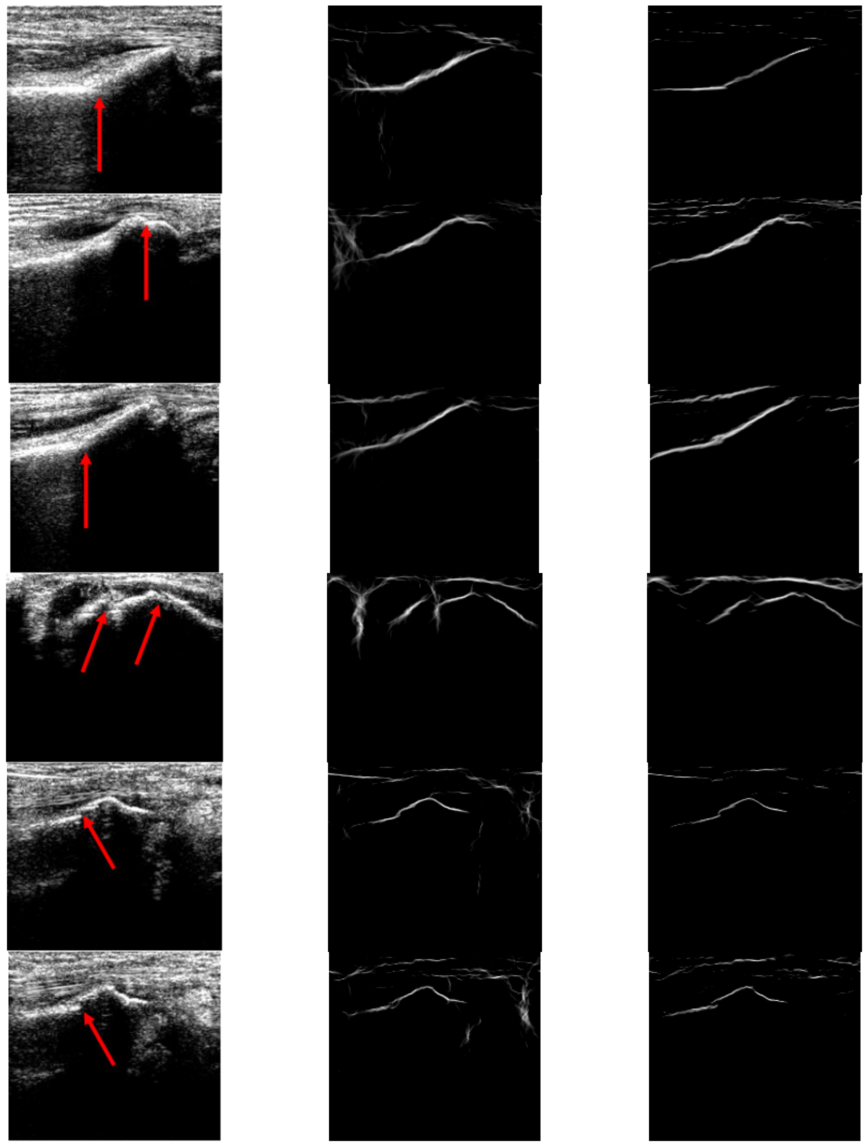

Fig.5.7 US images for case study 1. (a) B-mode US image, (b) PS image with empirical parameters used in chapter2, (c) Optimized PS image obtained using the proposed method in chapter 4. Red arrows in B-mode US images point to the location of fracture.

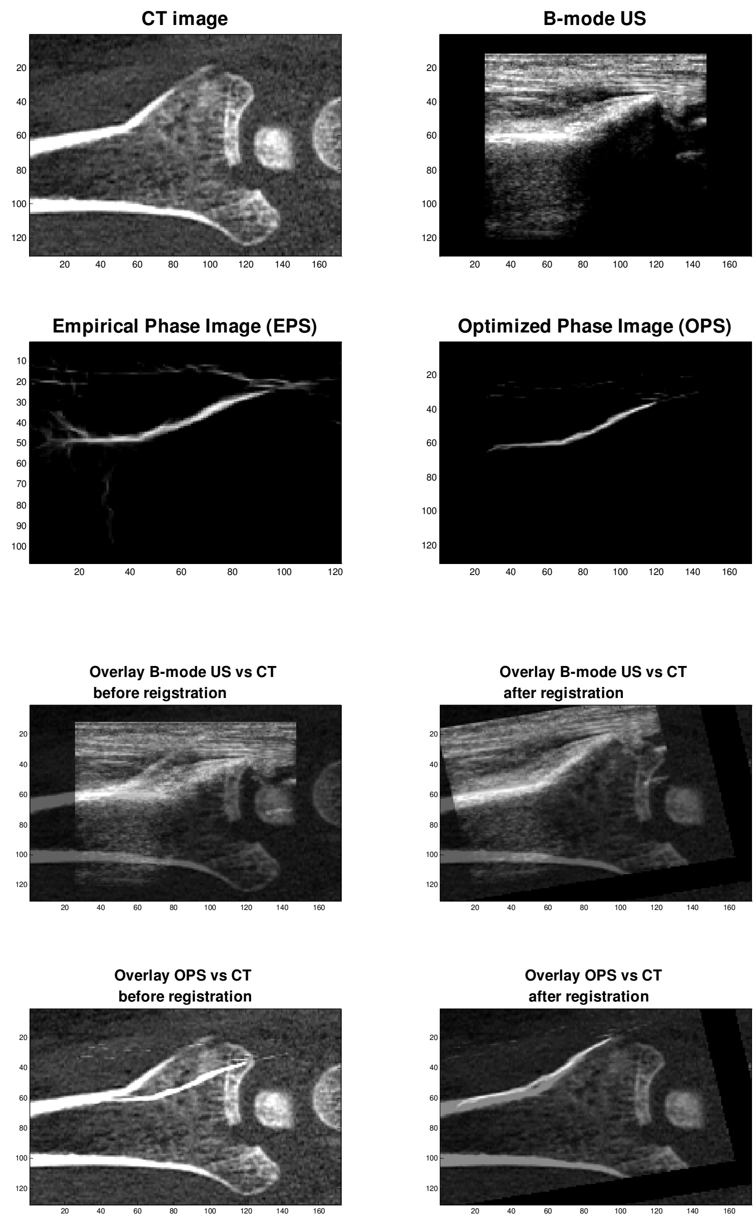

Fig.5.8 The analysis of “fitness” of bone surfaces extracted from B-mode US and corresponding PS images to the gold standard CT surface.

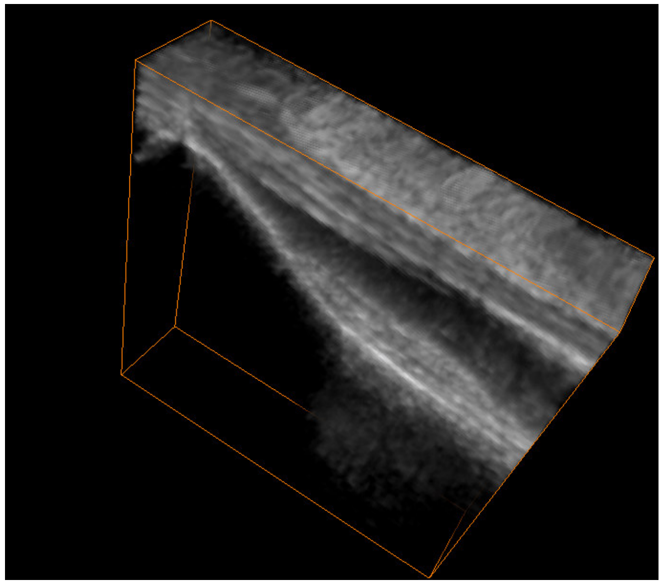

(a)

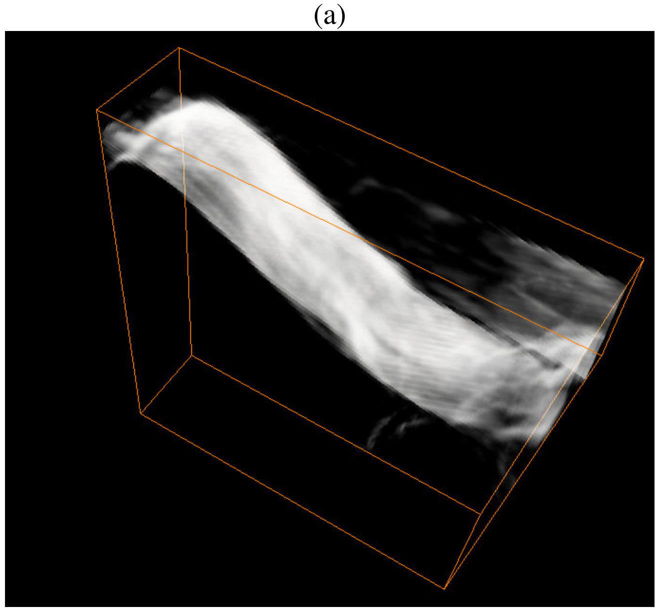

(b)

Fig.5.9 3D US images for case study 1. (a) 3D B-mode US volume, (b) corresponding 3D PS volume obtained by processing each individual 2D slice of the volume using the proposed method with empirical filter parameters.

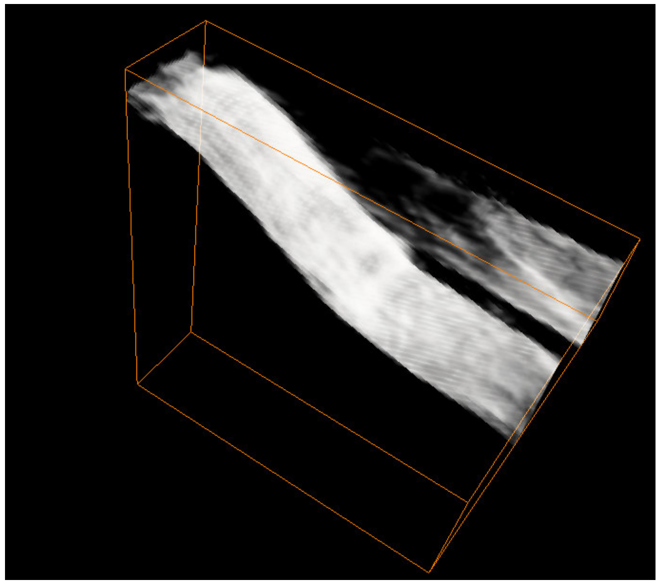

(a)

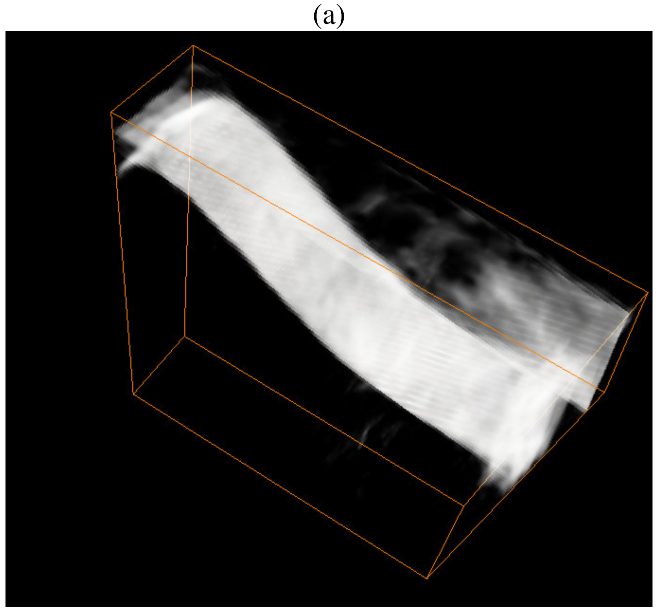

(b)

Fig.5.10 3D PS images for case study 1. (a) 3D PS volume obtained by processing the 3D B-mode US volume given in Fig 5.9 using optimized filter parameters. The volume is obtained by processing each individual 2D slice with the method proposed in chapter 4. (b) 3D PS volume obtained using 3D PS method explained in chapter 3.

Quantitative surface matching results are given in Table 5.1. Investigating Table 5.1 we can see that by optimizing the filter parameters using the proposed framework in chapter 4 we achieve a better localization accuracy. On the other hand 3D PS method achieves the best localization accuracy.

Table 5.1 Clinical validation Case 1 US to CT surface matching error results.

	EPS	OPS	3D PS
Average Mean Error (mm)	0.77	0.33	0.21
Std (mm)	1.10	0.52	0.47

Std: Standard deviation.

5.4.2 Case 2

The patient was presented to the emergency department with left wrist pain. The fracture was identified as a left distal radius fracture. Figures 5.11 and 5.12 are showing the conventional X-ray scans and gold standard CT scans respectively.

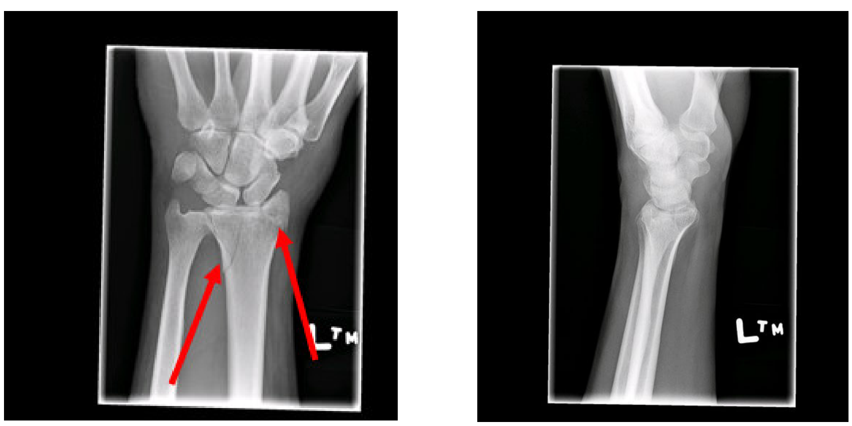

(a) (b)

Fig.5.11 Case study 2 conventional X-ray images. (a) Anterior posterior view on post attempted reduction, (b) Lateral view on post attempted reduction. Red arrows point out to the location of fracture.

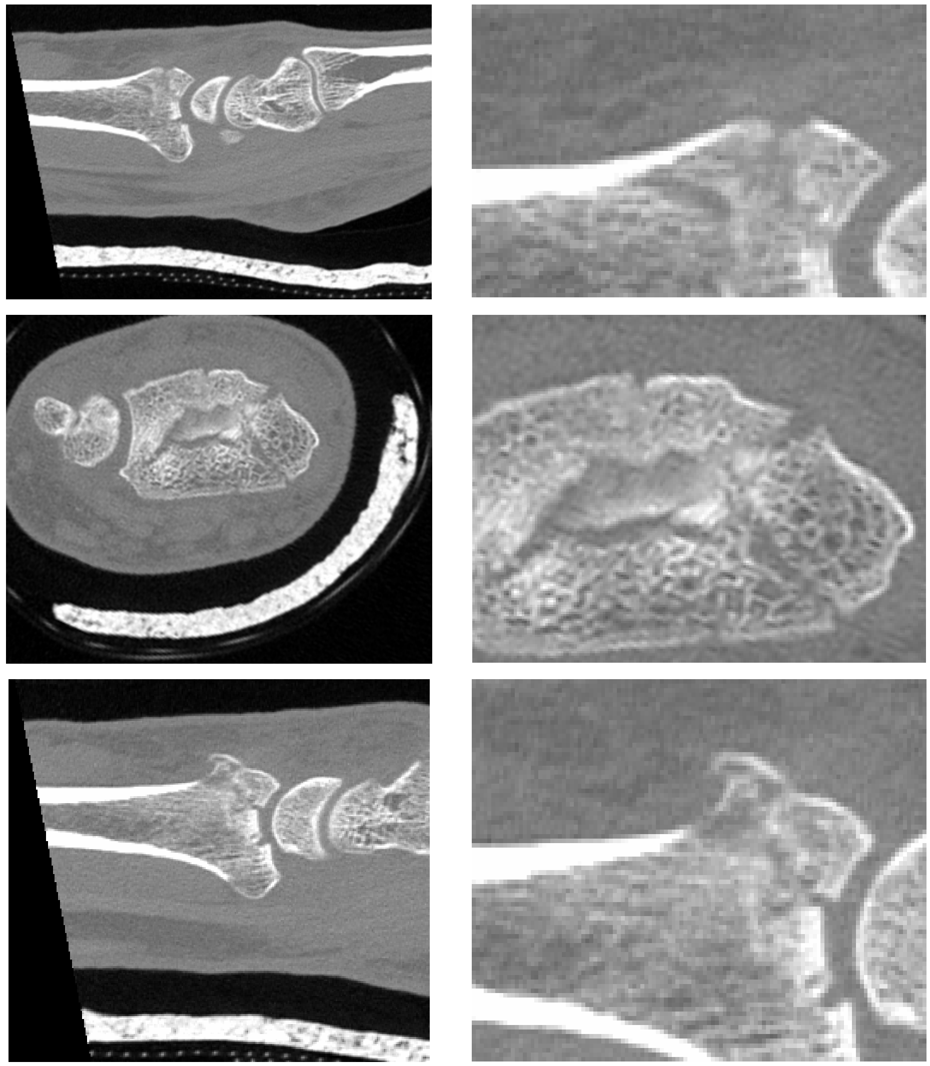

(a) (b)

Fig.5.12 Case study 2 gold standard CT surfaces. (a)Top to bottom: Sagittal, axial, and sagittal 2D CT slices. (b)Corresponding zoomed in images.

Fig 5.13 shows the corresponding US images for case study 2. Again distinct presentation of homogeneous, strong, bright reflective echoes with dorsal acoustic shadowing was the characteristic feature of the bone border in all scans. The PS images, obtained using the methods explained in chapter 2 and chapter 4, are shown in Fig. 5.13 (b) and (c) respectively.

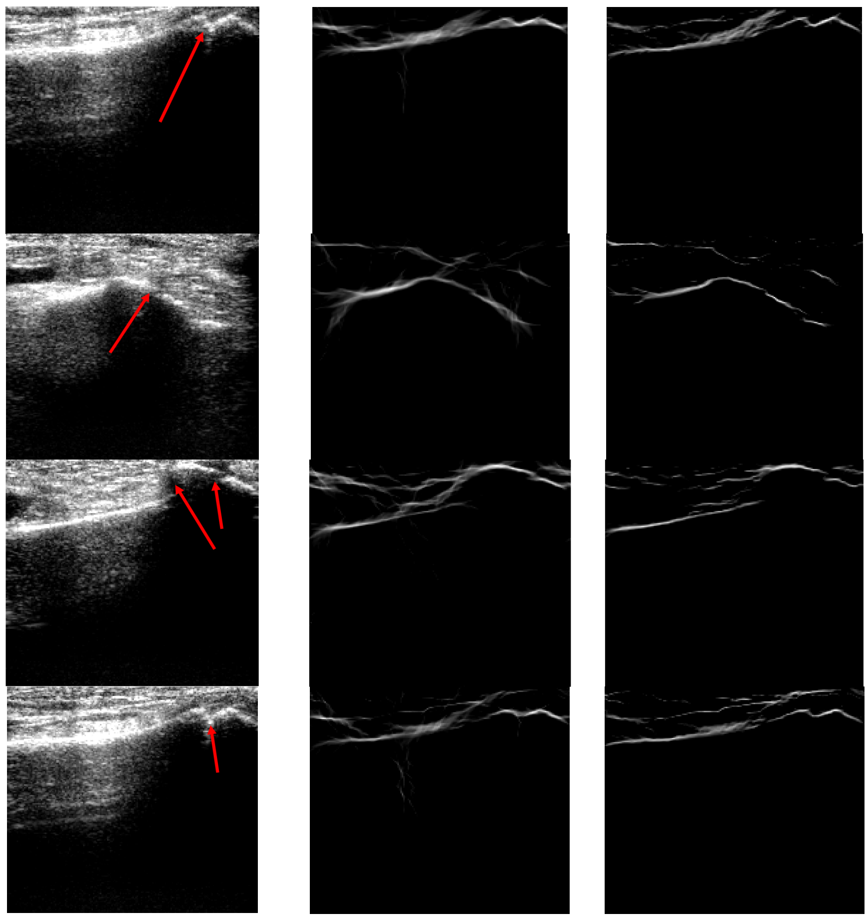

(a) (b) (c)

Fig.5.13 US images for case study 2. (a) B-mode US image, (b) PS image with empirical parameters used in chapter2, (c) Optimized PS image obtained using the proposed method in chapter 4. Red arrows in B-mode US images point to the location of fracture.

Finally we show 3D surfaces extracted using the proposed methods in Fig. 5.14 and Fig. 5.15.

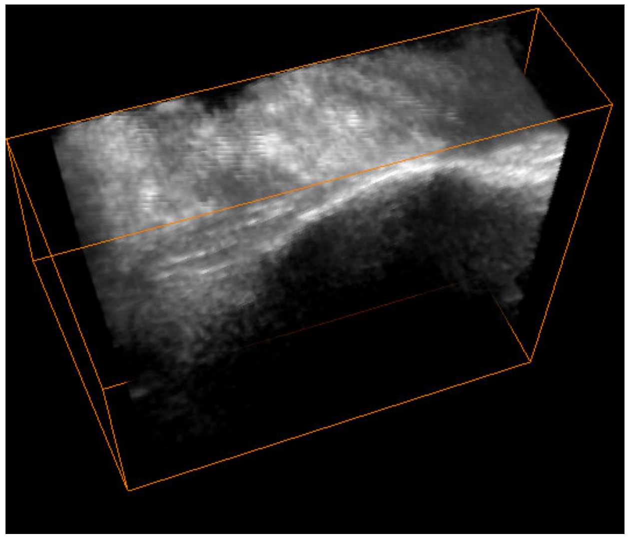

(a)

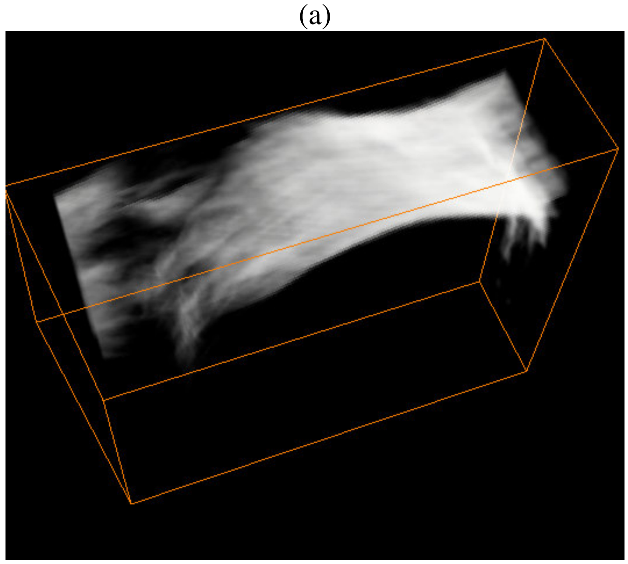

(b)

Fig.5.14 3D US images for case study 2. (a) 3D B-mode US volume, (b) Corresponding 3D PS volume obtained by processing each individual 2D slice of the volume using the proposed method with empirical filter parameters.

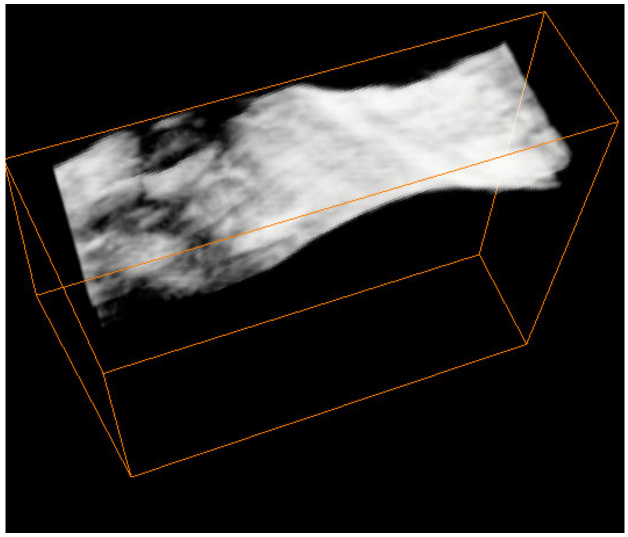

(a)

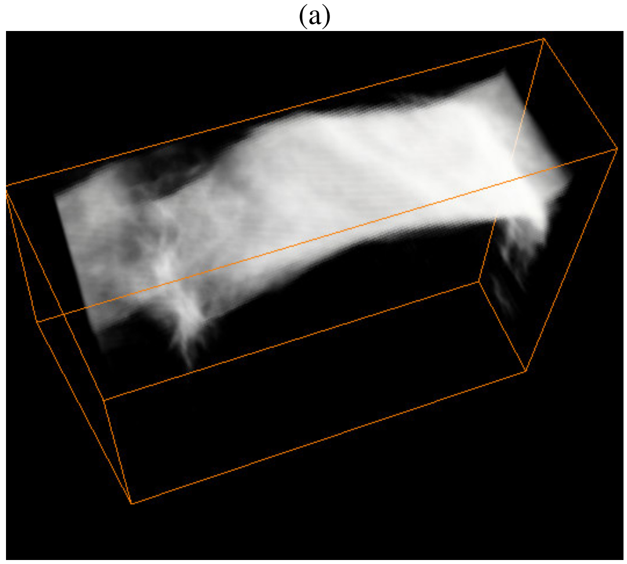

(b)

Fig.5.15 3D PS images for case study 2. (a) 3D PS volume obtained by processing the 3D B-mode US volume given in Fig 5.14 using optimized filter parameters, (b) 3D PS volume obtained using 3D PS method explained in chapter 3.

Quantitative surface matching results are given in Table 5.2. Investigating Table 5.2 we can see that by optimizing the filter parameters using the proposed framework in Chapter 4 we achieve a better localization accuracy. On the other hand 3D PS method achieves the best localization accuracy.

Table 5.2 Clinical validation Case 2 US to CT surface matching error results.

	EPS	OPS	3D PS
Average Mean Error (mm)	0.94	0.46	0.42
Std (mm)	1.45	0.55	0.65

Std: Standard deviation.

5.4.3 Case 3

The patient was presented to the emergency department with right wrist pain. The fracture was identified as a right distal radius fracture. Figures 5.16-5.18 show the US images for case study 3 with the corresponding gold standard 2D CT scans. Again distinct presentation of homogeneous, strong, bright reflective echoes with dorsal acoustic shadowing was the characteristic feature of the bone all scans. The PS images, obtained using the methods explained in chapter 2 and chapter 4, are shown in Fig. 5.16 -5.18 (b) and (c) respectively.

Investigating the figures we can se that the proposed method extracts bone surfaces without being affected too much by the typical US artifacts. However, due to the empirical filter parameter selection and without tuning the filter orientations to the specific bone appearance the empirical PS method also extract soft tissue interfaces which are not part of the bone surface. Furthermore, the empirical PS method also fails to identify the fracture in some scans (Fig. 5.16 and 5.18) whereas the parameter optimized 2D PS extracts the fracture clearly. The extracted 3D PS results using the method explained in chapters 2-3 and 4 are shown in figures 5.19 and 5.20.

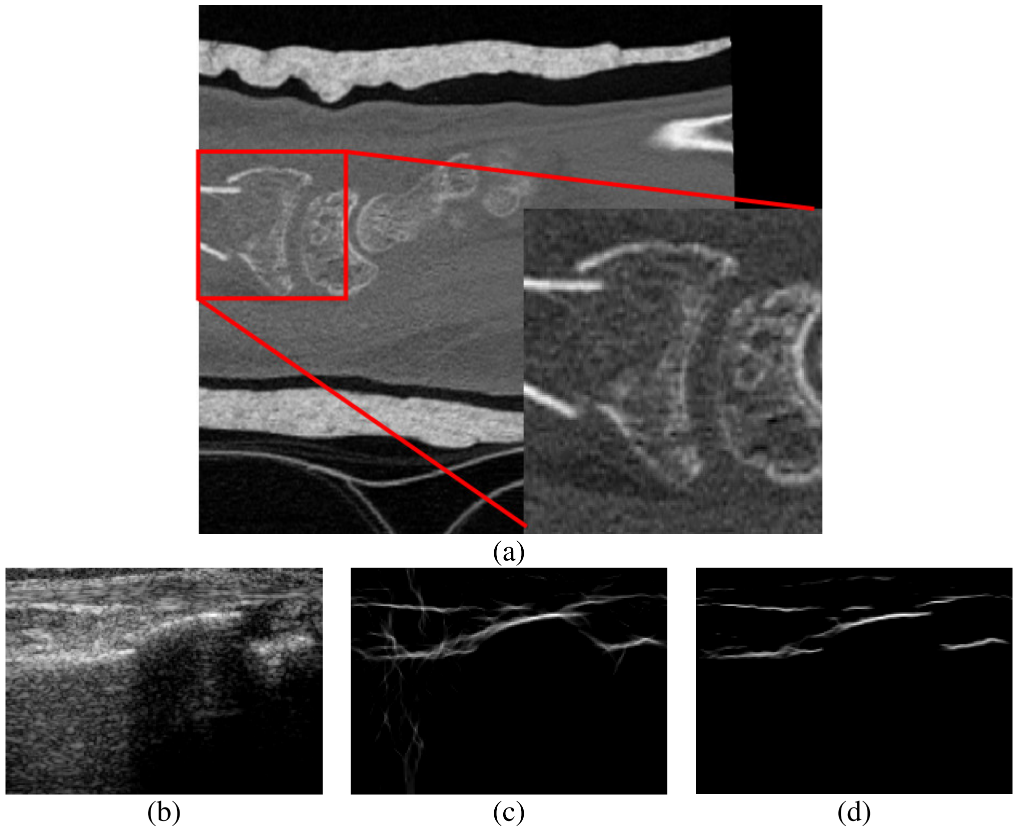

Fig.5.16 Case study 3. (a) Gold standard 2D sagittal CT slice where the zoomed in version shows a clear fracture, (b) 2D B-mode US image, (c) PS image with empirical parameters used in chapter 2, (d) Optimized PS image obtained using the proposed method in chapter 4.

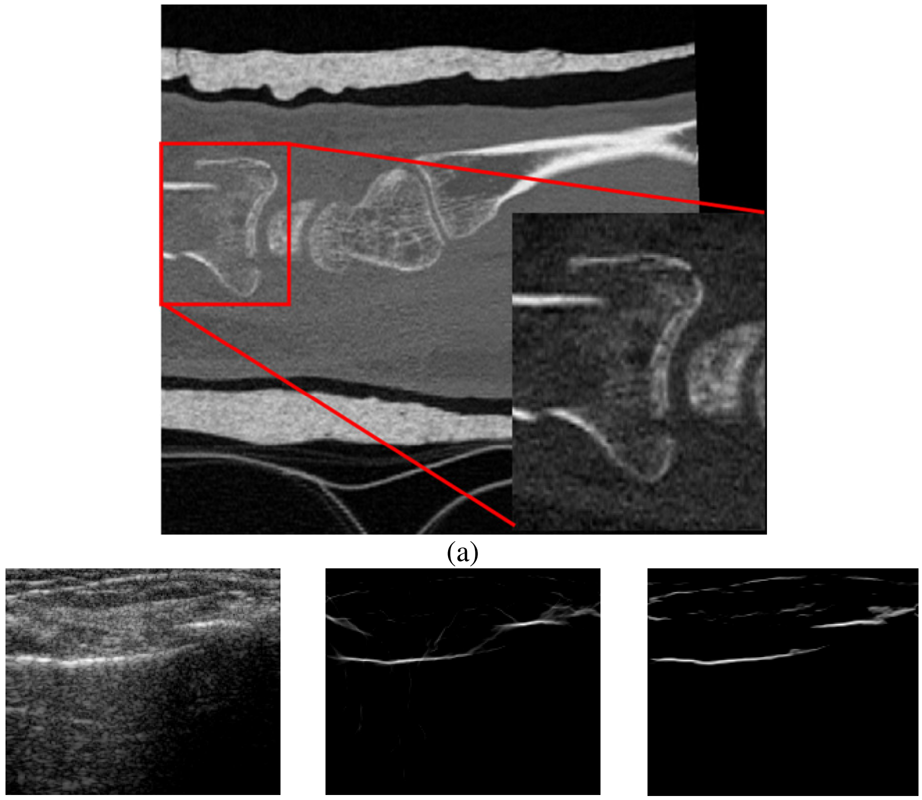

(a)

(b) (c) (d)

Fig.5. 17 Case study 3. (a) Gold standard 2D sagittal CT slice where the zoomed in version shows a clear fracture, (b) 2D B-mode US image, (c) PS image with empirical parameters used in chapter 2, (d) Optimized PS image obtained using the proposed method in chapter 4.

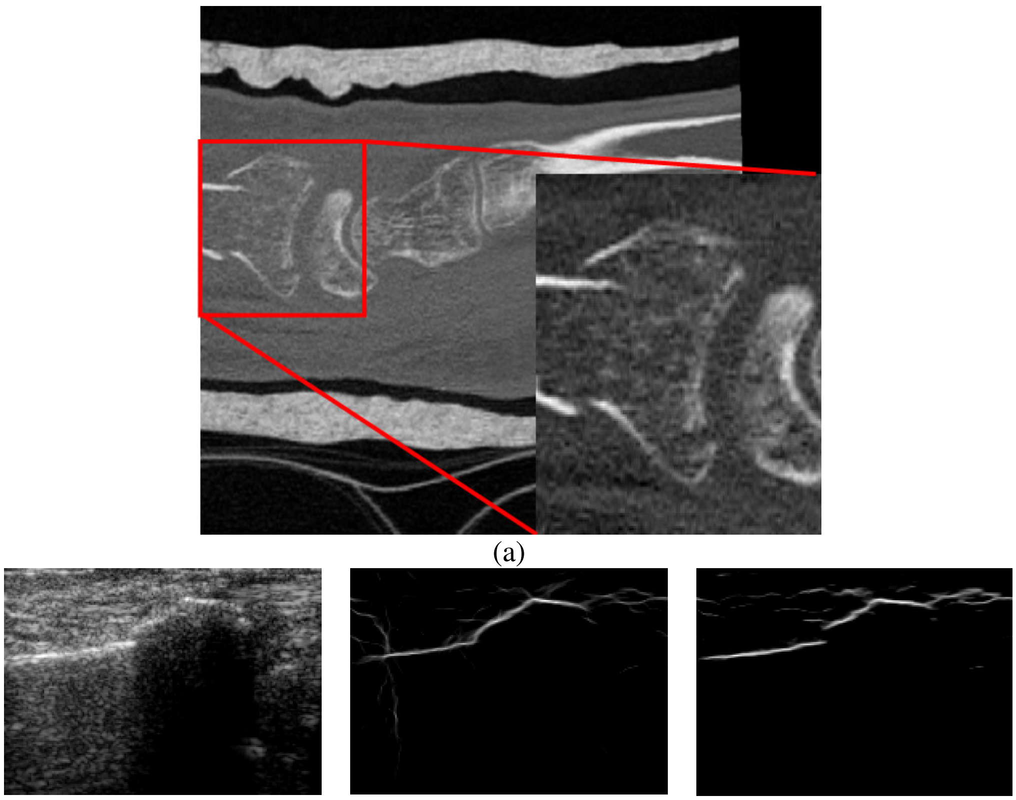

(a)

(b) (c) (d)

Fig.5. 18 Case study 3. (a) Gold standard 2D sagittal CT slice where the zoomed in version shows a clear fracture, (b) 2D B-mode US image, (c) PS image with empirical parameters used in chapter 2, (d) Optimized PS image obtained using the proposed method in chapter 4.

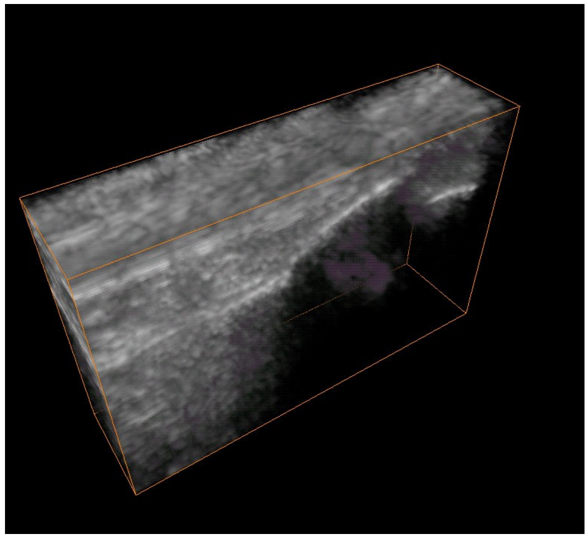

(a)

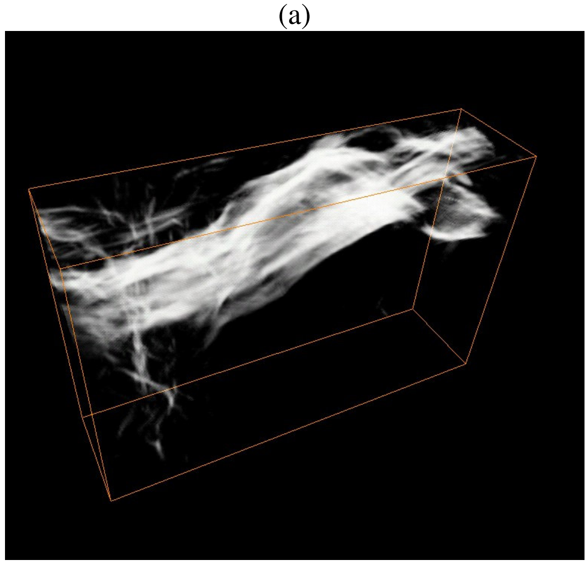

(b)

Fig.5. 19 3D US images for case study 3. (a) 3D B-mode US volume, (b) Corresponding 3D PS volume obtained by processing each individual 2D slice of the volume using the proposed method with empirical filter parameters.

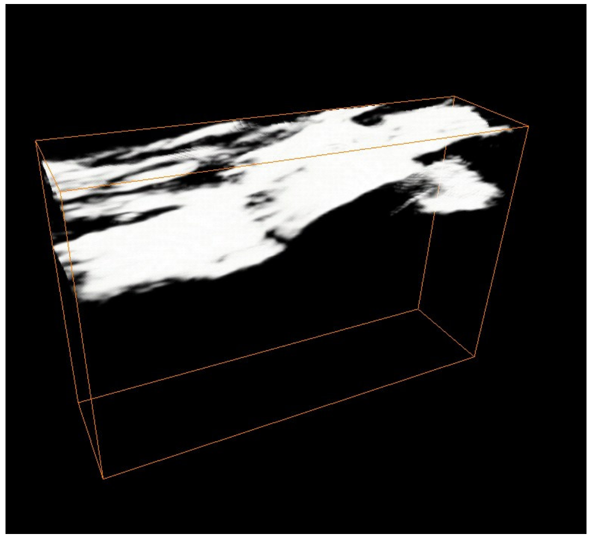

(a)

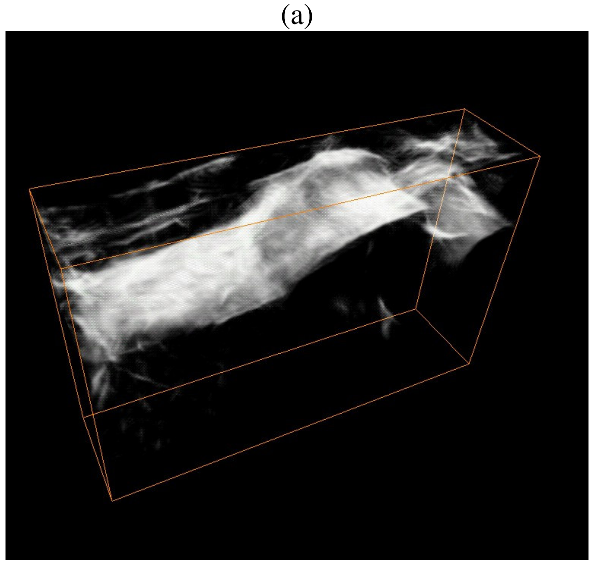

(b)

Fig.5.20 3D PS images for case study 3. (a) 3D PS volume obtained by processing the 3D B-mode US volume given in Fig 5.14 using optimized filter parameters, (b) 3D PS volume obtained using 3D PS method explained in chapter 3.

Quantitative surface matching results for case study 3 are given in table 5.3.

Table 5. 3 Clinical validation Case 3 US to CT surface matching error results

	EPS	OPS	3D PS
Average Mean Error (mm)	0.47	0.33	0.22
Std (mm)	1.39	0.88	0.77

Std: Standard deviation.

5.5 Discussion

With these three studies we have demonstrated our first clinical results using the proposed methods for extracting bone fractures from US images. With real-time scanning and confirmations obtained from the US and PS images we were able to identify the location of the fracture. Quantitative validation of the surface matching was also achieved by investigating surface matching between the surfaces extracted from B-mode US volumes using the proposed methods and gold standard CT surface. The surface results obtained from these two clinical cases were identical to the X-ray and CT findings. This similarity supports the hypothesis that real-time 3D US can provide real-time observation that can guide and confirm the fracture.

During these three studies we observed that proper alignment of the US transducer is of major importance in order to identify fractures. The scanning positions shown in Fig.5.4 provided good starting points.

Obtaining the US scans for case study 2 proved to be little bit problematic compared to the other cases since the fracture was very close to articular surface. Identification of the fractured part proved to be challenging and added extra time to the original scanning time. However, as we already know, observation of the articular surface is limited because of their deep-seated position. Furthermore, the articular surface is blocked by carpal components. Also, US cannot be used instead of radiographs to assess or confirm the quality of the reduction of intra-articular displacement of distal radial fractures, which is not uncommon. Finally, if the fracture is close to the articular surface or the soft tissue involves substantial swelling the extracted PS surfaces are affected from this by causing detection of unwanted soft tissue interfaces (Fig. 5.13).

While US has some limitations that prevent it from completely replacing conventional radiography, it can facilitate the reduction and prevent repeated reduction attempts. Despite the encouraging experimental results and clinical study which demonstrate the potential benefits of the proposed method additional clinical studies are required in order to fully address the potential opportunities and limitations of the proposed work.

Chapter 6
Conclusion and Future Work

6.1 Significance of the Research

In this thesis we investigated the employment of 3D US as an alternative safer imaging modality for a prospective minimally invasive computer assisted orthopaedic surgery system (CAOS) designed specifically for pre-operative bone fracture assessment and inter-operative guidance in fracture reduction procedures. We proposed several medical image processing methods for extraction of bone surfaces and fractures from 3D US volumes.

In the introduction we discussed the incidence rates of fractures and the importance of fracture treatment in orthopaedic surgery. We also discussed the current challenges faced in orthopaedic surgery during the treatment of fractures and the CAOS systems that were proposed to solve these problems. We introduced 3D US as a potential imaging modality in order to improve the problems associated with the current state of the art CAOS systems.

As with other imaging systems, US has many disadvantages over direct visual contact. The images are difficult to interpret, low resolution, and have a small field of view. However, there are features that can be taken advantage of to improve performance. First, 3D US is real-time volumetric data. There is no other medical imaging modality that provides volumetric data at the temporal resolution of ultrasound. In addition, it is non-ionizing, compatible with a wide range of materials and anatomy, and comparatively inexpensive. In chapter 2 we introduced the concept of phase symmetry for extracting bone surfaces from US data. The method was based on extracting local phase features using 2D Log-Gabor filters. We also showed for the first time that using the proposed method bone fragments could be extracted and tracked from US data using the proposed method. Knowing the location and orientation of the surgical instrument is arguably the most important piece of information for the surgeon. As a final application surgical tools were also extracted from US data with the proposed method. A key advantage of the proposed method is that it is fully automatic and intensity/amplitude invariant which makes it especially attractive for US image processing since the image gray value content depends on the orientation of the transducer and the US machine settings.

To further improve the extraction of bone surfaces from US data we extended the proposed method to 3D in chapter 3. By integrating bone surface information along the axis perpendicular to the US scan plane direction decreased the sensitivity of the algorithm to soft tissue interfaces/US artifacts and increased the localization accuracy. The significance of this method is that this is the first study to demonstrate the potential of 3D US in orthopaedic surgery.

In order to further improve the proposed method, in chapter 4, we investigated the effects of filter parameters on the extracted features. We developed a method that is based on the information obtained from the image content. With qualitative and quantitative results we demonstrated how the proposed framework captures essential aspects of US image feature enhancement based on local phase information, which would be of interest to developers of US based computer aided intervention systems.

Finally we demonstrate the clinical feasibility and effectiveness of the proposed system with three clinical studies in chapter 5.

6.2 Contributions

The main contributions of this thesis are summarized as follows:

- We introduced an automatic, fast and accurate method for extracting bone surfaces from 2D US data. The method is based on the design and use of 2D Log-Gabor in order to construct a local phase symmetry measure that produces strong responses at bone surfaces and suppresses responses elsewhere.
- We extended our original local phase based image processing technique from 2D to 3D US using 3D Log-Gabor filters. Extending the 2D method to 3D enables the extraction of much smoother and continues bone surfaces with increased localization accuracy. Furthermore, integrating the surface information along the axis perpendicular to the scan plane direction made the proposed 3D algorithm less sensitive to soft tissue artifacts and more sensitive to weak bone surface responses.
- We analyzed the ability of our proposed 2D/3D local phase based method to localize surgical tools from 2D/3D US scans. Using the proposed method we showed that even relatively small surgical tools (less than 2 mm in diameter) can be localized with sub-millimeter resolution in a soft tissue model.
- We presented extensive validation studies using carefully designed phantom, in-vitro and in-vivo experiments, and demonstrate the accuracy and robustness of our proposed approach for localizing fractured bone segments from 2D and 3D ultrasound data.
- We investigated the effects of Log-Gabor filter parameters on local phase-based feature extraction, specifically for bone surface localization. Although local phase measures can be quite successful in extracting important image features, they remain somewhat sensitive to the underlying filter parameters used. Therefore, we presented a

novel method for contextual parameter selection that is adaptive to image content. Our technique automatically selects the scale, bandwidth and orientation parameters of Log-Gabor filters for optimizing the local phase symmetry in ultrasound images. The proposed approach incorporates principle curvature computed from the Hessian matrix and directional filter banks in a phase scale-space framework.

- We demonstrated the clinical feasibility and effectiveness of the proposed system with three clinical studies.

6.3 Future Work

While the proposed US feature extraction methods have shown promising results, they still require further improvements to the implementation and must be further validated to be ready for a clinical application.

6.3.1 System Improvement

Intra-operative surgery necessitates real-time performance. To provide interactive feedback to the surgeons the data processing must occur in real-time as well. A number of improvements could be performed specifically to improve the speed and usability of the proposed system. The software platform used to develop the methods explained in this thesis was a high-level programming environment (MATLAB**,** The Mathworks Inc., Natick, MA, USA). Although the average time of the proposed method in this programming environment is an order of magnitude lower than acquiring a 3D fluoroscopy scan the processing time could be significantly reduced by implementing the algorithm in a lower-level language and optimizing the coding.

The image processing methods proposed in chapter 4 provides a significant first step for ultrasound guided orthopaedic surgery systems. However, the methods should be extended to 3D to fully address all the engineering challenges. The 3D RT is defined using 1D projections of a 3D object $f(x,y,z)$

where these projections are obtained by integrating *f(x,y,z)* on a plane with an orientation defined as $\vec{\alpha}$ (Fig.6.1).

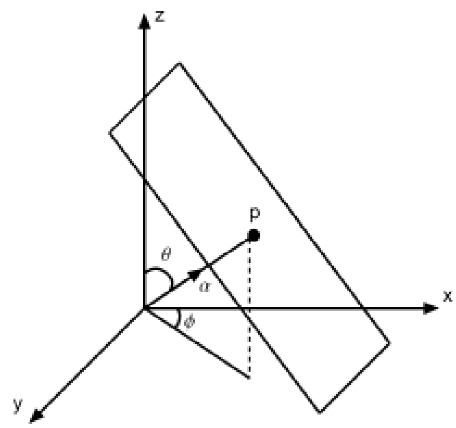

Fig.6.1 3D projection geometry.

Given a 3D function $f(\vec{x})=f(x,y,z)$ and a plane which is represented using the normal $\vec{\alpha}$ and the distance "*s*" which represents the distance of the plane from the origin, the 3D RT for this plane is defined as:

$$3DRT(\vec{\alpha},s)=\int_{-\infty}^{\infty}\int_{-\infty}^{\infty}\int_{-\infty}^{\infty} f(\vec{x})\delta(\vec{x}^{T}\vec{\alpha}-s)d\vec{x}$$

$$3DRT(\vec{\alpha},s)=\int_{-\infty}^{\infty}\int_{-\infty}^{\infty}\int_{-\infty}^{\infty} f(x,y,z)\delta(x\sin\theta\cos\phi+y\sin\theta\sin\phi+z\cos\theta-s)dxdydz \quad (6.1)$$

The 3DRT maps the spatial domain (*x,y,z*) to the domain ($\vec{\alpha}$,*s*). Each point in ($\vec{\alpha}$,*s*) space corresponds to a plane in the spatial domain (*x,y,z*). On the other hand the extension of the 2D hessian matrix to 3D is given as:

$$3DH=\begin{bmatrix} L_{xx} & L_{xy} & L_{xz} \\ L_{yx} & L_{yy} & L_{yz} \\ L_{zx} & L_{zy} & L_{zz} \end{bmatrix} \text{with } L_{ab}=\frac{\partial^2 L}{\partial a \partial b} \quad (6.2)$$

Despite the encouraging experimental results and clinical study which demonstrate the potential benefits of the proposed method, additional clinical studies are required in order to fully address the potential opportunities and limitations of the proposed work. These studies will eventually report the additional time introduced compared to the current reduction methods, reduction in the total amount of radiation exposure, achieved improvement in the reduction surgeries.

Finally, additional cadaver studies are required to compare fracture reduction accuracy, the number of attempts to achieve the desired bone alignment position, and the surgical and fluoroscopic times in 3D US guided and conventional (fluoroscopically guided) procedure. The cadaver studies will provide valuable feedback to identify the different error sources that contribute to the overall clinical accuracy, to investigate ways to measure this accuracy, to identify the main error contributors and finding ways to reduce the errors associated with these sources.

6.3.2 Other Applications

With the work presented here there are many promising new directions. Previously mentioned clinical studies such as pedicle screw placement, total hip replacement, or total knee replacement could benefit from the concepts introduced by this work.

However, the ultimate benefit of this work is more likely to be realized through the application to pelvic ring fractures where surgeons face considerable amount of difficulties during the alignment of the pelvic anatomical coordinate system. Furthermore, due to the difficulties faced during the intra-operative alignment and the use of a bigger C-arm unit (compared to mini-C arm which is used in distal radius surgeries) the amount of radiation exposure in pelvic surgeries is very high. Since post-operative CT scans are always available in these surgeries intra-operative registration of pre-operative CT data to the pelvic bone surfaces extracted using the proposed methods could be achieved. The previously proposed US based CAOS systems are based on the use of freehand 2D US transducers as an intra-operative imaging modality. Therefore, the collection of necessary data points in order to achieve successful point based registration, takes several minutes. We believe that providing real 3D surface information using the proposed methods would increase the registration accuracy and decreased operation time since the proposed methods are fully automatic and extraction of a 3D surface is sufficiently fast. Currently we are investigating the feasibility of the proposed method in extracting pelvic surfaces.

In order to use US in orthopaedic surgery applications there must be a direct line of sight between the transducer surface and the imaged bone anatomy. This could be problematic when imaging intra-articular fracture surfaces since the imaged anatomy will not allow a strong reflection from the top surface of the bones which in turn would results in an US image with a weak or no bone feature at all. However, in most of the intra-articular fracture cases there will be a pre-operative CT scan available. Again in the situations where the extraction of bone surfaces proves to be difficult an intra-operative registration of the distal part with the pre-operative CT data could be achieved.

6.3.3 US Image Registration

As mentioned in the previous section intra-operative registration is one of the most important steps in all US based CAOS systems. The ability to perform this registration accurately, automatically, and rapidly is critical for enabling more effective image guidance. The local phase features extracted using the proposed method could also be used in a registration framework which has already been investigated by our research group [1]. Since the proposed method is robust to typical US artifacts successful results were achieved in terms of registration accuracy. In chapter 4 we have also shown that RT provides useful information about the orientation and location of the bone boundaries in US images. Currently we are investigating the combination of

RT properties in a registration framework for extended field of view US and registering pre-operative CT data to intra-operative US images.

6.4 References

[1] R. Dalvi, I. Hacihaliloglu, R. Abugharbieh. "3D Ultrasound Volume Stitching Using Phase Symmetry and Harris Corner Detection for Orthopaedic Applications". *Accepted to SPIE Medical Imaging (MI)*, San Diego-USA, Feb 2010.

Appendix A
Clinical Evaluation Protocol Form

Background information

Distal radius and pelvic fractures are common injuries. Distal radius fracture is the most common fracture type in the forearm region. It is usually caused by a fall onto an outstretched hand (FOOSH). In the United States, fractures of the distal radius constitute about one sixth of all fractures seen in emergency department [1, 2, 3]. On the other hand, the incidence of pelvic fractures in the United States is estimated to be more than 100,000 per year [4] and typically occur in young patients and result from higher energy trauma.

Appropriate management and treatment of distal radius and pelvic ring fractures is important to prevent long-term disability and sequelae that may originate from the nature of the original fracture or complications of the treatment method.

A range of operative and non-operative treatment options are recommended based on injury and patient characteristics. In today's practice, methods for distal radius fracture fixation are based on either cast immobilization, percutaneous pinning, external fixation, internal fixation with plates, or combination treatments [5], while pelvic fractures are either managed non-operatively with protected mobilization or with internal and external fixation devices following reduction (realignment) of the fracture fragments [6,7,8]. Management for either injury is generally based on the fracture pattern, degree of displacement, other associated injuries, and the individual patient's needs and demands.

For distal radius fractures, other than casting, external fixation is considered the next least invasive procedure, which can be used to correct radial shortening and metaphyseal angulation, but may not always restore articular congruity in intra-articular fractures. For these situations a combination of open reduction and percutaneous pinning or internal fixation under fluoroscopic visualization is usually the favoured option and in many cases offers more secure fixation [9, 10].

The list of complications in malunited distal radius fractures is extensive and includes limitation of wrist mobility due to joint incongruencies, loss of radial length leading to impingement or subluxation of the distal radial joint, all causing a painful wrist, reduced grip strength, problems with the median nerve and, in later stages, carpal instability and secondary arthritic changes [11]. The treatment goals have therefore aimed at improving the radiographic alignment of fragments using the least invasive approach which will achieve this.

Similar treatment options, ranging from external fixation methods to open reduction and stabilization, are also available for pelvic ring fractures [6, 8]. External fixation devices cannot restore enough stability in the unstable complex fractures to allow mobilization of the patient without risk of redisplacement of the pelvis, which may lead to suboptimal functional results. In such cases, additional reduction manoeuvres are carried out, followed by internal fixation. The goal of the surgical treatment is to maintain anatomical shape of the pelvis and to reduce the fragments within 5-10mm of their normal location to maximize function.

Complications after operatively treated pelvic fractures include loss of the reduction; wound infection, neurological and/or vascular injuries, pain syndromes and leg length discrepancies which may result in permanent disability [6]. Of these, some may be related to inability to reduce the pelvis to an acceptable position or may be related to improper placement of implants. The main factors limiting the ability to reduce fractures and safely place implants are related to intra-operative fluoroscopy's limited ability (from 2-Dimensional images) to represent the complex 3-Dimensional structure of the pelvis and safely guide reduction and implant placement.

Imaging is therefore a critical component of adequate fracture treatment. The most commonly used medical imaging modalities in orthopaedic surgery are preoperative X-ray or computed tomography (CT) and intra-operative fluoroscopy for guidance during the surgery. Although these imaging modalities provide high quality visualization of bones, they still pose several challenges.

The traditional fluoroscopic images provide two dimensional (2D) representations of a 3D structure. Scans from different directions must therefore be obtained to visualize the 3D anatomical region undergoing surgery. This poses a particularly significant challenge during pelvic surgeries where large fragments are indirectly reduced back into position without direct visualization and implants are then placed to fix the fragments while avoiding important adjacent nervous and vascular structures (respectively the spinal canal and peripheral nerves, and major arteries and vessels). As no direct visualisation of the fragments or implants is possible during these operations, surgeons rely on 2-Dimensional images provided by intra-operative fluoroscopy to make decisions on a 3D environment.

Similarly during distal radius surgery, the surgeon must position the implant without direct visualization of all parts of the fracture or the implants. In order to determine the drill trajectory of K-wires, or screws commonly used for fixation during distal radius fracture surgeries, different 2D fluoroscopy images are taken assessing the quality of reduction, the position of implants particularly avoiding intra-articular penetration of the hardware.

CT imaging would on the other hand provide 3D information about the anatomical area with very good resolution but is limited to imaging before and after the surgical procedure. No intra-operative CT scanners are presently commonly in use. The preoperatively obtained 3D scans cannot at present be updated in the OR with CT once the reduction is achieved. It is therefore not possible to use this imaging modality in real time.

The pre and intra-operative imaging modalities currently employed in orthopaedic surgeries require the use of X-rays therefore exposing the surgical team and patients to potentially harmful ionizing radiation. It is reported that more than 15 million skeletal studies are performed yearly in the United States using radiography [14]. A recent study investigating the exposure of the orthopaedic surgeon's hands to radiation during the surgery found an exposure of 20mrem/case which is reported to be 187 times greater than the amount predicted by the manufacturer [15] (mrem represents the unit in radiation dose). For comparison, a chest x-ray exposes the patient to about 20mrem. The surgeries included in this study were treatments for distal radius fractures and malunions, scaphoid nonunion, small joint fusion, perilunate dislocation, and metacarpo-phalangeal joint arthroplasty. Both the National Council on Radiation Protection and the International Commission of Radiological Protection recommend a maximum exposure of the hands of 50000mrem, which allows up to 2500 cases per year. Though 20mrem/case is below this limit, however, receiving nearly the equivalent of a chest X-ray per case indicates special care must be taken especially if we think the amount of surgeries a surgeon has to perform. It is reasonable to keep the radiation exposure as low as possible, regardless of safety regulations and to strive to develop imaging modalities which avoid ionizing radiation whenever possible.

Since images used for guidance and fracture reduction assessment are 2D, the number of fluoroscopy images taken during the surgery increases depending on the experience of the surgeon. In a recent study, Blattert *et al* [16] formed two teams according to their professional qualification and clinical appointment in order to determine whether skill dependence affects the amount of radiation exposure to orthopaedic surgeons. The study showed that the mean time of fluoroscopy per operation was higher for the team which had less experienced surgeons.

Because of the difficulties encountered during the fixation of these fractures special interest has developed in computer assisted orthopaedic surgery (CAOS). Computer Assisted Surgery (CAS) was first introduced to locate brain tumors based on stereo tactics principles [19]. After that the CAS field has started to grow in different subspecialties; CAOS being one of them.

The most recent review about the latest developments of CAOS was conducted by Sugano [20] and Schep [21].Because of the rigid structure of the bone Orthopaedic surgeries are particularly suitable for CAS systems. There are two main categories in current Computer Assisted Orthopaedic Surgeries based on their imaging modalities and guidance capabilities: *Fluoroscopy Guided* and *Volumetric Image Guided* systems.

In Volumetric Image Guided systems preoperatively three dimensional (3D) models are created with the help of different imaging modalities such as computed tomography (CT), and magnetic resonance imaging (MRI). These models are then used together with the intra-operatively captured tracked two dimensional (2D) Fluoroscopic or 2D Ultrasound images to localize the patient in the OR and to guide the surgeon during the surgery. In CAOS systems CT is the most common used preoperative imaging modality. Because of its high resolution, and high contrast between the bone and surrounding tissue segmentation of bone is easy in CT. This imaging modality is used in several applications like: distal radius osteotomy [22, 23] spine pedicle screw insertion [24, 25, 26], total hip arthroplasty [27], total knee arthroplasty [28, 29], and reconstruction of knee cruciate ligaments [30].

For Fluoroscopic navigation; which is less costly than volumetric image based navigation, 2D Fluoroscopic images are used to construct the guiding process. A tracked C-arm, which is known as a mobile fluoroscopy device, is used during the surgery for data acquisition. The major disadvantage is the substantial exposure to ionizing radiation and fluoroscopy images only provide 2D planar view of the anatomical area being imaged.

Although these systems provide successful results there is still a need for a intra-operative real time 3D imaging modality in orthopaedic surgery.

The recently introduced 3D fluoroscopy units provide 3D visualization of the anatomical area of interest. However, the popularity of this technique is currently limited by the high cost of commercial systems, the limited field-of-view and inferior image quality compared with CT images. Furthermore, a rigid relationship must be obtained between the reference arc and the navigated anatomy in order to have an accurate 3D fluoroscopy unit. Finally there is still radiation exposure to the patient and surgical team.

Ultrasound has traditionally been used to image the body's soft tissue, organs, and blood flow in real time. Since there is no clinically reported risk of using ultrasound, it is still regarded as the only safe method to image a fetus. Consequently, in order to eliminate the substantial exposure of ionizing radiation to both the surgical teams and patients, which is inherent to fluoroscopic and volumetric image guided systems, special attention has been recently given to incorporating ultrasound imaging instead of fluoroscopy which completely eliminates the exposure of ionizing radiation [31-44]. Although unable to penetrate bone, ultrasound strategy is capable of delineating the surface of bone in 2 or 3 Dimensions, which may be used as an anatomical landmark. Our group's preliminary work on using 3D ultrasound has shown promising laboratory results; supporting the present pilot proposal to investigate the technologies capabilities in a clinical setting [45-47].

Purpose

The purpose of this research proposal is to determine the effectiveness and demonstrate the clinical feasibility of using 3D ultrasound imaging modality for assessing distal radius and pelvic fractures in emergency departments. Using real time 3D ultrasound we would ultimately aim to decrease the amount of time spend in the emergency department, to decrease the radiation exposure to patient and to staff, and to increase the accuracy of reduction and implant placement in fracture fixation cases. The present goals are limited to the feasibility outcomes listed below.

Hypothesis

Our hypothesis is that 3D real time ultrasound can provide useful information about the fractured anatomical area.

The specific research questions we aim to answer are:

- Can distal radius and pelvic ring fractures be assessed from 3D ultrasound scans using state of the art image processing techniques?
- Is the ultrasound procedure well tolerated by patients? (questionnaire, rate of refusal) Separate document: 3D ultrasound patient assessment questionnaire:
- Can we obtain the same or more information from this 3D scans compared to plain X-rays or CT?
- Which characteristics of the fractured bone surfaces can we detect?
- To what extent can we match the surface detected on ultrasound to that of X-ray or CT image?
- Are the measures of post reduction as assessed by 3D ultrasound similar those assessed by traditional imaging modalities such as post reduction X-ray and CT?

This in turn will help us in the future design, develop, and evaluate a 3D ultrasound based CAOS system which could:

- Improve performance by providing better assessment and placement of the fracture fragments which could in turn improve reduction and decrease the operation time
- Promote minimally invasive surgery (MIS) by minimizing soft tissue exposure
- Decrease cost and improve efficiency by replacing fluoroscopy at key points in the diagnosis and treatment
- Decrease the amount of radiation exposure to patients and to staff
- Decreasing the post operative complications related to fracture fragment reduction and implant position, which are encountered because of imaging limitations.

This research will introduce the concept of using radiation-free real time 3D ultrasound imaging modality for fracture assessment in emergency departments. It could provide a method which will be robust, fast and easy to use and which will allow imaging of the fracture at the time of presentation and during surgery.

Furthermore, it will be invaluable for all future imaging studies with ultrasound for fracture reduction assessment in orthopaedic surgeries.

Methods

The components of the proposed research method are an ultrasound scanner and a ultrasound probe. By interacting with the ultrasound probe the surgeon can acquire 3D ultrasound scans from the fractured wrist or pelvic area. The acquisition time for one ultrasound volume is approximately 30 seconds, translating into 2 minutes (4 sides) to assess an area, and doubling to 5 minutes per area scanned to factor in positioning time.

Due to the physics of ultrasound imaging ultrasound signals cannot penetrate the bone surface. Therefore, only the bone surface which is perpendicular to the probe surface can be scanned and visualized. In order to span all the fractured bone area different ultrasound volumes will be obtained from dorsal, volar, radial and ulnar sections of the distal radius, and the superior and lateral portions of the iliac crest on the pelvis using the sterile-bag covered ultrasound probe. As stated, actual scanning time is expected to be 2 minutes per area of interest. Considering the need for repositioning we expect this will take 5 minutes per scan. As we will need to scan patients 2 to 3 times over the course of care we expect the total time demand increase from usual care would be 10-15 minutes, which we expect would not affect the patients outcome.

Ultrasound scans will be obtained from patients who arrive to the emergency department with a distal radius or pelvic ring fracture. Enrollment in this pilot study will be limited to 20 patients who have already been diagnosed with a fracture in this area and who have been referred to the Orthopedic Trauma team at VGH for consultation and treatment. The patient will have already undergone a standard investigation procedure, which involves anatomical investigation by the surgeon and obtaining X-ray scans (if necessary a CT scan). Once the area (wrist or pelvis) is confirmed to involve a fracture requiring further care, the patient will be informed about the study and invited to participate. Informed consent will be obtained. The time allowed for the patient to make a decision after he/she is informed about the study will be limited to 2 hours.

Inclusion criteria:

- Patients presenting to VGH Emergency Room with a diagnosis of distal radius or pelvis fracture, who are referred to the orthopaedic Trauma team.

Exclusion criteria:

- Patients with skin conditions, skin breakdown, or allergy which precludes the use of ultrasound gel.
- Patients who have sustained a previous pelvis or distal radius fracture.
- Patients unable to provide informed consent.

The scanning will start after voluntary consent is obtained. For comparison of anatomical alignment and to ease study participant concerns related to an unfamiliar imaging modality involving gel and a probe, the uninjured wrist or pelvis of the patient will first be examined with ultrasound machine.

US technique: Before starting the ultrasound scan a special ultrasound gel (the amount equivalent to the tip of a thumb) will be spread into the skin surface. The gel makes the probe movement much easier and effective. It also helps coupling the probe interface with the skin surface which makes the image quality much better. The gel has no perfumes, no color, is hypoallergenic and is water-soluble. During the scanning no additional pain will be caused to the patient and the total scanning time will be limited to 15 minutes.

The acquired ultrasound volumes will be analyzed with state of the art image processing techniques after transferring them to a computer workstation.The reliability and accuracy of ultrasound will be compared with the standard imaging modalities which are currently being used in emergency departments to assess the fracture as part of their usual care. Consequently, we will also ask for permission from the study participant to review the X-ray and CT scans (if available), collect the information and transform it to compare the ultrasound results to X-ray and CT scans.

Analysis: After transferring the US scans to a workstation (PC) located at UBC-Department of Electrical and Engineering we will extract the 3D bone surfaces from the US scans by using state of the art image processing techniques that are already being developed by our group [45-48]. The gold standard comparison will be provided by the 3D surfaces extracted from the CT scans. The analysis will be done by assessing the "fitness" of US derived surfaces to the gold standard. Moreover, the reliability and accuracy of using US imaging in comparison with that of conventional X-rays for fracture fragment detection will also be evaluated by investigating the derived bone surfaces.

References

[1] Hanel D.P., Jones M.D, Trumble ., T.E., "Wrist fractures", Orthop Clin North Am; 33(1): pp.35-57, 2002.

[2] McMurtry R.Y., Jupiter J.B., Browner B.D., "Fractures of the distal radius", Skeletal Trauma: Fractures, Dislocations, Ligamentous Injuries. Philadelphia: WB Saunders Co, pp.1063-91, 1997.

[3] Brooks KR, Capo JT, Warburton M, Tan V., "Internal fixation of distal radius fractures with novel intramedullary implants", Clin Orthop Relat Res. Pp:42-50, 2006.

[4] Rice PL Jr, Rudolph M., "Pelvic fractures", Emerg Med Clin North Am., 25(3), pp.795-802, 2007.

[5] Muller M.E., Allgower M., Schneider R., Willenegger H, Manual of Internal Fixation, Springer-Verlag, 1991.

[6] Hirvensalo E., Lindahl J., Kiljunen V., "Modified and new approaches for pelvic and acetabular surgery", Injury, 38(4),pp. 431-441, 2007.

[7] Nunn T., Pallister I., "Fractures of the pelvic ring", Surgery (Oxford),25(10),pp. 420-423, 2007.

[8] Stephen D. J. G., "Management of high-energy pelvic fractures", Current Orthopaedics, 17(5), pp: 335-345, 2003.

[9] Geissler W., Fernandez D., "Percutaneous and limited open reduction of intra-articular distal radial fractures", Journal Hand Surgery, Vol.5, pp. 85-92, 2000.

[10] Grewal R., Perey B., Wilmik M., Stothers K.," A randomized prospective study on the treatment of intra-articular distal radius fractures: Open reduction and internal fixation with dorsal plating versus mini open reduction, percutaneous fixation, and external fixation", Journal of Hand Surgery, Vol. 30A, pp 764-772, 2005.

[11] Croitoru H., Ellis R.E., Small C. F., Pichora D. R., "Fixation based surgery: A new technique for distal radius osteotomy", Medical Image Computing and Computer Assisted Intervention, pp. 1126-1135, 2000.

[12] Cimerman M., Kristan A., "Preoperative planning in pelvic and acetabular surgery: The value of advanced computerized planning modules", Injury, 38(4), pp.442-449, 2007.

[13] Edwards II, C.C., Christopher J.H., McGillivary G.R., Gutow A.P., "Intra-articular distal radius fractures: arthroscopic assessment of radiographically assisted reduction", The Journal of Hand Surgery, pp.1036-1041, 2001.

[14] Herscoici D., Sanders R.W., "The effects, risks, and guidelines for radiation use in orthopaedic surgery", Clinical Orthopaedics and Related Research, pp 126-132, 2000.

[15] Singer G., "Radiation exposure to the hands from mini C-arm fluoroscopy", The Journal of Hand Surgery, Vol 30A, pp 795-198, 2005.

[16] Blattert R.T., Fill U.A., Kunz E., Panzer W., Weckbach A., Dieter F.R., "Skill dependence of radiation exposure for orthopaedic surgeon during interlocking nailing of long bone shaft fractures: a clinical study", Arch. Of Orthopaedic Trauma Surgery, pp. 659-664, 2004

[17] Kachalia a., Gandhi T.K., Puopolo A.L., Yoon C., Thomas E.J., Griffey R., Brennan T.A., Studdert A.M., " Missed and delayed diagnoses in the emergency department: a study of closed malpractice claims from 4 liability insurers", Annals of Emergency Medicine, VOl. 92, pp.196-205, 2007

[18] Guly H.R., "Diagnostic errors in accident and emergency department", Emergency Medicine Journal, pp. 263-269, 2001.

[19] Bown R.A., "A computerized tomography- computer graphics approach to stereotaxic localization", Journal of Neurosurgery, 50, pp.715-720, 1979.

[20] Sugano N., "Computer Assisted Orthopaedic Surgery", *Journal of Orthopaedic Science,* 8:442-448, 2003.

[21] Schep N. W. L., Broeders I. A. M. J., "Computer Assisted Orthopaedic and Trauma Surgery state of the art and future perspective", Injury,34:299-306,2003.

[22] Athwal G. S., Ellis R. E., Small C. F., Pichora D. R., "Outcomes of Computer Assisted Distal Radius Osteotomy", Journal of Hand Surgery, 28:951, 2003.

[23] Croitoru H., Ellis R. E., Smal C. F., Prihar R., Pichora D. R., " Fixation Based Surgery: A new technique for distal radius osteotomy", Journal of Computer Aided Surgery,6:160, 2001.

[24] M. Arand, E. Hartwig, L. Kinzl, "Spinal navigation in cervical fractures-a preliminary clinical study on judet-osteosynthesisof the axis", Journal of Computer Aided Surgery,6: 170-175, 2001.

[25] M. Kamimura, S. Ebara, H. Itoh, "Accurate pedicle screw insertion under the control of a computer assisted image guiding system: laboratory test and clinical study", Journal of Orthopaedic Science, 4: 197-206, 1999.

[26] P. Merloz, J. Tonetti, A Eid, " Computer assisted spine surgery", Clinical Orthopaedics,337: 86-96, 1999.

[27] A. M. DiGioia, B. Jaramaz, M. Blackwell, "The otto aufranc award: image guided navigation system to measure intraoperatively acetabular implant alignment", Clinical Orthopaedics, 355:8-22, 1998.

[28] S. L. Delp, S. D. Stulberg, B. Davies, "Computer assited knee replacement", Clinical Orthopaedics, 354:49-56, 1998.

[29] K. A. Krackow, M. Bayers-Thering, and M. J. Phillips, "A new technique for determinng proper mechanical axis alignment during total knee arthroplasty: proress toward computer assisted TKA", Orthopaedics, 22:698-702, 1999.

[30] T. V. Klos, R. J. Habets, A. Z. Banks, "Computer assistance in arthroscopic anterior cruciate ligament reconstruction", Clinical Orthopaedics, 354: 65-69, 1998.

[31] Chen T.K., Abolmaesumi P., Pichora D.R., Ellis R.E., "A system for ultrasound-guided computer assisted orthopaedic surgery", Journal of Computer Aided Surgery, Vol. 10, pp. 281-292, 2005.

[32] Amin D.V., Kanade T., DiGioia A. M., Jaramaz B., "Ultrasound registration of bone surface for surgical navigation", Computer Aided Surgery, pp.1-16, 2001.

[33] Herring J. L., Dawant B. M., Maurer Jr. C.R., "Surface based registration of CT images to physical space for image guided surgery of the spine: a sensitivity study", IEEE Transactions on Medical Imaging, pp.743-752, 1998.

[34] Kryvanos A., Computer assisted surgery for fracture reduction and deformity correction of the pelvis and long bones, PhD thesis, University of Manheim, Germany, 2002.

[35] Barratt D.C., Penney P.G., Chan S.K., Slomczykowski M., Carter T.J., Edwards P.J., Hawkes D.J., "Self calibrating 3D-ultrasound-based bone registration for minimally invasive orthopaedic surgery", IEEE Transactions on Medical Imaging, Vol. 25, No. 3, March 2006.

[36] Penney G.P., Barratt D.C., Chan C.S.K., Slomczykowski M., Carter T.J., Edwards P.J., Hawkes D.J., "Cadaver validation of intensity-based ultrasound to CT registration " , Medical Image Analysis, Vol 10, Issue 3, June 2006.

[37] Muratore D. M., "Towards an image guided spinal surgical system using three dimensional ultrasound: from concept to clinic", PhD thesis, Vanderbilt University, USA, 2002.

[38] Carrat L., Tonetti J., Lavallee S., "Percutaneous computer assisted iliosacral screwing", Medical Image Computing and Computer Assisted Intervention Conference, pp.84-91, 1998.

[39] Carrat L., Tonetti J., Merloz P., "Percutaneous computer assisted iliosacral screwing: Clinical validation", Proc. Medical Image Computing and Computer Assisted Intervention Conference, pp.1229-1237, 2000.

[40] Muratore D. M., Russ J. H., Dawant B. M., “Three dimensional image registration of phantom vertebrae for image guided surgery: A preliminary study”, Computer Aided Surgery, pp.342-352, 2002.

[41] Tonetti J., Carrat L., Blendea S., Merloz P., Troccaz J., Lavallee S., Chirossel J.P., ” Clinical results of percutaneous pelvic surgery: Computer assisted surgery using ultrasound compared to standard fluoroscopy”, Journal of Computer Aided Surgery, Vol. 6, January 2001.

[42] Kowal J., Amstutz C.A., Nolte L.P., “On B-mode ultrasound based registration for computer assisted orthopaedic surgery”, In: CAOS, pp. 35, 2001.

[43] Talib H., Rajamani K., Kowal J., Styner M., Ballester M.A.G., “Assessing the feasibility of ultrasound initialized deformable bone models”, Proc. of SPIE Medical Imaging, 2006.

[44] Daanen V., Tonetti J., Troccaz J., “A fully automated method for the delineation of osseous interface in ultrasound images”, Medical Image Computing and Computer Assisted Intervention Conference, pp. 549-557, 2004.

[45] Hacihaliloglu I., Abugharbieh R., Hodgson A.J., Rohling R.N., "Bone Segmentation and Fracture Detection in Ultrasound Using 3D Local Phase Features". Accepted to Medical Image Computing and Computer Assisted Intervention (MICCAI), NY-USA, Sep 2008

[46] Hacihaliloglu I., Abugharbieh R., Hodgson A.J., Rohling R.N., O'Brien P., Guy P.," Surgical Tool Localization From 3D Ultrasound Volumes Using 3D Phase-based Features", CAOS 2008, Hong Kong-China, 2008.

[47] Hacihaliloglu I., Abugharbieh R., Hodgson A.J., Rohling R.N., O'Brien P., Guy P., " Distal radius and K-wire localization in 3D ultrasound using local phase information", Proceedings of the 7th Annual Meeting of CAOS International CAOS 2007, Heidelberg-Germany, 2007, pp. 572-575.

[48] Hacihaliloglu I., Abugharbieh R., Hodgson A.J., Rohling R.N.,, “Enhancement of bone surface visualization from 3D ultrasound based on

local phase information", IEEE International Ultrasonics Symposium, Vancouver-Canada, 2006, pp. 21-24.

Appendix B

Clinical Evaluation Patient Consent Form

Bone Fracture Alignment Assessment Using 3D Ultrasound Imaging – A Pilot Study

STUDY PARTICIPANT CONSENT FORM

Principal Investigator: Pierre Guy, MDCM, MBA, FRCSC, Assistant Prof.
UBC Department of Orthopedics
Div of Ortho Trauma
Ph: +1 604-875-5239
Fax: +1 604-875-4438

Co-Investigator: Dr. Anthony J. Hodgson, Associate Prof.
UBC Department of Mechanical Engineering
Ph: +1 604-822-3240
Fax: +1 604-822-2403

Co-Investigator: Dr. Rafeef Abugharbieh, Assistant Prof.
UBC Department of Electrical and Computer Engineering
Ph: +1 604-822-6034
Fax: +1 604-822-5949

Co-Investigator: Dr. Robert N. Rohling, Associate Prof
UBC Department of Electrical and Computer Engineering
UBC Department of Mechanical Engineering
Ph: +1 604-822-2045
Fax: +1 604-822-5949

Co-Investigator: Ilker Hacihaliloglu, PhD, Candidate
UBC Department of Electrical and Computer Engineering
Ph: +1 604-822-4988
Fax: +1 604-822-5949

Description

You have been invited to participate in this study because you have a distal radius fracture in your forearm region or a fracture of your pelvis bone. Before you decide, it is important for you to understand what the research involves. This consent form will tell you about the study, why the research is being done, what will happen to you during the study and the possible benefits, risks and discomforts.

If you wish to participate, you will be asked to sign this form. If you do decide to take part in this study, you are still free to withdraw at any time and without giving any reasons for your decision.

If you do not wish to participate, you do not have to provide any reason for your decision not to participate nor will you lose the benefit of any medical care to which you are entitled or are presently receiving. Please take time to read the following information carefully and to discuss it with your family, friends, and doctor before you decide.

This research is currently being carried out as an internal study by the investigators listed above and is conducted by the University of British Columbia, Department of Orthopaedics, Department of Mechanical Engineering and Department of Electrical and Computer Engineering.

Background

Appropriate management and treatment of fractures is important to prevent long-term disability that may originate from the nature of the original fracture or its treatment. A variety treatment options involving either surgery or no surgery are commonly recommended for fractures, depending on the bone involved, the extent of the injury, the patient's needs, and the ability to restore function. Your surgeon has recommended a treatment based on these criteria. This treatment (or procedure) involves realigning and holding into position the different fragments of your fracture with or without an operation.

The study we are inviting you to take part in **will not** influence which treatment to choose but aims at performing an ultrasound to display the different fragments of your broken bone using ultrasound technology.

Imaging is one of the main components of all fracture assessment and treatment methods. It uses a range of technologies to show physicians the extent of an injury, for example which bone is broken and to what extent. The most commonly used medical imaging modality in emergency departments and orthopaedic surgery are X-rays. These are usually done prior to any type of procedure to allow physicians to better define the injury. Along with the usual X-rays, CT scans are also obtained to define in additional detail the injured bone if the injured region can not be identified clearly from the previously obtained X-rays. Imaging is also performed during and after a procedure to confirm the proper position of the fracture.

Although these imaging modalities provide high quality visualization of bones, they have limitations.

Traditional X-rays provide two dimensional (2D) representations of your bones which are three dimensional (3D) structures. To compensate for that, X-rays must be taken from different directions to visualize the anatomical region being imaged or operated on. A lot of skill is required to visualize 3D anatomy based on information obtained from 2D images and perform the necessary surgical action accordingly.

Another type of imaging we already mentioned, CT imaging, on the other hand can provide 3D information, but as it is not readily available during a procedure or in the operating room it is therefore not a practical option to assist treatment.

X-rays are also used during procedures such as orthopedic surgery to monitor the position of fragments but also to confirm the proper position of implants (wires, plates, screws) which are used to keep bones together. Surgeons use their knowledge of a bone's anatomy to properly realign it and fix it with implants. The result is usually confirmed during surgery by additional X-rays. Operation time, quality and accuracy of the surgical procedure and reproducibility of the surgical actions therefore largely depend on information obtained from 2D X-ray images and the experience of the surgeon.

Although safe because used in small radiation doses, one final area of concern is that imaging modalities, such as X-rays, currently employed to monitor the position of fracture fragments and during surgery requires the use of X-rays, which expose the surgical team and patients to potentially harmful ionizing radiation. Note that the doses of radiation used for each operation remain within a safe range for patients and repeated doses are safe for surgical team staff.

In contrast, Ultrasound is non ionizing imaging modality that involves no radiation and no known harmful side effects to humans. It is utilized to image soft tissues inside the body but can also show the contour of more solid structures such as bone. Many people would be familiar with the use of Ultrasound to image a baby or fetus prior to birth. In this study we will image fractures and surrounding bone with similar ultrasound technology with additional 3D capacity.

The ability of 3D ultrasound to show fractures have not yet been established. This research will introduce the concept of using radiation-free real time 3D ultrasound imaging modality for fracture assessment in emergency department and in the operating room. Our aim is to compare this new technology to the usual one in its ability to image the fractured bone prior to and after repositioning.

Furthermore, it could be helpful in developing new minimally invasive techniques for these surgeries, reducing amount of radiation, decreasing the post operative complications encountered because of the approaches (placement of implants) applied in today's practice. This would involve other types of research than the one we are proposing to you.

Purpose

- The purpose of this study is to demonstrate the *clinical feasibility* of using three dimensional (3D) ultrasound, an imaging modality that involves no ionizing radiation, for assessing distal radius fractures and pelvis fractures in the emergency department and in the operating room. We will achieve this by performing to the usual imaging that is done for the type of injury you have, then additionally imaging the area with 3D ultrasound. Having done both, we will be able to find 3D Ultrasound's ability to identify the usual imaging information.

Who can participate?

Patients who present to the Emergency Department at Vancouver General Hospital with a distal radius fracture or a pelvis fracture will be invited to participate.

Who should not participate?

Patients who do not have a distal radius fracture or a pelvis fracture should not participate in this study. Patients who have previously sustained a radius fracture or a pelvis fracture which has now healed should also not participate. Moreover, patients who have a skin condition, skin breakdown, or allergy which precludes the use of ultrasound gel over the area should also not participate.

Study Procedure

The study will take place in the Emergency Department and the Operating Room of Vancouver General Hospital (VGH, Vancouver, BC, Canada). Enrollment will be limited to 20 patients who have given their consent. All other patients will receive the usual level of care provided at VGH for these injuries.

The components of the proposed research involve an ultrasound scanner and a 3D ultrasound probe. Before scanning the area on your body (wrist or pelvis) an ultrasound gel will be spread into the skin surface. The gel makes the probe movement much easier and effective, and also improves the image quality. The gel has no perfumes, no color, is hypoallergenic and is water-soluble.

The ultrasound probe will then be placed on the skin over the fractured bone 4 times (once in each direction: superior, inferior, medial, lateral) for about 30 seconds each (total ultrasound time of 2 minutes). A sterile technique will be used keeping the gel and probe away from any planned or performed surgical incisions.

The obtained images will be analyzed and compared with the standard imaging modalities (X-rays, CT scan) which were used to assess the fracture and which we will also use to analyze. .

For comparison of anatomical alignment your uninjured wrist or pelvis will also be examined with 3D ultrasound using the same type of gel and probe; however no specific X-ray of this area will be taken.

Risks

As this study does not influence treatment and uses technology which is commonly used in other fields of medicine we foresee no additional risks from participating in this study. We expect the ultrasound procedure you will undergo will take an additional 5 minutes everytime the ultrasound is used. As the ultrasound will be used 2 and perhaps 3 times, depending on the number of attempts at realigning the bone (reductions) to be done, we expect an additional 10-15 minutes will be added to the usual care. This would be a small amount of time not expected to influence the outcome of your injury.

Cost and Payments

You will incur no additional cost and will not receive any payment for participation in this study. Your participation is purely voluntary.

Benefits

There are no direct benefits to you for participating of this study. We hope that the information learned from this study will help in developing 3D ultrasound imaging for fractures of the distal radius and the pelvis and be a potential benefit to future patients.

Discomforts

As described, Ultrasound imaging involves the placement of a gel over the area to scan followed by the sliding of a probe on the gel and skin surface to visualize the area of interest. This procedure involves a very small amount of pressure over your wrist or pelvis. As ultrasound is often successfully used over affected tender areas of the body (for example to identify a fluid collection in a swollen area or on the infected skin overlying an abscess) we expect this test to be well tolerated and no more painful than the usual X-rays done for the injury.

The usual care for the assessment and treatment of a fracture would involve you receiving analgesic medication, which we expect would be sufficient to allow you to undergo the usual X-rays and an Ultrasound.

The Ultrasound will first be performed on your *uninjured* side; we expect this will allow you to appreciate the extent of the procedure.

You may request to have the procedure stopped at any time for discomfort or any other reason.

Alternative Treatments

If you decide not to participate in this study, you will be treated with the standard procedure and a treatment method will be conducted depending on the fracture type.

Privacy

Your rights to privacy are protected by the Freedom of Information and Protection of Privacy Act of British Columbia. This act lays down rules for the collection, protection and retention of your personal information by public bodies, such as the University of British Columbia and its affiliated teaching hospitals. Further details about this Act are available upon request.

Confidentiality

Your confidentiality will be respected. No information that discloses your identity will be released or published without your specific consent to the disclosure. However, research records and medical records identifying you may be inspected by representatives of the UBC Research Ethics Board for the purposes of monitoring the research in the presence of the Investigator or his or her designate. No records which identify you by name or initials will be allowed to leave the Investigator's offices.

Contact

If you have any questions about the procedures employed in this study, if you desire further information with respect to this study, or if you experience any adverse effects you should contact Ms Raman Johal or Dr. Pierre Guy at 604-875-5239 or Dr. Antony J. Hodgson at 604-822-3240. If you have any concerns about your treatment or rights as a research subject, you may contact the Director of the Office of Research Services at the University of British Columbia at 604-822-8598.

Summary

The proposed procedure requires your consent to proceed with ultrasound imaging of your uninjured wrist or pelvis, followed by ultrasound of the injured side. Finally consenting to use the images obtained in the course of your care (X-ray and/or CT scan) to compare ultrasound's ability to match the images they provide.

Voluntary Consent

I understand that participation in this study is entirely voluntary and that I may refuse to participate or I may withdraw from the study at any time. The study doctor(s)/investigators may decide to discontinue the study at any time, or withdraw me from the study at any time, if they feel that it is in my best interests.

I also understand that if I choose to withdraw at any time, the data collected during my enrollment will be retained for analysis.

I understand that signing this form in no way limits my legal rights as a patient. I also understand that participating in the study, refusing to participate or withdrawing from the study at any point in time has no affect whatsoever on my medical care.

I have received a copy of this Consent Form for my own records. I have carefully reviewed all the pages of this form and I hereby consent to participate in this study.

_____________________ _________________________ _____________________

Printed name of participant Signature Date

___________________________ __________________ _____________________

Printed name of witness Signature Date

___________________________ ______________ _____________________

Printed name of principal
Investigator Signature Date

Appendix C

Clinical Evaluation Patient Questionnaire Form

SUBJECT QUESTIONNAIRE FORM

Study Title: Bone Fracture Alignment Assessment Using 3D Ultrasound Imaging

A Pilot Study

Principal Investigator: Pierre Guy, MDCM, MBA, FRCSC, Assistant Prof.
UBC Department of Orthopedics
Div of Ortho Trauma
Ph: +1 604-875-5239
Fax: +1 604-875-4438

Co-Investigator: Dr. Anthony J. Hodgson, Associate Prof.
UBC Department of Mechanical Engineering
Ph: +1 604-822-3240
Fax: +1 604-822-2403

Co-Investigator: Dr. Rafeef Abugharbieh, Assistant Prof.
UBC Department of Electrical and Computer Engineering
Ph: +1 604-822-6034
Fax: +1 604-822-5949

Co-Investigator: Dr. Robert N. Rohling, Associate Prof
UBC Department of Electrical and Computer Engineering /
UBC Department of Mechanical Engineering
Ph: +1 604-822-2045
Fax: +1 604-822-5949

Co-Investigator: Ilker Hacihaliloglu, PhD, Candidate
UBC Department of Electrical and Computer Engineering
Ph: +1 604-822-4988
Fax: +1 604-822-5949

Emergency Telephone Number: Ms Raman Johal or Dr. Pierre Guy at 604-875-5239 or Dr. Antony J. Hodgson at 604-822-3240. If you have any concerns about your treatment or rights as a research subject, you may contact the Director of the Office of Research Services at the University of British Columbia at 604-822-8598.

Thank you for taking the time to participate in this study. As the Ultrasound scanning procedure has finished we would like to take some time to ask you a few questions.

Questions:

1) How painful was your wrist while waiting in the Emergency Room prior to being seen by a physician? Please place a vertical mark on the line below to indicate how bad you felt you pain prior to seeing a doctor..

No Pain Worst Pain

2) How painful was the process of scanning with the ultrasound probe and gel? Please place a vertical mark on the line below to indicate how bad you felt you pain was during scanning

No Pain Worst Pain

3) Would you agree to the use of this ultrasound guided procedure performed again in the future?

No Yes

Appendix D

UBC Research Ethics Board Approval Certificates

The University of British Columbia
Office of Research Services
Clinical Research Ethics Board – Room 210, 828 West 10th Avenue, Vancouver, BC V5Z 1L8

ETHICS CERTIFICATE OF EXPEDITED APPROVAL

PRINCIPAL INVESTIGATOR:	INSTITUTION / DEPARTMENT:	UBC CREB NUMBER:
Pierre Guy	UBC/Medicine, Faculty of/Orthopaedics	H06-03147

INSTITUTION(S) WHERE RESEARCH WILL BE CARRIED OUT:

Institution	Site
Vancouver Coastal Health (VCHRI/VCHA)	Vancouver General Hospital

Other locations where the research will be conducted:

The investigation of the obtained scans (Ultrasound, CT, and X-ray) using state of the art image processing techniques will be done at the Biomedical Signal and Image Computing Laboratory- Department of Electrical and Computer Engineering, UBC campus.

CO-INVESTIGATOR(S):

Rafeef Abugharbieh
Ilker Hacihaliloglu
Antony J. Hodgson
Robert N. Rohling

SPONSORING AGENCIES:

N/A

PROJECT TITLE:
Bone Fracture Alignment Assessment Using 3D Ultrasound Imaging – A Pilot Study

THE CURRENT UBC CREB APPROVAL FOR THIS STUDY EXPIRES: September 11, 2009

The UBC Clinical Research Ethics Board Chair or Associate Chair, has reviewed the above described research project, including associated documentation noted below, and finds the research project acceptable on ethical grounds for research involving human subjects and hereby grants approval.

DOCUMENTS INCLUDED IN THIS APPROVAL:

Document Name	Version	Date
Protocol:		
Protocol for bone fracture assessment using 3D ultrasound	Version 1	August 6, 2008
Consent Forms:		
Revised Consent form for bone fracture assessment using 3D ultrasound	Version 2	September 5, 2008
Advertisements:		
revised Recruitment for bone fracture assessment using 3D ultrasound	Version 2	September 5, 2008
Questionnaire, Questionnaire Cover Letter, Tests:		
Questionnaire for bone fracture assessment using 3D ultrasound	Version 1	August 6, 2008

APPROVAL DATE:

September 11, 2008

CERTIFICATION:

In respect of clinical trials:

1. The membership of this Research Ethics Board complies with the membership requirements for Research Ethics Boards defined in Division 5 of the Food and Drug Regulations.

2. The Research Ethics Board carries out its functions in a manner consistent with Good Clinical Practices.

3. This Research Ethics Board has reviewed and approved the clinical trial protocol and informed consent form for the trial which is to be conducted by the qualified investigator named above at the specified clinical trial site. This approval and the views of this Research Ethics Board have been documented in writing.
The documentation included for the above-named project has been reviewed by the UBC CREB, and the research study, as presented in the documentation, was found to be acceptable on ethical grounds for research involving human subjects and was approved by the UBC CREB.
Approval of the Clinical Research Ethics Board by one of: **Dr. Gail Bellward, Chair**

The University of British Columbia
Office of Research Services
Clinical Research Ethics Board – Room 210, 828 West 10th Avenue, Vancouver, BC V5Z 1L8

ETHICS CERTIFICATE OF EXPEDITED APPROVAL: RENEWAL

PRINCIPAL INVESTIGATOR:	DEPARTMENT:	UBC CREB NUMBER:
Pierre Guy	UBC/Medicine, Faculty of/Orthopaedics	H06-03147

INSTITUTION(S) WHERE RESEARCH WILL BE CARRIED OUT:

Institution	Site
Vancouver Coastal Health (VCHRI/VCHA)	Vancouver General Hospital

Other locations where the research will be conducted:

The investigation of the obtained scans (Ultrasound, CT, and X-ray) using state of the art image processing techniques will be done at the Biomedical Signal and Image Computing Laboratory- Department of Electrical and Computer Engineering, UBC campus.

CO-INVESTIGATOR(S):

Rafeef Abugharbieh
Ilker Hacihaliloglu
Antony J. Hodgson
Robert N. Rohling

SPONSORING AGENCIES:

N/A

PROJECT TITLE:

Bone Fracture Alignment Assessment Using 3D Ultrasound Imaging – A Pilot Study

EXPIRY DATE OF THIS APPROVAL: August 14, 2010

APPROVAL DATE: August 14, 2009
CERTIFICATION: **In respect of clinical trials:** 1. The membership of this Research Ethics Board complies with the membership requirements for Research Ethics Boards defined in Division 5 of the Food and Drug Regulations. 2. The Research Ethics Board carries out its functions in a manner consistent with Good Clinical Practices. 3. This Research Ethics Board has reviewed and approved the clinical trial protocol and informed consent form for the trial which is to be conducted by the qualified investigator named above at the specified clinical trial site. This approval and the views of this Research Ethics Board have been documented in writing. The Chair of the UBC Clinical Research Ethics Board has reviewed the documentation for the above named project. The research study, as presented in the documentation, was found to be acceptable on ethical grounds for research involving human subjects and was approved for renewal by the UBC Clinical Research Ethics Board.
Approval of the Clinical Research Ethics Board by one of: Dr. Peter Loewen, Chair Dr. James McCormack, Associate Chair